UPPER BODY COORDINATION AND MOVEMENT CONTROL OF UNCONSTRAINED VISUALLY GUIDED THREE-DIMENSIONAL REACH MOVEMENTS

by

Shin-Yuan Yu

A dissertation submitted in partial fulfillment
of the requirements for the degree of
Doctor of Philosophy
(Biomedical Engineering)
in The University of Michigan
2010

Doctoral Committee:

Associate Professor Bernard J. Martin, Chair
Professor Arthur D. Kuo
Assistant Professor Kathleen H. Sienko
Research Associate Professor Matthew P. Reed
Assistant Professor Diane E. Adamo, Wayne State University

To Renee

Table of Contents

List of Figures

Figure

List of Tables

Table

ABSTRACT

Reaching is a basic component of human movements requiring the coordination of the eyes and multiple body segments including the hand, forearm, arm and torso. Although this movement has been studied extensively, the theory bridging the explicit reaching behavior (coordinated movement of body segments) and the implicit reaching strategy (control mechanisms) is limited. Hence, modeling unconstrained reach movements as a result of coordination remains a difficult task.

The aims of the present study were to investigate the relationships defining the coordination pattern, control mode composition and movement phase transition in order to develop a model of coordinated reach movements. This work focuses more particularly on the characterization of body segment kinematics in movement phases and control mode transition in relation to visual information. A novel approach to determine control mode transition is proposed by using changes in curvature of the elbow swivel angle (ESA) combined with the content of visual information. The results show that this approach seems to be a good indicator of control mode transition in reach movements. The relative durations of movement control modes were therefore determined and modeled as a function of reaching requirements. In addition, the use of the swivel angle enables the reduction of the degrees of freedom and contributes to a simplification of arm movement models. Two strategies of movement execution were observed as a function of

the availability of the visual information. In absence of vision, the movement variability was significantly reduced in order to constrain the system degrees of freedom. Furthermore, the orientation of the movement errors strongly support that in the present context, movements are planned in a local coordinate system and the head is the origin of that frame of reference.

A coordination model was developed to describe the timing and kinematics of three-dimensional reach movements. This model also includes the relationship between the eyes and body segment movements. With a generalized hand trajectory, the proposed model generates the sequence of movement phases and drives a multi-linkage system as a function of target locations.

CHAPTER 1

Introduction

1.1 Background and significance

Reaching is a basic component of human movements which requires the coordination of the eyes and multiple body segments including the hand, forearm, arm and torso. It represents a major activity in everyday life and more specifically in the manufacturing industry as it plays a crucial role in object manipulation. As any hand movement starts with a reach, it explains why this activity has been widely studied since the early ’50 (Lashley, 1951). Moreover, several pathological syndromes, resulting from cerebral palsy, stroke, Parkinson’s disease, etc., cause spatial and temporal deficiency of reach movements whose specific characteristics help understand the control of reaching movements. Rehabilitation programs relying on a solid understanding of the planning and coordination are needed as an increasing number of patients suffer from strokes (America Heart Association, 2006 & 2007) and Parkinson’s disease (Albert et al., 2000). It has been also suggested that coordinative rules of movement in healthy adults provide a framework from which to interpret deficits following nervous system injury, and assist clinicians in advancing neurorehabilitation (Bastian 1997; Bastian et al.2000; Beer et al. 2000). Additionally, general features of adult reaching provide potentially important variables to track in the development of reaching in infants (von Hofsten and Roennqvist 1988; Zaal et al. 1999). Thus, a general model of upper body coordination based on motor control principles may help to generate realistic movements using computer assisted design and possibly determine the alteration of specific mechanisms by some diseases.

1.1.1 Kinematics and modeling of reach movements

Reaching is the essential transport element of the hand movement in order to grasp a selected object (Jeannerod et al., 1998; Paillard and Beaubaton, 1978). Several studies have focused on the grip pre-shaping and opening linked to the reaching program (Castiello et al., 1993a, b; Gentillucci et al., 1991; Stelmach et al., 1994). A reaching-to-grasp model has been proposed as a program coordinated via a time-based module (Hoff and Arbib, 1993). The temporal coordination between reaching and grasping has been well studied and characterized by prehensile behavior derived from empirical data (Jeannerod, 1984; Jackobson and Goodale, 1991; Chieffi and Gentilucci, 1993). Although it was suggested that all joints begin to move together in two-dimensional movements (Hoff & Arbib, 1993; Vercher et al., 1994; Sailer et al., 2005), the temporal organization of body segments still requires further examination and study.

Extending from the same framework, several studies have investigated reach-grasp coordination when two effectors are involved. According to the work of Churchill et al. (1999), the temporal parameters of reaching and grasping are the same in bimanual and unimanual conditions. Similar results related to bimanual tasks have been reported (Castiello, 1997; Castiello and Bennet, 1997; Castiello et al., 1993a; Tresilian and Stelmach, 1997). These results indicate that the overall timing and kinematics of reach-to-grasp movements are similar for both bimanual and unimanual conditions. Hence, they also suggest that the coordination of reaching may present the same pattern for single and bimanual tasks.

Regarding different approaches of reach movement studies, it was originally proposed from a neurophysiological approach that reaching programs were controlled by two loosely coupled visuomotor channels (Jeannerod 1981, 1984). The inferior premotor cortex linked to the inferior parietal lobe was suggested to play a major role in spatial positioning of the arm (Jeannerod et al., 1995). At the cerebellar level, the posterior interpositus nucleus and the adjacent dentate were assumed to influence reaching accuracy and arm stability (Gibson et al., 1998; Mason et al., 1998, 2001). Moreover, experiments in cerebellar subjects showed that the cerebellum may be involved in the coupling of reach and grasp movements (Zackowski et al., 2002).

From the muscle dynamics point of view, it is proposed that movements are organized such that reactive forces not only fail to disrupt movement but directly support movement. Interaction effects, although passive, have been referred to as the offspring of muscle activation as they are ultimately generated from muscle forces (Bernstein, 1996). There is growing evidence that the nervous system anticipates these effects when planning arm muscle activity or muscle torque, particularly for the initial motion of the arm toward a target (Sainburg et al., 1999). Several specific control issues of reaching have been addressed using select intersegmental dynamic variables and methods. Studies have reported muscle torque across multiple directions (e.g., Buneo et al., 1995; Gottlieb et al., 1997), or multiple torque components for a few directions (e.g., Beer et al., 2000; Cooke and Virji-Babul, 1995; Ghez and Sainburg, 1995; Gribble and Ostry, 1999; Hollerbach and Flash, 1982; Sainburg and Kalakanis, 2000; Sainburg et al., 1999). Taken together, these studies suggest that intersegmental dynamics can differ across joints for different areas of the workspace.

Reaching involves the coding of spatial parameters, such as direction and amplitude, and of temporal parameters, such as velocity (Oliver et al., 2004). In the 1980's, human arm reach movements kinematics were investigated to understand the central nervous system (CNS) strategy to plan reaches and to improve rehabilitation processes. Many studies show that humans tend to choose unique trajectories with a fairly straight and smooth path exhibiting a bell-shaped velocity profile for the hand (Morasso, 1981, Abend, 1982). These invariant features of human movements reveal the internal representation of the movements in the CNS (Bernstein, 1967). In accordance to these invariant features reach movements were approached using optimization method. A number of two-dimensional (2-D) reach movement and multi-joint arm movement control models were formulated in the task space for co-planar movement using a minimum jerk criterion (Flash et al., 1985, Hogan 1985, Hoff et al., 1993; Jordan et al., 1994). Additionally, other studies (Uno et al., 1989; Dornay et al., 1992) suggested a minimum joint torque change criterion implying that the CNS plans the reach movements based on the dynamic formulation. Generally, the approaches are divided into two groups assuming that the CNS strategy is based on specific different coordinates – kinematic and dynamic coordinates (Wolpert et al., 1995). However, the choice of a coordinate system

remains an open debate, according to the results of kinematic and dynamics characteristics (Kawato, 1996 and 1999; Flash et al., 2003).

Expanding from the 2-D reach movement studies, three-dimensional (3-D) reaching models have been attempted to predict reach movements by predicting reaching postures or aiming at specific operational needs. (Zhang and Chaffin, 1997, 1999 and 2000; Galloway et al., 2002). The role of head movements and visual feedback has been investigated (Kim, 2005), and physiological consideration were also proposed (Siebert et al., 2007, Ren et al., 2007). According to the kinematics of the head and hand, Kim (2005) divided the unconstrained visually-guided reach movements into a lift-off, transport, and landing phases. The lift-off phase was defined as the initiation of hand movement regardless of the reaching direction, the transport phase corresponded to the directional reach segment of the movement, which was distinguished from the landing phase when gaze aimed at the target and the hand entered the estimated perimeter of the foveal field of view. Although the developed models were adapted to fit specific tasks, a more general 3-D reaching model is still needed to simulate and understand non-constrained movements.

1.1.2 Role of proprioception in goal directed movements

The role and contribution of proprioception to movement perception and control have been extensively studied. Proprioceptive information encoded by muscle spindles (Sherrington, 1906; Goodwin et al., 1972; McCloskey, 1973; Burgess et al., 1982) plays a major role in the control of voluntary movements (Gandevia et al., 1992; Ghez et al., 1995; Hasan, 1992; Roll et al. 2000). Proprioceptive feedback has been found to be critical in controlling muscle interaction torques (Sainburg et al., 1993; Ghez and Sainburg, 1995), the timing of limb segments during multi-joint movement (Cordo et al., 1994, 1995; Devanne and Maton, 1998), movement trajectories (Roll et al., 2000; Sauter and Martin et al. 1991), and providing internal models of limb representation (Roll and Roll, 1998) used in skilled movement (Kawato and Wolpert, 1998).It is also suggested that proprioception is involved in the control of limb posture (Goodwin et al. 1976; Rothwell et al. 1982; Sanes et al., 1985; Adamo and Martin 2009) and the specification of movement direction and extent (Ghez et al., 1990; Rothwell et al., 1982; Saling et al.,

1992; Sanes et al., 1985). The relationship between joint kinematic information and discrete movement show that proprioceptive information is also used to coordinate joint movements (Cordo et al., 1994). However, most proprioceptive studies have not considered the interaction of vision and proprioception. Based on the assumption that the sequencing of body segment initiation is triggered by joint rotation, visual feedback was excluded in these studies.

1.1.3 Vision and movement control

Visual feedback is supported by eye and head movements. It has been shown that visual targets presented in peripheral locations are likely to induce head movements for gaze displacements in order to obtain accurate visual information (Fuller 1992; Gauthier et al. 1986; Guitton et al. 1987; Stahl 1999, Kim 2005; Kim and Martin 2007) from the foveal field of view (FFoV). Visual feedback contains information not only about the current state of the moving limb (Carlton, 1981), but also about the location of the target and the relative positions of limb and target (Prablanc et al. 1986). A study of eye movements during transient target disappearance suggested that the CNS plans the eye position based on the expected target location and velocity. The resulting eye movement is achieved through the synergy of saccades and smooth pursuit (Orban de Xivry et al., 1996). It has been also shown that eye movements are modulated by the movement of the whole body and the hand (Gauthier et al 1986; Martin et al. 1991; Delleman et al., 2001; Tipper et al., 2001). Furthermore, visual perception of the environment was found to be modified by the adjustments of stance control (Peterka et al., 1995; van der Kooij et al., 2001), torso movements (Cohn et al., 2001), and head movements (Kim, 2005).

Eye-hand coordination is essential for reaching and pointing movements. It has been first shown that wrist-rotation in rapid aiming movements is highly dependent on the type of eye movements involved (Abrams et al. 1990). In addition, it has been shown that gaze supports hand movement planning by marking key positions to which the fingertips or grasped object are subsequently directed (Flanagan and Johansson 2003; Johansson et al. 2001; Neggers and Bekkering 2000, 2001). It is also estimated that gaze aims at the target by the time the corrective movements take place (Uemura et al., 1980; Biguer et al., 1984; Carnahan & Marteniuk, 1991; Vercher et al., 1994) Furthermore,

gaze and body segment movements tend to move in a similar manner in reaching movements. Some studies on unconstrained three-dimensional movements (Desmurget & Prablanc, 1997; Pelz et al., 2001; Flanagan & Johansson, 2003) reported the eye-hand coordination features and the temporal organization. For each segment, a large initial undershoot is followed by one or more corrective movements to reach their respective final position (Helsen et al. 2000; Kim et al., 2007). Moreover, a study of the relationship between limb proprioception and oculomotor signals in 2-D reaching suggests that the required direction of a saccade indicated by the relative initial position of the eye and hand affects the average direction and variability of saccades during hand movements, which are not affected by the direction of the hand movement (Vercher et al., 1994; Ren et al., 2007). It is proposed that any misestimating error of the hand trajectory derived from visual information may not be responsible for gaze movement errors. The errors in defining saccade vectors rather arise from a process of comparing proprioceptive information of initial eye and limb positions. Furthermore, the performance of reaching movement relative to target and arm visibility suggests that movements appear to be planned to start in a direction that deviates from the direction of the actual straight line between the initial and target positions (Sittig et al., 1994; Kim et al. 2007). This result shows that deviations of the initial movement direction of goal-oriented arm movements are not primarily visually based (de Graaf et al., 1991a, 1991b, 1994; Kim et al. 2007).

1.2 Applied problem

To the human movement control, the contribution of major feedback mechanisms, vision and proprioception, needs a further investigation and quantification. The primary focus in this work is the effect of visual feedback in movement planning. According to the studies concerning visual guidance for reach and movement control, it may be suggested that the CNS, while planning and executing a movement, simultaneously controls multiple subsystems that pursue individual and shared goals (guiding the hand, displacing the gaze, etc) in order to achieve the general aim of the task (reaching to a target). It also implies that visual feedback plays an important role in determining reach movement control and coordination. Hence, in the context of this work reach movements

are assumed to be multi-phasic. It is hypothesized that the control mode transition is relative to the availability and characteristics of visual information.

The following phases will be included in the model of reach movement coordination:

1. Lift-off phase:

The lift-off phase may be initiated before visual acquisition of a target. The hand movement during that phase may simply correspond to an elevation without a specific direction. The joint initiation sequencing and timing found from the experiments and feed-forward control will be used to generate the limb movements during their own movement time.

2. Transport phase:

This phase may be initiated after the visual acquisition of the target of interest. Hence, transport phase is defined to be the stage after which target location is visually acquired and the end effector is moving toward the target under open-loop control. It is assumed that the peak horizontal velocity occurs during the transport phase.

3. Landing phase:

Derived from gaze movements, the estimated instant at which the hand enters the foveal field of view (FFoV) when the hand is close to the target location is assumed to be the indicator of the phase transition. Additional aid with the body segment kinematic information needs to be used to precisely determine the phase initiation. In this phase, movement can be adjusted by feedback (closed-loop) control using visual feedback (if the hand remain in the FFoV) or estimated proprioceptive feedback (if the hand is not in the FFoV) until the hand reaches the target with a predetermined estimated error.

1.3 Specific aims of the thesis

Reaching is one of the important activities among multi-segmental goal directed movements. Several factors, such as perception, control modes, and kinematics of body segments, might affect the performance of human reach movements. These movements have been studied extensively; however, the theory bridging the explicit reaching behavior (coordinated movement of body segments) and the implicit reaching strategy

(control mechanisms) is limited. Hence, modeling multi-functional reach movements remains a difficult task.

In this work, the relationship between reach movement characteristics and the factors contributing to movement phases and multi-segmental organization are investigated. These relationships, which define coordination, are governing the timing, duration, sequencing, and displacement of body segments as well as control modes and movement phase transitions. This work will focus more specifically on the characterization of upper-body segment sequencing (including the gaze), movement phase composition and the role of visual feedback in movement phase transitions. As shown in Figure 2.1, the coordination of reach movements can be divided into two components, which relate to body segment kinematics and control mechanisms respectively. Coordination of movements is assumed to be characterized by two aspects such as timing/phase change and body segment interaction. Given the known control mode mechanisms (open-loop and closed-loop control) their sequencing can be dependent on sensory information such as vision and proprioception, as illustrated in Figure 2.2.

The specific aims of the present dissertation are as follows:

1) To determine movement control mode transition during one-handed reach activities.
2) To determine the sequencing of 3D upper-body reach movements and to define eye-head and upper body coordination of unconstrained reach movements.
3) To determine the contribution of visual feedback mechanisms to movement phase transition and to the reaching precision of the hand in unconstrained reach movements.
4) To develop a model of upper body coordination that simulates realistic reach movements based on control principles.

CHAPTER 2

Movement Characteristics of Body Segments during Reach Movements

2.1 Abstract

Coordination of reach movements is related to body segment control and movement timing. In this chapter, the initiation sequencing and movement characteristics of body segments were extracted from recordings performed with motion capture systems. The movement characteristics represented by the end effector trajectory and torso angles reveal a dependence on target azimuth. Besides, the eye-head coordination results support the necessity of the precise eye movement information to determine the availability of the visual feedback in movement control. Combining visual feedback information and kinematics data of body segment movements during reach, the results of arm joint initiation show the combination of the feed-forward and feedback control mechanisms exists based on the hypothesis that the implicit sequence of body segments in reach movement can be inferred in part from kinematic characteristics and associated visual feedback information. The overall torso displacement and the initiation timing of arm joint angles show a dependence on the target azimuth and can be further used for the coordination model development.

2.2 Introduction

A number of single and multi-joint arm movement control models have been proposed for the simulation of co-planar movements (Flash et al., 1985, Hogan 1985) and 3D reaches (Zhang and Chaffin, 1997, 1999 and 2000, Galloway et al., 2002). In a previous study, reach movement models were extended by inclusion of head movements

as estimation of eye gaze direction (Kim, 2005). Nevertheless, a deeper understanding of movement control and coordination is necessary to develop more general models of 3-D reaches to simulate a larger variety on unconstrained movements including all body segments involved in a movement. These models are necessary for realistic representation of industrial and vehicle design applications.

Coordination of human movements is assumed to be characterized by two aspects such as timing/phase change and body segment interaction (Figure 2.1). Following coordination studies presented before (Sober & Sabes, 2003; Todorov, 2004; Kim, 2005), the timing/phase change was the focus of this chapter. Given the known control modes involved in a reaching movement, feed-forward (open-loop) and feedback (closed-loop) modes, their sequencing can be dependent on visual feedback as illustrated in Figure 2.2.

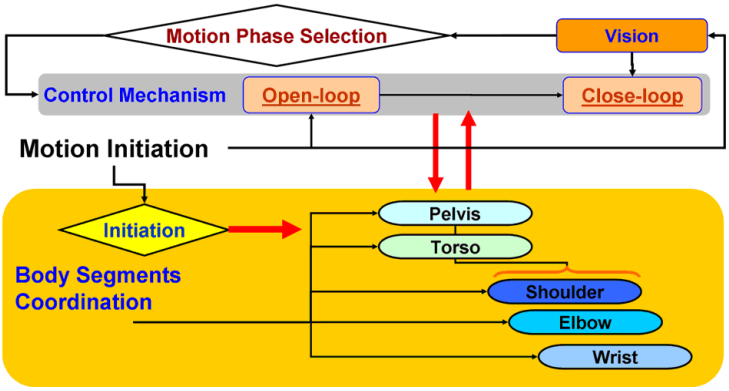

Figure 2.1. General hypothetic structure of movement coordination

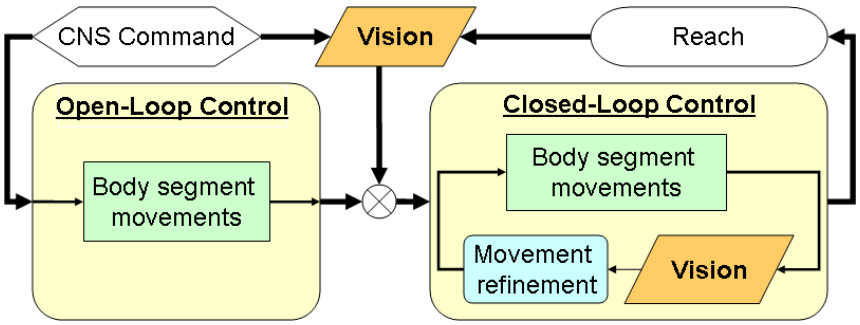

Figure 2.2. Hypothetic sequencing structure of movement control

The eye-head interaction, the end effector trajectory and the overall torso angular displacement for reaching to different target azimuth and distance was investigated in order to verify the approach of this study and to compare with the previous ones.

Furthermore, the timing for the arm joint angle initiation in related to the visual feedback was also studied to determine the sequencing of the joint initiation in reach movements.

2.3 Methods

In this chapter, movement capturing techniques was used as the experimental approach for the study. Data of body segment movements, eye movements and visual scene were collected to define the relationship between movements and visual feedback information.

2.3.1 Participants

Six young adults (three females and three males) participated in this preliminary study. Their average age was 21 ± 2.7 years and average stature of 1.74 ± 0.09 m. The height of the seat pan was about 56 cm (adjusted according to their comfortable seating posture) and the seated elbow height was about 82.6 cm. The average arm reaching length was 66.0 ± 3.7 cm. The participants were all right-handed and free from any neuromuscular disorders. All signed an informed consent for participation in an experiment approved by the internal review board of the University of Michigan.

2.3.2 Experimental setup

Participants were comfortably seated to perform right-hand reaches. Twelve targets were distributed along horizontal concentric circles centered at the participant's right shoulder (Figure 2.3a) with an elevation corresponding to elbow height. The targets were divided into two groups, near and far, as a function of their distance from the shoulder, which was defined by the radii of two circles. Radii (distances) for the near and far groups corresponded to 80% and 120% of the arm reaching length defined as the distance between the acromion and the tip of the index finger when the elbow is fully extended.

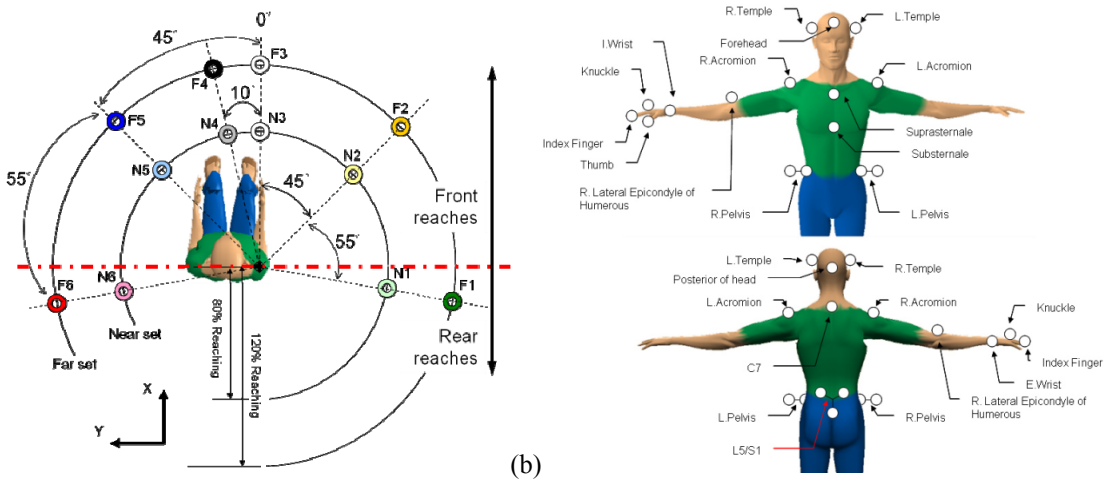

Figure 2.3. Experimental setup. a) Target locations; b) Retro-reflective marker set used to track whole-body motion

Whole-body movements were recorded by an infrared motion capturing system including eight cameras (Qualysis® ProReflex 240-MCU). Twenty-two retro-reflective markers were placed on selected body landmarks (Figure 2.3b). An Eye Tracking System (ASL Eye-Trac®), which includes both an infra-red eye movement camera and a scene camera fixed on a on a head mount, was used to record eye movements and subject's visual scene simultaneously (Figure 2.4). In order to determine the visual acquisition of the target to be reached during each movement, both body and eye movements were sampled at 60 Hz and the respective data were synchronized (Figure 2.5).

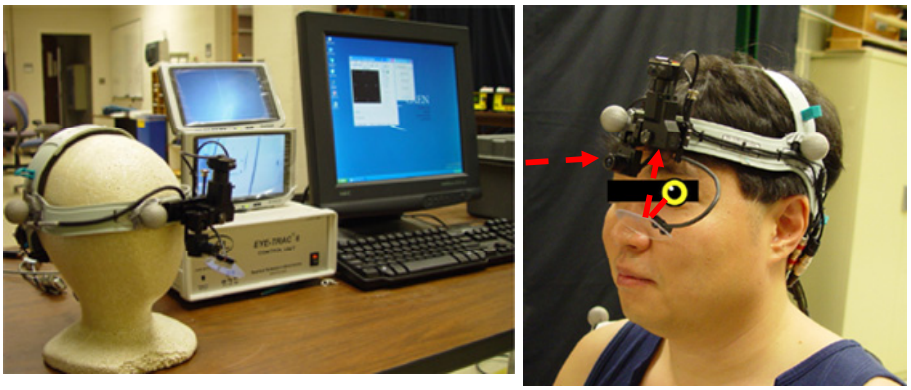

Figure 2.4. Eye tracking system (left) and configuration when mounted on a subject (right)

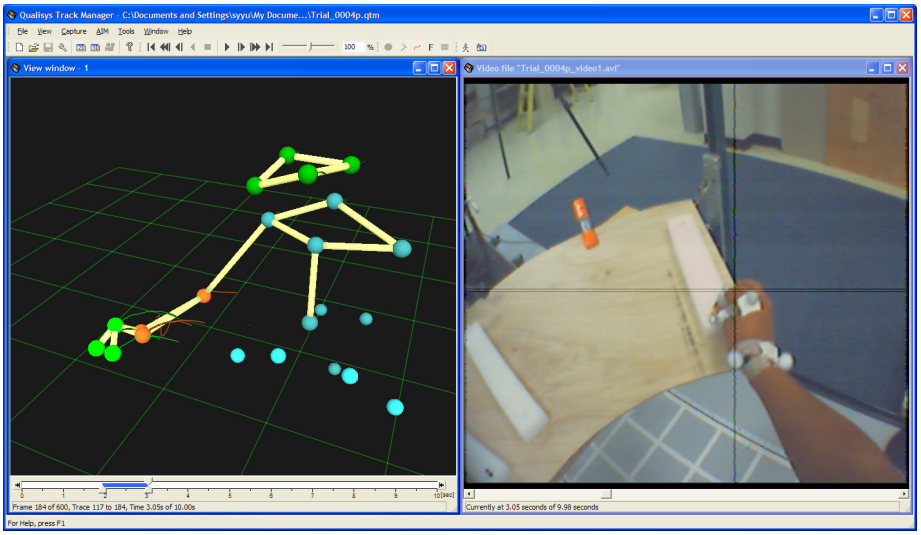

Figure 2.5. Synchronized Motion and Eye tracking system (visual scene)

2.3.3 Experimental protocol

The experiment was divided into two sessions conducted sequentially.

1st Session: Anthropometric Measurements & Calibration

Anthropometric data including stature, reach length, seat height, elbow height and shoulder height when seated were measured for each individual. Target distances and elevation were determined accordingly. Then the eye tracking system was placed on the subject's head. To obtain an accurate direction of gaze, the eye tracking system was carefully calibrated with a 9-point panel which covered the field of view and was placed to face the subject vertically and centered at the neutral gaze orientation.

2nd Session: Motion Capturing

Retro-reflective markers were placed on the subject (Figure 2.3b) and a digitization procedure was executed to define the location of additional body landmarks such as the eyes and the low back (L5/S1) with respect to the optical makers placed on the corresponding body link. Digitized locations were later combined with three-dimensional marker data to determine the position of the eyes in the head and create a linkage representation of the human body (Reed et al., 1999; Kim, 2005).

Each trial (movement to a target) started from an initial posture in which the arm is resting on the thigh with the hand on the knee while the eyes fixate a reference visual target placed at eye level in the mid sagittal plane (Figure 2.6a). The targets were reached at a comfortable self-imposed pace in a random order (Figure 2.6b). For each trial, the instructed target location was indicated visually with a reaching configuration graph on a panel placed in front of the subject beyond the reach destination. The subject was also instructed to return to the initial posture and gaze after each reaching movement. The sequence of reaching to different target location was random and each target was reached by the subject with repetition of three in total.

(a) (b)

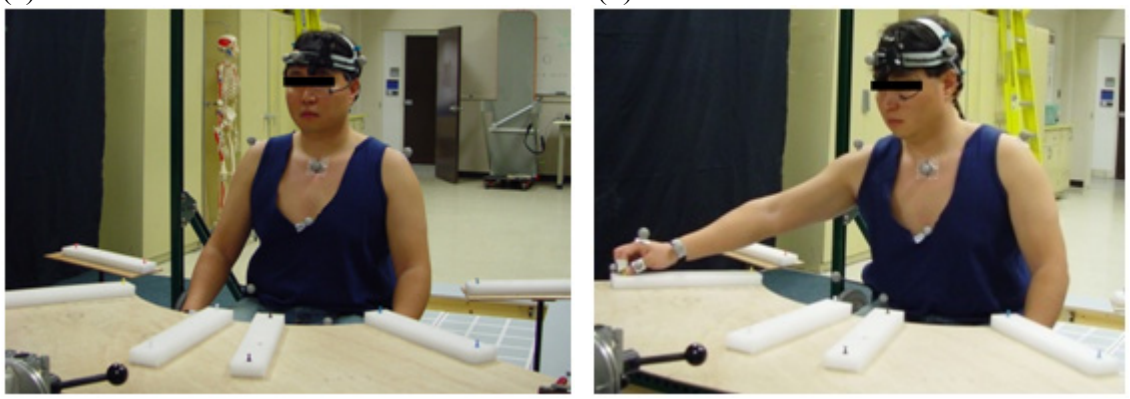

Figure 2.6. Typical initial posture (a) and final reach posture (b)

2.3.4 Reconstruction of gaze orientation

The direction of gaze was reconstructed from the eye tracking data to find the instants at which visual information may be used to control the hand movement and thus identify phase transitions in hand movements. Since the eye tracking data was recorded as the planar movement of the eye within the orbit, the local 2-D coordinate system of the eye in the head (orbit) requires a homogeneous transformation for a representation in the global coordinate system with which the body segment kinematic data were expressed (Figure 2.7a). By representing the gaze orientation vector within a local coordinate system established from the three markers on the head (frontal, left and right temporal markers) ($\vec{G}^{head}$) and using the size of the eye (van den Bosch et al., 1999), then the gaze

orientation vector in the global coordinate system ($\vec{G}^{global}$) can be reconstructed and represented by the following equation:

$$\vec{G}^{global}(t) = T_{head}^{global}(t) \cdot \vec{G}^{head} \qquad \text{(Eq. 2.1)}$$

where T_{head}^{global} is the homogeneous transformation matrix from the local (head) to the global coordination system, and $T_{head}^{global} = \left[\mathrm{x}_{\mathrm{head}}^{\mathrm{gaze}} \quad \mathrm{y}_{\mathrm{head}}^{\mathrm{gaze}} \quad \mathrm{z}_{\mathrm{head}}^{\mathrm{gaze}} \right]$. An example of the result of this gaze reconstruction process is illustrated in Figure 2.7b.

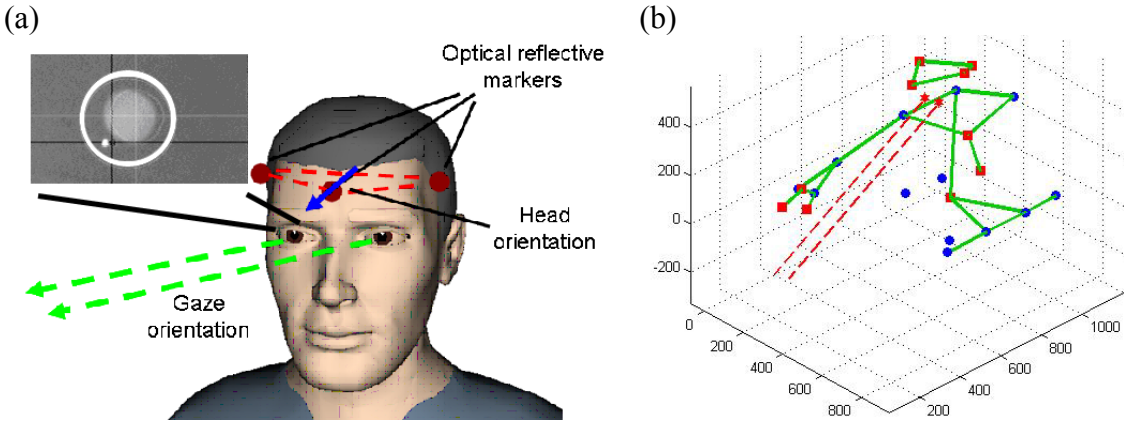

Figure 2.7. Gaze reconstruction. a) Image captured from Eye Camera and Head-Eye integration; b) Example of the reconstruction of gaze orientation (dash lines)

2.3.5 Data processing and analysis

The movement of the end effector (hand) in reach/pointing movements is characterized by its trajectory whose characteristics also needs to be investigated. Hence, the straightness error (SE) was defined and used to determine the deviation from a straight line between the initial and terminal position of the end effector. SE is defined as:

$$SE = \frac{A_{err}}{l^2} \qquad \text{(Eq. 2.2)}$$

where l represents the horizontal displacement of the hand (the hand traveling distance) and A_{err} the area enveloped by the horizontal projection of the hand trajectory and SE is a dimensionless index representing the deviation of the hand traveling path from a straight line connecting the initial and terminal position of the hand (Figure 2.8).

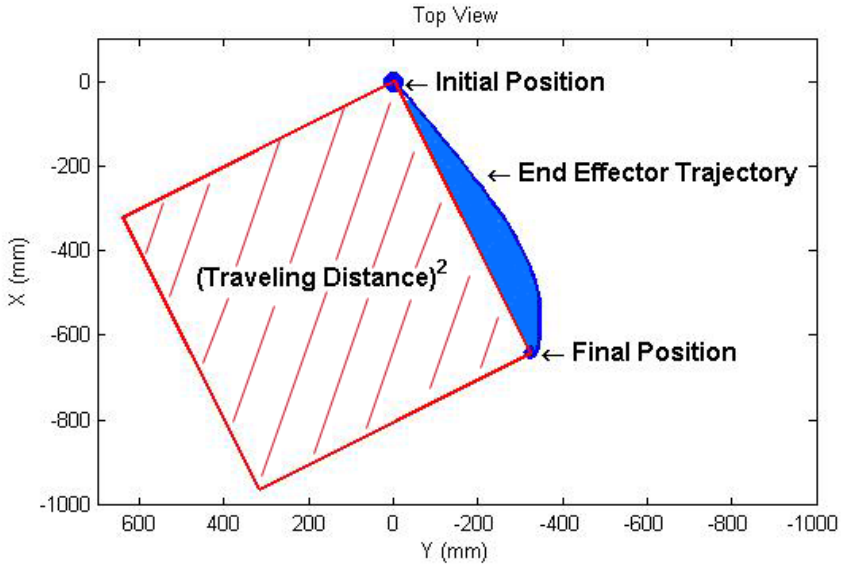

Figure 2.8. Illustration of the straightness error (deviation from a straight line) for the end effector trajectory – reaching to the rear right target location.

Kinematic data of each body segment were used to quantify time variations of joint rotations and to determine their sequencing. They were also used to find the onset and termination of the reach movements. The initiation of the end effector was determined by using a 2% threshold of the total hand horizontal velocity change. A reach to a target was determined by the position of the end effector and its velocity at the beginning and end of the movement. Then, the total movement time (MT) was determined by the duration between the initiation of the end effector and the achievement for the reach movement. The initiation of each arm joint movement was determined by using a 2% threshold of the total change of joint angle between the initial and end posture. For a better comparison between individuals, the temporal axis of kinematic data was normalized by MT.

The movement refinement may rely on the content of the visual feedback information. Given the hypothetic model for the role of visual feedback in movement control, gaze-on-target (GOT) is defined to be the timing when the gaze locates on the target to acquire the exact spatial information about the target for CNS. For each collected reaching movement, the origin of time was shifted to be at the GOT instant. Hence, the magnitude of an arm joint angle initiation is negative when it was initiated before GOT, and vice versa.

In this study, focus was taken on the movement properties of the end effector and body segments. To understand the kinematic characteristics of body segments, analysis was performed to the movement properties from the trials of all subjects, such as straightness errors and maximum vertical displacement of the end effector trajectories, total torso angular displacement (axial rotation, lateral bending and anterior flexion), and the initiation timing for the joint angles which include elbow extension, shoulder azimuth and elevation for the arm, and axial rotation, lateral bending and flexion for the torso. Since each target was reached more than once in a series of reaches for each subject, a repeated measure analysis of variance (ANOVA) and the Tuckey's honestly significant difference criterion (HSD) for all trials were used to determine the influence of target azimuth and distance on the properties of the hand and body segment movements.

2.4 Results

2.4.1 Eye-head coordination

Visual acquisition of the target usually occurs earlier than head movement regardless of the reaching direction, as illustrated in Figure 2.9. The action of the vestibulo-ocular reflex (VOR) , which helps maintain the eye on target when the head rotates is illustrated in Figure 2.9c and d for different targets to show the differences in eye-head interaction as a function of target azimuth (upper and lower panels). The interaction of the VOR is significant for eccentric targets (45° azimuth), while it is negligible for targets in the mid sagittal plane (0° azimuth).

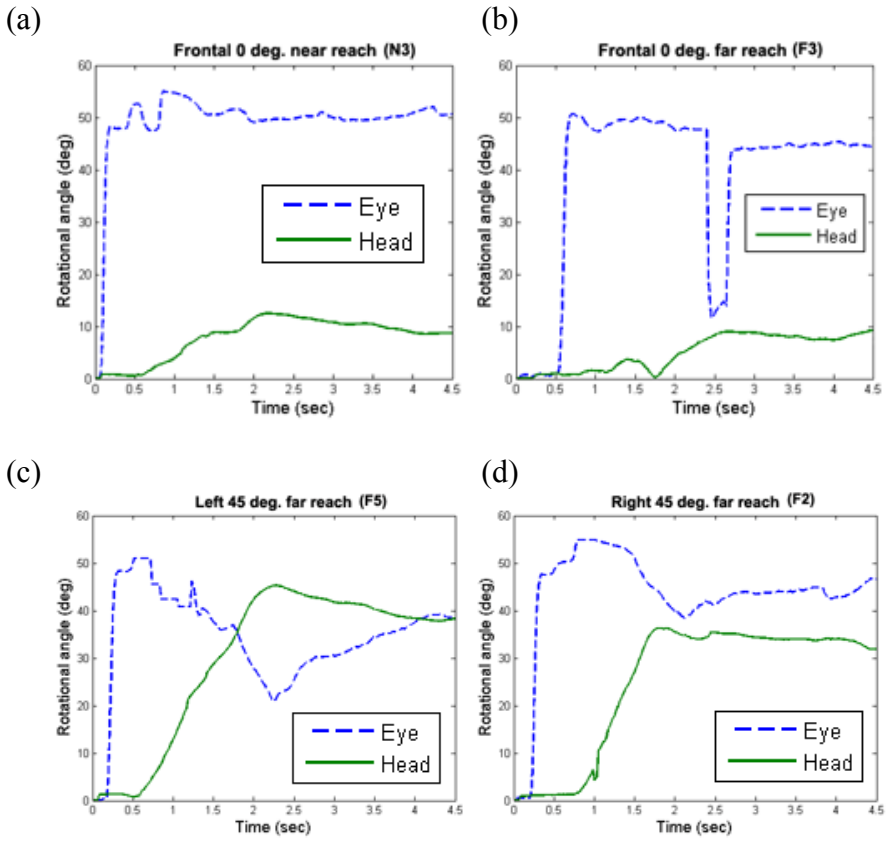

Figure 2.9. Head and eye orientation time profiles for near and far medial targets (left and right panel in upper panels) at 0° and 45° azimuths (upper and lower panels)

2.4.2 End effector trajectories

A typical example of reach movements to each target location is shown in Figure 2.10. For the sake of representation clarity, reach movements are illustrated at a frame rate corresponding to a 20 Hz sampling rate.

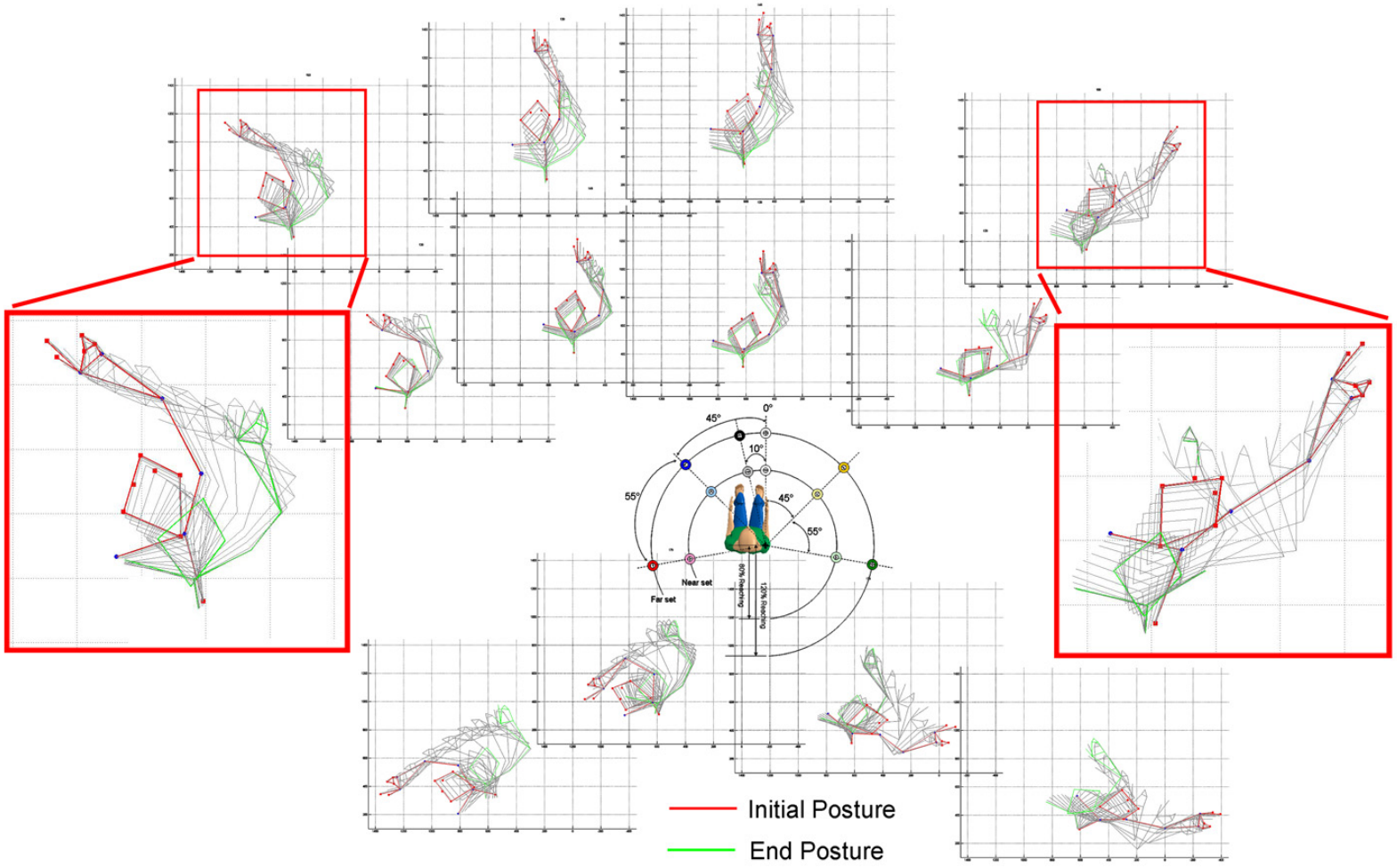

Figure 2.10. Example of reach movements to each target location at a sub sampling rate of 20 Hz (0.05 ms /frame)

An example of 3D end effector trajectories to each target location is presented in Figure 2.11. The horizontal path (horizontal projection of the trajectory- Figure 2.11, top view) of the hand is only slightly curved. While the hand moves mostly in a plane, the trajectory is significantly curved in the vertical direction (Hore et al., 1992, 1994; Miller et al., 1992; Wolpert et al., 1994; Gielen et al., 1997).

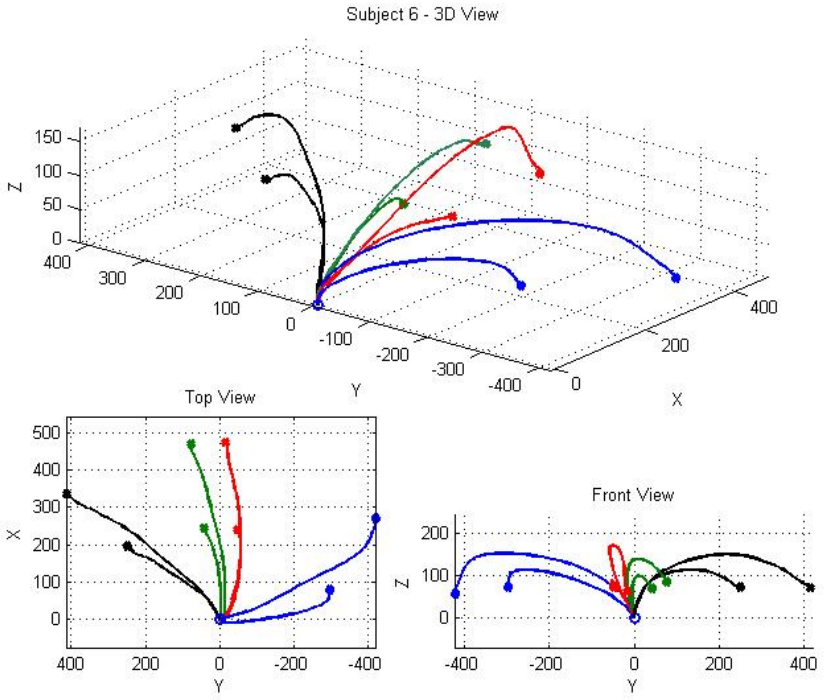

Figure 2.11. Examples of end effector trajectories – frontal reaches

Horizontal component

The influences of target azimuth and reaching distance are significant with p values less than 0.05 (Table 2.1) and there is no interaction between target azimuth and distance. The comparison of SE for each target azimuth as a function of distance is presented in Figure 2.12. In general, the hand traveling path is fairly straight for all reaches except reaching to the rear left target, as the SE values show, are less than 12%. Comparing the frontal (0º front F & N3, and 10º left F & N4) and rear (rear right F & N1, and left F & N6) reaches, the path of the hand is significantly ($F = 37.01$, $p < 0.01$) curved more for rear than front reaches with an average SE of 10.3% ± 7.2% and 4.7% ± 2.9% , respectively. Furthermore, the path is significantly curved more for the near reaches than the far reaches ($F = 5.96$, $p = 0.01$) with an average SE of 7.9% ± 6.5% and 6.0% ± 4.5%,

respectively. The straightness errors are listed in Table 2.2. The standard deviations of the rear left reaches to the far (F6) and near (N6) are 4.0 and 6.4 respectively while those of the exact frontal (medial) reaches are only 1.7 (F3) and 2.7(N3) for the far and near target respectively

Table 2.1. ANOVA table of the SE

	DoF	F	p
Azimuth	5	32.1	<0.01
Distance	1	1.75	0.04
Azim. × Dist.	5	0.84	0.81

(Shaded cells correspond to significant values.)

Table 2.2. Straightness errors of end effector trajectories with respect to target location

(%)	Rear Right	45º Right	0º Front	10º Left	45º Left	Rear Left	$F_{5,102}$
Far set	4.7 ± 3.8	6.2 ± 2.9	4.6 ± 1.7	3.0 ± 1.9	4.7 ± 3.7	13.0 ± 4.0	23.09*
Near set	6.4 ± 6.4	7.5 ± 4.5	5.9 ± 2.7	5.5 ± 4.0	5.0 ± 5.0	17.1 ± 6.4	14.93*
$F_{1,34}$	0.83	1.12	4.14	5.27	0.05	5.24	
p value	0.3698	0.2983	0.0453	0.028	0.8225	0.0284	

(Shaded cells correspond to significant values.) *p < 0.01

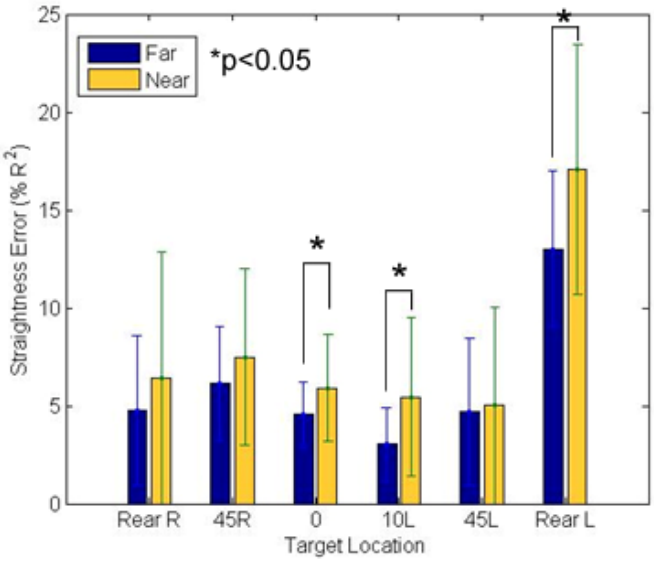

Figure 2.12. Straightness errors of end effector trajectories with respect to target location

The curvature tended to increase with eccentricity but the azimuth effect is significant only for the rear left reach. The path curvature for rear left reach is significantly larger than all other reaching azimuth ($p < 0.05$). Reaching to far right target (F2) is also significantly larger than reaching to the far 10 degree left target (F4). The curvature also tended to increase with distance; however this tendency was significant only for the front reaches (F&N3 and 4) and rear left one (F&N6).

Vertical component

As shown in Table 2.1 and Table 2.2, the maximum vertical displacement of the end effector trajectory significantly increases with reaching distance. From the Tukey's HSD, there is no significant difference among all frontal reaches (F & N2 - 5). Among the near reaches, only reaching to the rear left is significantly larger than other reaches by about 50 mm; while the two rear reaches have a significantly larger amount the frontal ones by about 50 mm as well. The average maximum vertical displacement of the frontal reaches is 103 mm and 71 mm for the far and near reaches respectively. The comparison of maximum vertical displacement for each target azimuth as a function of distance is presented in Figure 2.13.

Table 2.3. ANOVA table of the Max vertical displacement

	DoF	F	p
Azimuth	5	18.37	< 0.01
Distance	1	4.56	< 0.01
Azim. × Dist.	5	0.35	1

(Shaded cells correspond to significant values.)

Table 2.4. Max vertical displacement of the end effector trajectories with respect to target location

(mm)	Rear Right	45º Right	0º Front	10º Left	45º Left	Rear Left	$F_{5,102}$
Far set	136 ± 33	98 ± 31	101 ± 33	104 ± 33	109 ± 33	166 ± 48	13.44*
Near set	80 ± 29	71 ± 26	67 ± 29	70 ± 38	75 ± 29	123 ± 32	11.2*
$F_{1,34}$	39.37	11.02	13.99	11.06	14.47	12.79	
p	< 0.01	< 0.01	< 0.01	< 0.01	< 0.01	< 0.01	

(Shaded cells correspond to significant values.) *p < 0.01

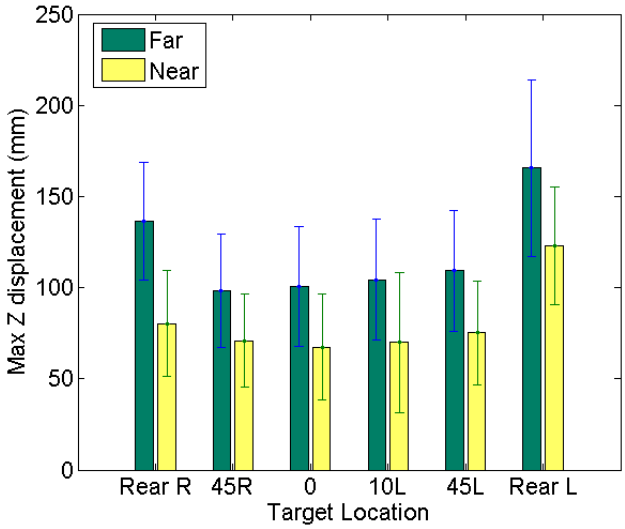

Figure 2.13. Max vertical displacement of the end effector trajectories with respect to target location (p values for all pairs are less than 0.01)

2.4.3 Joint angles

Torso angles

The torso is an important body segment in the coordination scheme as it may contribute significantly to both the direction and distance of reaches. In collected data, the torso was represented by the markers placed on C7, the suprasternale, and substernale, and the axis of rotation was located at L5/S1 (Figure 2.3b). The overall torso movement was represented by the angular displacements corresponding to axial rotation, anterior flexion, and lateral bending. The influences of target azimuth and reaching distance on the torso angles are shown in Table 2.5 from ANOVA. It shows that torso lateral bending for the far and near reaches may not significantly different ($p = 0.22$), and target azimuth and reaching distance might have interaction for all torso angles ($p<0.01$). Azimuth and distance has significant interaction for all torso angles ($p<0.01$).

Table 2.5. ANOVA table of the torso angular displacement

	Axial rotation			Anterior flexion			Lateral bending		
	DoF	F	p	DoF	F	p	DoF	F	p
Azimuth	5	485.4	< 0.01	5	218.6	< 0.01	5	63.73	< 0.01
Distance	17	29.2	< 0.01	17	19.2	< 0.01	17	1.41	0.22
Azim. × Dist.	85	3.4	< 0.01	85	8.3	< 0.01	85	6.9	< 0.01

(Shaded cells correspond to significant values.)

The average torso angles and their standard deviation related to different reaching azimuths across all subjects are presented in Table 2.6. For far reaches, torso anterior flexion shows a consistency with the region divided by the frontal plane of subject. Torso anterior flexion angles are all positive in the front region, while those are negative for rear reaches. For the near reaches, however, anterior flexion angles are also negative when reaches to the left (N5 and N6). This might result from the self-interference and coordination of body segments. In addition, the variance of all torso angles when reaching to the rear targets (target 1 and 6) is higher for the left side (F6 and N6) than the right one (F1 and N1) ($p<0.01$).

Table 2.6. The torso angles with respect to the reaching azimuth

(Unit: deg.)		Rear Right	45º Right	0º Front	10º Left	45º Left	Rear Left	$F_{5,102}$
Axial Rotation	Far	-23.7 ± 7.7	7.4 ±3.9	24.9 ±3.8	28.4 ±4.6	39.6 ± 5.6	70.5 ± 9.6	613.64*
	Near	-18.9 ±7.6	-0.8 ±3.7	6.7 ±2.6	8.6 ±2.4	17.7 ± 4.5	50.4 ± 8.6	429.41*
Anterior Flexion	Far	-6.5 ±3.2	14.0 ±3.2	13.1 ±5.0	11.6 ±3.8	3.7 ± 3.1	-16.3 ± 3.6	265.36*
	Near	-2.8 ±2.1	2.1 ±3.1	0.9 ±2.0	0.9 ±2.4	-1.0 ± 1.8	-10.9 ± 3.9	78.32*
Lateral Bending	Far	14.9 ±3.3	15.4 ±1.9	0.8 ±3.0	-3.8 ±4.2	-8.3 ± 4.3	-13.4 ± 4.3	264.45*
	Near	-0.7 ±3.5	1.8 ±2.9	-0.5 ±1.7	-1.5 ±1.7	-2.8 ± 3.7	-0.9 ± 5.3	4.82*

(Shaded cells correspond to significant values.) *$p < 0.01$

Figure 2.14 show the three torso angles as a function of target azimuth for the far (a) and near (b) reach distances. Torso axial rotation shows as a quasi linear increase with target azimuth, while anterior flexion and lateral bending tend to vary with target azimuth for far targets only and remain the same regardless of the target azimuth when reaching to near targets. Torso lateral bending for the near reaches is not significantly affected ($p=0.32$) by the reaching distance. Furthermore, the torso anterior flexion for the near frontal reaches (N2 to N5) is significantly affected by the azimuth ($p < 0.01$).

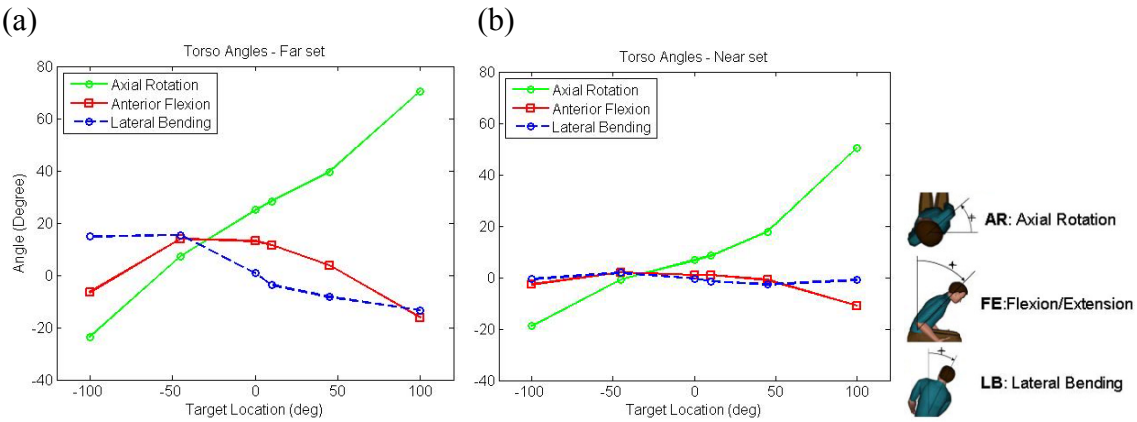

Figure 2.14. Total torso angular displacement with respect to reaching azimuth angles. a) Far set; b) Near set

Joint space angles of the arm

In collected movement data, the arm was represented by markers placed on the right acromion, humerus lateral epicondyle and wrist (Figure 2.3b). Between the initial and terminal posture, the overall arm movement was quantified by the angular displacement of its joint space angles which correspond to elbow extension, shoulder azimuth and shoulder elevation. The center of rotation of the elbow was determined by the location of the humerus lateral epicondyle marker, and elbow extension angle was determined by the angle between upper arm and forearm. Shoulder azimuth and elevation were derived from the projection of the angle between the upper arm and torso onto the horizontal and vertical plane, respectively. Through 2-way ANOVA, Table 2.7 shows the effect of target azimuth and distance and their interaction on each joint space angle. Notice that shoulder azimuth angles is not significantly affected by reaching distance ($p = 0.22$); while neither is shoulder elevation varied by target azimuth ($p = 0.15$). There is no evidence of an interaction effect of the target azimuth and distance given the interaction p values of 0.98, 0.88 and 0.99 for elbow extension, shoulder azimuth and shoulder elevation, respectively.

Table 2.7. ANOVA table of the joint angular displacement analysis

	Elbow extension			Shoulder azimuth			Shoulder elevation		
	DoF	F	p	DoF	F	p	DoF	F	p
Azimuth	5	4.98	<0.01	5	53.32	<0.01	5	1.65	0.15
Distance	17	17.58	<0.01	17	1.29	0.22	17	7.39	<0.01
Azim. × Dist.	85	0.66	0.98	85	0.78	0.88	85	0.58	0.99

(Shaded cells correspond to significant values.)

Averaged over all subjects, Table 2.8 shows the mean values of the joint space angles and its standard deviation with respect to target azimuth for far and near set. The shoulder azimuth angle has the highest variance among the three joint space angles. Notice that the elbow extension angle is not significantly affected by target azimuth when reaching to the near ($F = 0.96$, $p = 0.44$). Given the p value less than 0.05 for all joint space angles to the far and elbow extension angle to the near, the arm movement is significantly affected by the target azimuth.

Table 2.8. The joint angular displacement with respect to the reaching azimuth

(Unit: deg.)		Rear Right	45º Right	0º Front	10º Left	45º Left	Rear Left	$F_{5,102}$
Elbow Extension	Far	59.7 ± 3.3	59.7 ± 3.7	55.3 ± 3.8	59.3 ± 2.6	53.6 ± 3.0	40.4 ± 2.3	5.54*
	Near	25.7 ± 3.8	28.1 ± 3.4	26.3 ± 3.0	23.7 ± 3.6	22.6 ± 2.7	19.1 ± 2.7	0.96†
Shoulder Azimuth	Far	-9.6 ± 12.0	19.3 ± 8.6	67.1 ± 7.4	70.5 ± 7.7	97.9 ± 10.1	136.2 ± 14.1	26.21*
	Near	-42.1 ± 12.9	11.3 ± 6.3	59.3 ± 8.2	58.8 ± 6.6	78.4 ± 5.8	115.7 ± 14.2	33.0*
Shoulder Elevation	Far	41.2 ± 1.7	38.5 ± 1.3	38.1 ± 1.5	36.8 ± 2.0	34.3 ± 2.3	33.5 ± 0.8	2.87*
	Near	25.7 ± 2.3	23.2 ± 2.0	24.3 ± 2.6	23.8 ± 1.9	22.5 ± 2.1	33.0 ± 2.0	3.21*

(Shaded cells correspond to significant values.) * $p < 0.05$; † $p = 0.44$

As illustrated in Figure 2.15, shoulder azimuth angle shows as a function of target azimuth for the far (a) and near (b) reach distances. It has a quasi linear increase with target azimuth. On the other hand, shoulder elevation angles seem to remain the same regardless of the target azimuth ($p = 0.15$). Regardless of target azimuth, the magnitudes of elbow extension angles are significantly larger for the far than the near set ($F = 17.58$, $p < 0.01$) with values of 144° and 111°, respectively; while shoulder elevation remain about the same for both reaching distances. Furthermore, the final arm posture, as

indicated by the elbow angle, is straighter for reaches to the right than the left region, with an average terminal angle over all subjects of 129° and 117°, respectively.

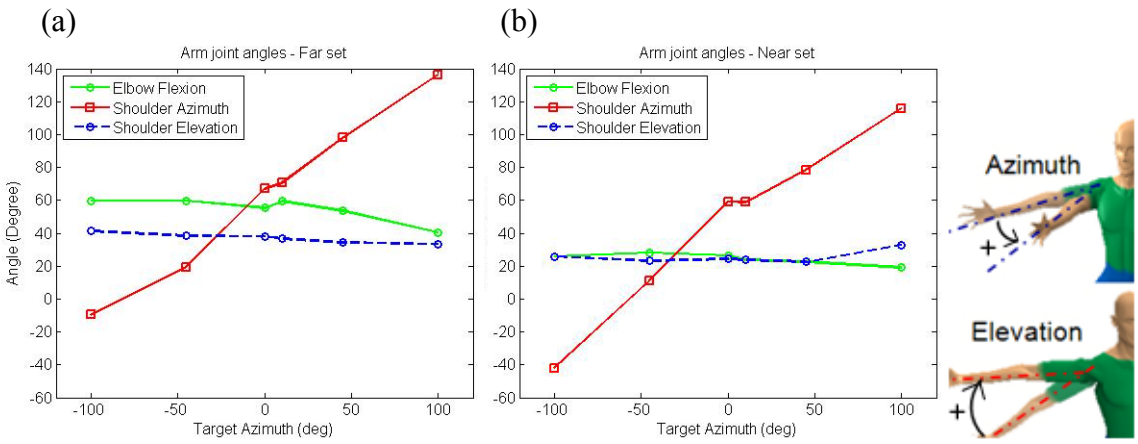

Figure 2.15. Arm joint angles with respect to reaching azimuth angles. a) Far; b) Near set

2.4.4 Relationship between gaze and body segment initiation - Initiation timing and sequencing

To determine an association between visual feedback and phase transition, the timing of body segment movement initiation relative to the time at which the target entered the foveal field of view was computed. A 2-way ANOVA determined the main and interaction effects of target azimuth and distance for each joint angle of the arm (elbow extension, shoulder azimuth, and shoulder elevation) and torso angle (axial rotation, lateral bending, and flexion). The results of these analyses are presented in Table 2.9. Figure 2.16 to Figure 2.18 show the initiation timing of each joint relative to gaze-on-target time for each target location (see Figure 2.3a for target identification).

Table 2.9. ANOVA table of the joint initiation timing analysis

Torso joints	Axial Rotation			Lateral Bending			Anterior Flexion		
	DoF	F	p	DoF	F	p	DoF	F	p
Azimuth	5	3.41	< 0.01	5	1.77	0.12	5	5.88	< 0.01
Distance	1	1.83	0.18	1	2.92	0.09	1	4.05	0.05
Azim. × Dist.	5	0.83	0.53	5	0.47	0.80	5	0.31	0.90

(Shaded cells correspond to significant values.)

Arm joints	Elbow extension			Shoulder azimuth			Shoulder elevation		
	DoF	F	p	DoF	F	p	DoF	F	p
Azimuth	5	10.32	< 0.01	5	5.56	< 0.01	5	6.17	< 0.01
Distance	1	3.2	0.08	1	7.58	< 0.01	1	0.8	0.37
Azim. × Dist.	5	1.03	0.40	5	1.72	0.13	5	1.16	0.34

(Shaded cells correspond to significant values.)

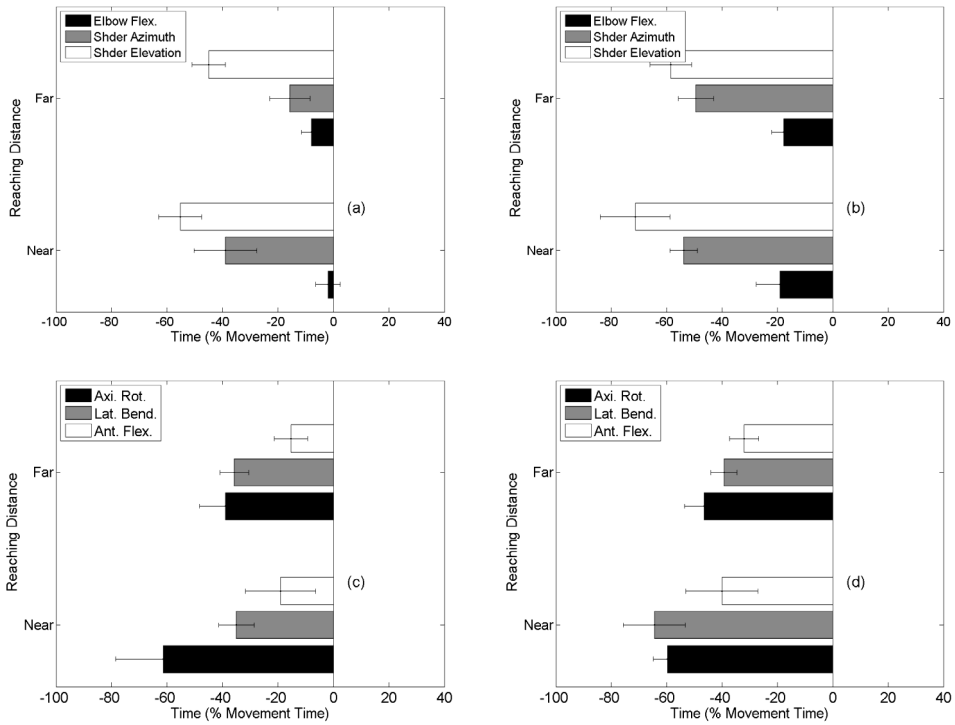

Figure 2.16. Joint angle initiation timing of rear reach (a) right side (F & N1), (b) left side (F & N6)

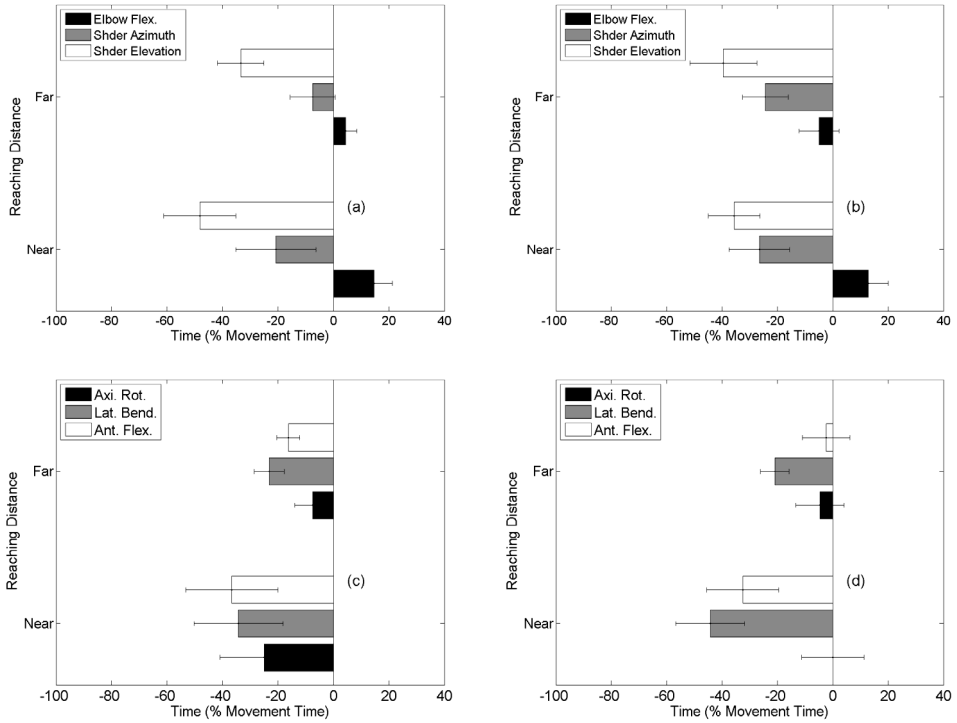

Figure 2.17. Joint angle initiation timing of front 45º reach (a) right side (F & N 2), (b) left side (F & N 5)

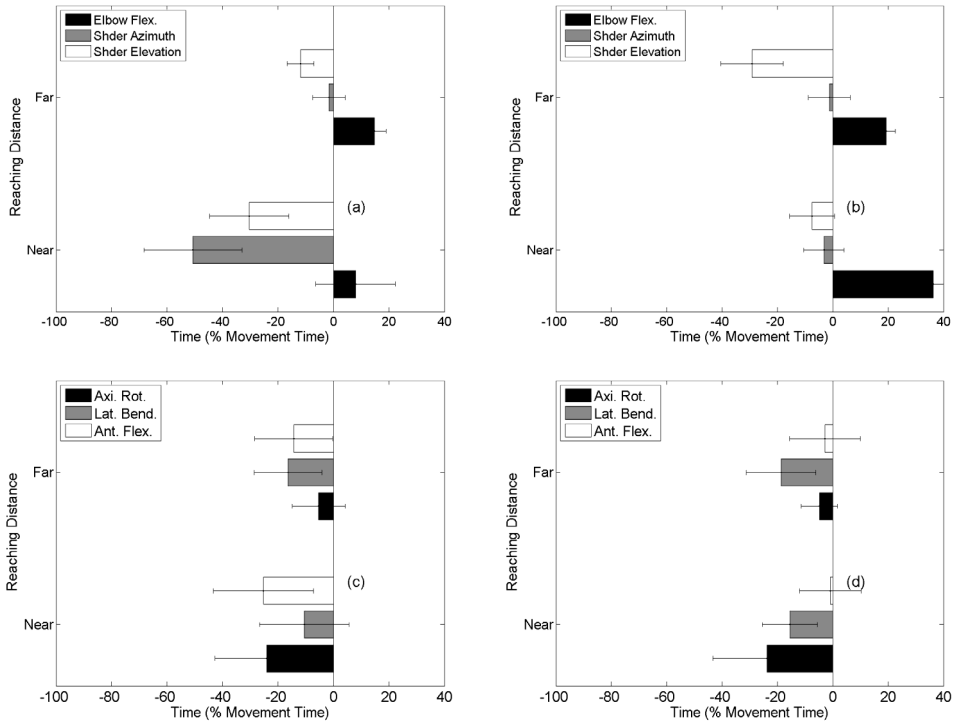

Figure 2.18. Joint angle initiation timing of front reach (a) 0º front (F & N 3), (b) 10º front (F & N 4)

Arm joint angle initiation timing

The initiation timings for all three arm joints were significantly advanced with the eccentricity of target azimuth ($p < 0.01$). Except shoulder azimuth ($p < 0.01$), reaching distance has no significant effect on arm joint initiation timing. There is no evidence of an interaction effect between azimuth and distance for all arm joint angles as indicated by p values 0.40, 0.13 and 0.34 for elbow extension, shoulder azimuth and elevation angle, respectively.

As shown in Figure 2.16 to Figure 2.18, the initiation sequence of arm joint angles is a function of target azimuth, but not related to target distance in general. Generally, the movements of the shoulder and elbow joints were initiated earlier for the rear and left reaches than the medial and right reaches. Arm joint angles (upper panels in Figures) were initiated in a sequence of shoulder elevation, shoulder elevation and then elbow extension in general. In other words, the initiation of shoulder joint is prior to elbow.

Torso angle initiation timing

As the ANOVA results show in Table 2.9, the initiation timings of torso axial rotation and flexion are significantly influenced by the target azimuth; while those for torso lateral bending show no difference with target azimuth. However, the comparisons with HSD for the torso axial rotation shows that only the reach to rear left has significant difference from the medial reaches (0º front and 10º left) in the initiation timing of torso axial rotation. And there is no significant difference between far and near set for the axial rotation. Therefore, the average initiation timing would be used for all frontal reaches as 23% of MT before GOT for the both far and near reaches. The average initiation timings for rear left and rear right are 51.9% and 35.4% of MT before GOT.

The initiation timing of torso lateral bending has no significant changes with target azimuth and distance. Hence, the average initiation timing of 19.8% of MT before gaze for all reaches.

For the torso flexion, the HSD shows that the initiation timing of the frontal reaches are significantly different from rear reaches for both near and far set. There is no significant difference among frontal reaches, neither between two rear reaches. Therefore,

average values of 5.6% and 18.2% of MT before GOT was obtained for the initiation timings of the far and near frontal reaches, respectively. Between the rear reaches, the initiation timings are 42.7% and 60.5% of MT before GOT for the far and near set, respectively.

Overall, the initiation timing related to GOT for each torso angle was determined empirically as a function of target location. The results are summarized in Table 2.10. The negative sign stands for the initiation is prior to GOT.

Table 2.10. Torso initiation timing

	Rear left			Frontal (45º left – 45º right)			Rear right		
% MT	AR	LB	AF	AR	LB	AF	AR	LB	AF
Far	-51.9%	-19.8%	-42.7%	-23%	-19.8%	-5.6%	-35.4%	-19.8%	-42.7%
Near			-60.5%			-18.2%			-60.5%

AR: Axial Rotation; LB: Lateral Bending; AF: Anterior Flexion

2.5 Discussion

In the context of this experiment, it was observed that visual acquisition of the target occurred before the head moved for the medial target (target location 3) and thus visual information about the target location can be used to guide the reach movements. In addition, visual fixation to the target may occur earlier than the achievement of final position of the head. Based on the results, it is suggested that information about the eye movement is required to precisely study the relationship and coordination between visual feedback and body segment movement.

In this chapter, the kinematics and movement characteristics of the end effector and body segments represented by the joint angles during reaching tasks were presented. While the hand moves mostly in a vertical plane, the hand trajectories were reported as approximately straight lines in the horizontal plane, and significantly curved in the vertical direction, as found in other studies as well (Hore et al., 1992, 1994; Miller et al., 1992; Wolpert et al., 1994; Gielen et al., 1997).

The joint movements are context dependent (target azimuth and distance). Furthermore, the initiation of joint space angles was all in advanced of the timing of

gaze-on-target. It also shows a dependency on reaching context. The empirical results including torso and arm joint angular displacement magnitudes, initiation time of torso and arm joints, and the time delay between the eye-on-target and the initiation of reach movements are to be used in the development of the coordination model presented in Chapter 6.

2.5.1 Trajectory of the end effector

For unconstrained reach movements, the results of the hand trajectory exhibit the same behavior – a mostly planar traveling path - as suggested earlier (Georgopolous et al., 1981; Abend et al., 1982) for targets beyond the frontal plane focusing on the hand movement only. However, for targets behind the frontal plane (rear targets) the trajectory is no longer planar and is more variable. These results may reflect the increase in degree of freedom (DOF) to be controlled due to the recruitment of a larger number of joints and thus a more complex arm-torso coordination (Soechting et al., 1995; Admiraal et al., 2004).

When comparing the results for the far and near set, it was found that hand trajectory deviation from a straight line is greater for near than far targets regardless of the reaching direction (azimuth). Since the magnitudes of the overall joint angular displacements (i.e. torso and arm joints) are lower for the near reaches than the far reaches, the smaller displacement may contributes to a higher curvature in the hand trajectories. This result may reflect, for short traveling distances, a central control trade-off between complex coordination to achieve a straight line and simpler control with small angular displacements leading to a curved trajectory. Even though curvatures differ between the near and far reaches, the results show that the trajectory of the hand during a reach movement is consistent from trial to trial both within subjects and across subjects (Georgopolous et al., 1981; Soechting & Lacquaniti, 1981). This suggests that reach movements may be planned at a kinematic level and a pre-planned scheme may exist to yield consistency in unconstrained reach movements.

2.5.2 Kinematics of body segments

As shown in Figure 2.10, the magnitude of elbow extension differs between the near and far set of targets as expected from the difference in reaching distance. In addition, the end postures relative to the reaching direction can be divided between reaches to the right and left of the sagittal plane according to the joint conformation. Elbow extension is significantly larger when reaching to the right than to the left region. This feature is illustrated in Figure 2.15 for both reaching distances. It may relate to the self-interference of body segments when reaching to the left and joint ranges of motion with comfort.

Furthermore, the orientation of torso axial and shoulder rotation in the end posture are consistent with the target azimuth. Both joint angles are quasi-linear functions increasing with the reaching azimuth (Figure 2.15). It has been proposed that torso movements might be influenced by joint ranges of motion, especially at the shoulder (Reed et al., 2004). However, torso axial and shoulder axial rotations are both recruited, although not necessary, to accomplish reaches for slightly eccentric targets (such as 10º left and 45º right) which are within the shoulder rotational range of motion. This indicates that shoulder and torso contributions must be coordinated as a function of reaching direction. Hence, the recruitment of the shoulder and torso should be included in a coordination model.

Torso anterior flexion movements are observed to decrease with eccentricity of the far targets (rear right and left) (Figure 2.14). For the medial target locations (0 º front and 10º left), the torso forward bending increase about 10º more for the far than the near reaches. On the other hand, torso lateral bending is highly correlated with the laterality of frontal targets (45º right and left). These results and the indication of torso axial rotation as a function of target azimuth, suggest that torso movements are necessary to extend the reach distance and compensate the limitations in direction and distance of the range of motion of the arm alone.

Shoulder axial rotation varies with azimuth suits the purpose of reaching direction. However, the shoulder elevation angle does not vary significantly with azimuth for both far and near targets. The displacement magnitude is similar for the same target distance except for reaching to the near rear left target. This might be expected since torso lateral

bending is less in the direction of the target in that case. Shoulder elevation might be therefore increased to avoid the discomfort induced by torso/arm self-interference and to facilitate the pick-up of the push pin with the hand. This is in accordance with a previous result that the hand posture for grasping (supination/pronation) may alternate the arm joint rotation (Roby-Bami et al., 2003). These angles adjustments illustrate the assistance of the chain of links to the end effector trajectory, as proposed by Bernstein (1967).

Reaching distance. The elbow extension is larger for the far than the near reaches, as indicated above. A greater shoulder azimuth angle (more counter clockwise shoulder axial rotation) may be induced by the greater elbow extension for far reaches. For the near reaches, reaching length should be already integrated by the CNS so the torso should not move if energy was optimized. However, some joints may need to move much (e.g. 100º right for the shoulder azimuth) relative to their range of motion to accomplish a task and it may not be comfortable as it may stretch too much on some shoulder muscles. So a compromise is made to move the torso. On the other hand, since the peripheral visual feedback is not accurate enough for movement correction or the range of motion for the head-eye system does not cover the visual need for eccentric targets, the subject has to moves the torso during the movement to compensate for the distance and orientation.

Control mode transition. A movement feature change might be expected when the movement control mode changes. From this perspective, angular movements of the elbow, shoulder azimuth and elevation were plotted in the joint space, together with the superimposed indication of gaze-on-target (GOT) (Figure 2.19**Error! Reference source not found.**). The corresponding graph shows that the joint space curve presents a significant change after GOT. This indicates that GOT might serve as a good indicator for movement control mode transition. This is in agreement with the assumption that a directional movement requires a precise spatial /mapping of the target location.

Figure 2.19. Example of arm joint angles in the joint space when reaching to the rear right target.

Furthermore, the use of an egocentric or exocentric coordinate system for the elaboration of reach movements is still debated. It has been proposed that the CNS may switch from one system to the other during the movement as a function of the context or the availability of spatial information used to calibrate the egocentric system (Kim, 2005). Present results support the utilization of both coordinate systems during a movement. The planning strategy may be inferred from the joint space plot (Figure 2.19). The trajectory represented in the joint space shows a significant change in direction when the precise spatial location of the target is determined by visual feedback. It is suggested that the joint space coordinate system (egocentric system) based on muscle proprioception might be first adopted at movement initiation when the target space is not completely calibrated by visual information, and then transforming to the target space system (exocentric system) when visual feedback provides the localization of the target in the extra-corporal space. This is also in agreement with previous studies suggesting that this coordinates transformation corresponds to a visually derived representation of target location (Andersen, 1987; Soechting & Ross, 1984; Soechting et al., 1989).

2.5.3 Initiation of joints – Sequencing of body segment movements

The movement phase transition may depend on the availability of visual information and its content. Hence, the timing of gaze on target (GOT) was used as an indicator of this transition. If an arm joint angle is initiated before GOT, the initial mode of control for the hand movement is likely to be under feed-forward (open-loop) control or mainly using proprioceptive feedback; however, it is generally recognized that the initial control of a reaching movement is based on a feed-forward control mode, generally followed by a feedback control mode. The movement phases before and after GOT are denoted the lift-off and transport phases since the directional movement can only be made after GOT to obtain the target spatial information.

It has been reported that torso angular movements are initiated almost simultaneously with upper limb joint movement, but usually do not end at the same time during a reach (Paillard & Amblard, 1985; Jeannerod, 1988). This characteristic is in agreement with the hypothesis of a multi-phasic composition of multi-link movements based either on an elaborate motor program and/or online adjustments based on visual information. For both near and far rear reaches shown in Figure 2.16, arm joint movements are initiated before gaze reached the target, and hence before acquiring precise visual information. This behavior suggests a movement preparation phase (lift-off phase), which is probably used to refine the motor program and activate the muscles to facilitate the access of the movement command to the motor neurons (Desmurget & Prablanc, 1997; Brown & Cooke, 1981) and thus reduce the overall movement duration. In addition, the time profile of gaze orientation reveals that "searching" was involved when reaching to rear targets. These results indicate that the precise target location information does not account for the joint initiation and strongly support an initial open-loop control of the movement. This strategy may be a general characteristic of human movement behavior since in the present context movement time was not constrained.

Regardless of reaching direction, the movements of the elbow were initiated significantly earlier ($p<0.01$) for the near than the far reach (Figure 2.16 to Figure 2.18). As shown in Table 2.9, the initiation timing depends significantly on the reaching direction for frontal reaches (45º right to 45º left). Among the frontal reaches, the activation timing of body segments have similar pattern for the left-hand side reaches

with the same distance (far or near). Furthermore, the duration of the lift-off phase (before GOT) seems to be shorter for reaches to medial (Figure 2.18) than reaches to eccentric targets (Figure 2.17). This might be due to the smaller eccentricity of the medial targets and their easy access locations which are close to the initial visual field of view.

CHAPTER 3

Temporal Aspects of End Effector and Eye-hand Coordination

3.1 Abstract

Temporal aspects of reach movements, such as movement time and time to peak velocity of the end effector, as well as time variations of gaze orientation associated with the visual acquisition of targets, were investigated. Reach movements with different requirements were conducted to collect the eyes and hand movements simultaneously. The time to peak velocity (TP) and total movement time (MT) of the hand were computed. The timing of the gaze-on-target (GOT) was quantified with respect to the total movement time. The result shows that the time to peak velocity reveals a movement scaling property in the context of self-imposed movement speed. In addition, both movement time and the proportion of the initial (lift-off) phase, which is defined by the timing of GOT, vary with target location (azimuth and distance). Variation of the peak velocity is also found to be a function of target location. Peak velocity and the proportion of the lift-off phase as a function of target azimuth were represented by a quadratic regression model. The temporal scaling effect was identified in the TP/MT ratio and the lift-off phase was found to be in proportion to the total movement time.

3.2 Introduction

Coordination of human movements is assumed to be characterized by three aspects including timing, phase changes and body segment kinematic interaction. Movement coordination is also associated with movement control (Rosenbaum et al., 1995; Admiraal et al., 2004). Furthermore, reach coordination also includes the

consideration of the head movements since they are modulated by the movement of the whole body and the hand (Delleman et al., 2001; Tipper et al., 2001; Kim, 2005, Kim et al. 2007; Kim et al. 2009). Since the early initiation of the gaze with respect to the hand has been generally observed (Carnahan & Marteniuk, 1991; Fuller, 1992; Helsen et al., 2000; Flanagan & Johansson, 2003), reach movement models shall include the temporal characteristics of gaze and its corresponding head movement as well as the interaction between gaze and hand movement.

As stated in section 1.2, the multi-phasic movement model of reach, which includes three movement phases – the lift-off, transport, and landing – were hypothesized to be determined by the content of visual feedback information. In this study, the lift-off phase is assumed to be the period during which the exact spatial information about the target has not been perceived by the CNS. When the eyes acquire the target, the corresponding spatial information is obtained by the CNS. Hence, it can be expected that the lift-off phase spans from the initiation of a reach movement to the moment at which gaze is aligned with the target azimuth.

Using this definition, the temporal characteristics of the lift-off phase were quantified. This work investigates the correlation of eye and hand movements to address their coordination and the role of visual feedback in reaching movements. A motion tracking system and an eye tracking system were used synchronously to record the displacement of selected body landmarks and the eyeball.

3.3 Methods

3.3.1 Participants

Eight young adults (three females and five males) participated in the experiments. Participants had an average age of 27 years and an average stature of 1.78 m. Measured from the acromion to the tip of the index finger when the elbow is fully extended, their average arm reaching length was 65.8 cm. All participants were right-handed and free from any neuromuscular disorders. All signed an informed consent for participation in an experiment approved by the internal review board of the University of Michigan.

3.3.2 Experimental setup

Twelve targets were distributed along horizontal concentric circles centered at the right shoulder (Figure 2.3a) with an elevation corresponding to elbow height. The targets were divided into two groups, near and far, as a function of their distance from the shoulder. Radii (distances) for the near and far group corresponded to 80% and 120% of arm reaching length, which is defined as the distance between the acromion and the tip of the index finger when the elbow is fully extended.

Eye movements were recorded by an Eye Tracking System (ASL Eye-Trac®) to determine the direction of gaze during each movement (see section 2.3.4). Whole-body movements were recorded and quantified by an infrared motion tracking system including eight cameras (Qualysis® ProReflex 240-MCU). Twenty-two retro-reflective markers were placed on selected body landmarks (Figure 2.3b). Both movement tracking systems were synchronized to sample data at a rate of 60Hz.

3.3.3 Experiment design

After measuring and recording anthropometric data including stature, reach length, seat height, elbow height and shoulder height when seated, target locations were determined and set accordingly.

The eye tracking system was placed onto the subject's head and carefully calibrated to obtain an accurate direction of gaze. Then retro-reflective markers were placed on the subject (Figure 2.3b) and a digitization procedure was executed to define the location of additional body landmarks such as the eyes and the low back (L5/S1) with respect to the optical makers around them. The location of digitized points and digitizing procedures were as stated in chapter 2 (Reed et al., 1999; Kim, 2005).

Each participant was instructed to reach at a comfortable self-imposed pace each target, presented in a random order. Each trial (movement to a target) started from an initial posture in which the elbow angle was 90° with the hand is on a given starting point while the eyes fixate a reference visual target placed at eye level in the mid sagittal plane. For each trial, the target to be reached was visually indicated by an illustration of the reaching environment on a panel placed in front of the subject beyond the reach

destination. The subject was also instructed to return to the initial posture and gaze after each reaching movement.

The procedures were reviewed and approved by the University of Michigan Health Sciences Institutional Review Board for compliance with appropriate guidelines, state and federal regulations.

3.3.4 Data processing and analysis

The linear velocity of the end effector and the peak value for each trial was computed off-line. The displacement of the hand during reach movements was represented by the wrist displacement in order to rule out the randomness and inconsistency of the unintended wrist motion. Velocity in the horizontal plane was computed as the resultant velocity of X and Y directional components.

The approach in this study was intended to facilitate the integration of the current data into real time simulation models. Hence, in this chapter, two temporal aspects were investigated. The duration of the lift-off phase is approached from the real time unit (i.e. in second) perspective and its relationship with the end effector traveling distance, which corresponds to the horizontal displacement of the hand.

Duration of the lift-off phase was normalized as a percentage of the total movement time of the hand in order to facilitate comparisons and to eliminate the effect of the randomness in movement speed. The hand traveling distance during the lift-off phase was also normalized by the total hand traveling displacement (in the horizontal plane). This fractional hand traveling distance was used as another dimension to be quantified for the lift-off phase.

Focusing on the hand movement, a repeated measure analysis of variance (ANOVA) was used to determine main effects of target azimuth and distance and their interactions on movement time, peak velocity, and time to peak velocity for the end effector, and hand fractional traveling displacement and duration for the lift-off phase.

3.4 Results

3.4.1 Peak velocity and movement time of end effector

Table 3.1 shows the results from the two-way ANOVA. The peak velocity is significantly influenced by target azimuth and distance. In addition, the interaction between these two factors is also significant.

Table 3.1. ANOVA table of the horizontal peak velocity

	DoF	F	p
Azimuth	5	54.41	< 0.01
Distance	1	24.03	< 0.01
Azim. × Dist.	5	1.56	0.006

(All entries are significant.)

As shown in Figure 3.1, the peak velocity of the hand in the horizontal plane shows the same tendency for the far and near sets of reaches. The distribution of peak velocity magnitudes is a function of target azimuth and distance. For the same reaching distance, the peak velocity was significantly greater for rear than the front reaches ($p<0.01$). In addition, the peak velocity tends to be slower for the medial than eccentric targets. When comparing the near and far set, the peak velocity for the 0 and 10 degree front reaches is significantly slower for near than far reaches ($F = 10.23$, $p < 0.01$). Furthermore, variability of the peak velocity is significantly larger ($F = 4.99$, $p = 0.028$) for the far than near set of targets. Since movement time was not constrained the between subject variability was not negligible.

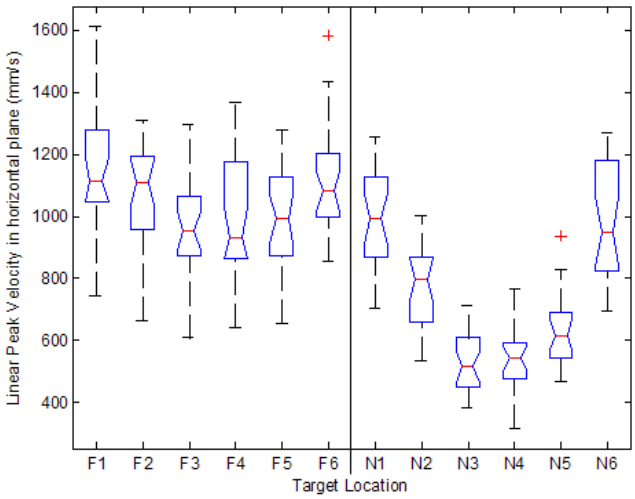

Figure 3.1. Box plot for peak horizontal velocity of the end effector. The left and right panels correspond to far (Fi) and near (Ni) reaches, respectively.

To describe variations in peak velocity as a function of reaching direction, a 2nd order regression was used to model their relationship (Figure 3.2). The following equations represent these variations for far and near targets, respectively:

$$V_p^{Far} = 0.0136\theta^2 - 0.3361\theta + 992.27$$
$$V_p^{Near} = 0.0424\theta^2 - 0.3252\theta + 569.11 \qquad \text{(Eq. 3.1)}$$

where θ represents the target azimuth angle (in degree). The coefficients of determination (R^2) for the far and near group are 0.90, 0.93 respectively.

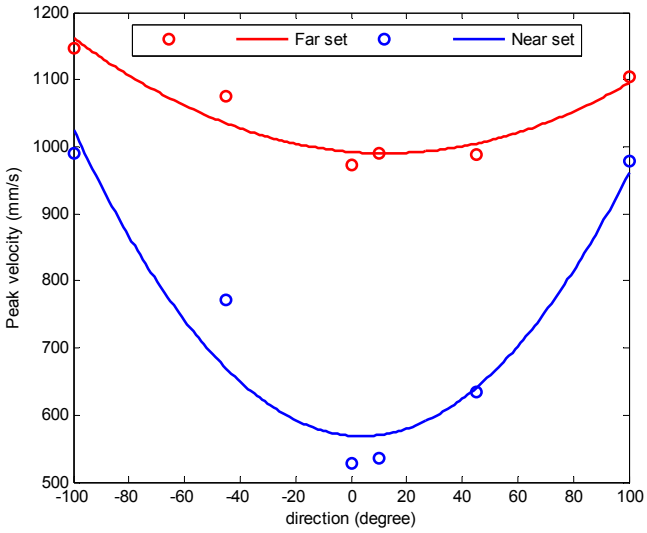

Figure 3.2. Estimated peak velocity, with respect to direction for each target distance, derived from quadratic regressions

The time to peak velocity (TP), which corresponds to the movement acceleration phase, relative to the total movement time (MT) is consistent across reaching distances. The ANOVA shows the MT and TP were not significantly affected by target azimuth for the frontal reaches ($p = 0.38$). As shown in Figure 3.3, the MT and TP are significantly greater ($p < 0.05$) for far than near targets. However, the ratio of time to peak velocity over movement time (50%) is not significantly different ($F = 20.95$, $P < 0.01$) between near and far targets. These results strongly support movement scaling (Plamondon et al., 1995; Grinyagin et al., 2005) for unconstrained movements.

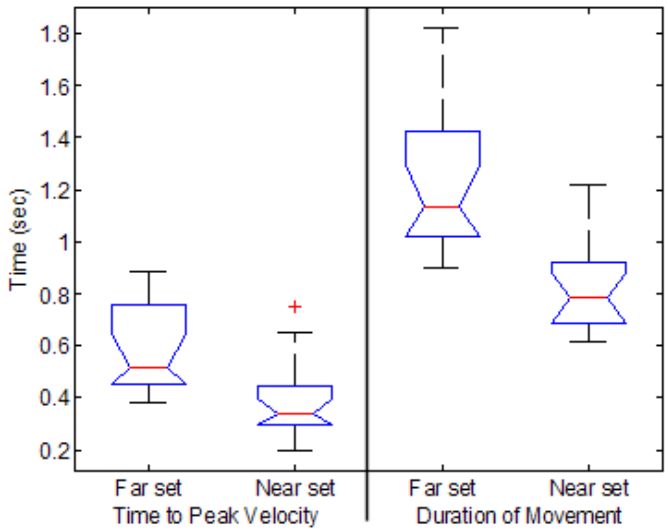

Figure 3.3. Box plot of time requirements with respect to distance

3.4.2 Duration of the lift-off phase

The duration of the lift-off phase, which corresponds to the period preceding the visual acquisition of the target, was quantified as function of target azimuth and distance to determine whether movement scaling properties also applied to this phase.

The two-way ANOVA indicates that azimuth and distance have a significant influence on the lift-off phase duration (Table 3.2), as the p values are both less than 0.01 for these factors. However, their interaction is not significant ($p = 0.56$). The results indicate that the duration of the lift-off phase has a stronger dependence on target azimuth than distance. The standard deviations for each type of reach are similar ($p = 0.02$). When comparing the near and far reaching to the same azimuth direction, the phase duration

difference between the far and near set is not significant except the pair for the rear left and 45° right reach.

Table 3.2. Statistical results for the proportion of lift-off phase duration relative to the total movement time as a function of target azimuth and distance.

% MT	Rear Right	45º Right	0º Front	10º Left	45º Left	Rear Left	$F_{5,138}$
Far sets	42.9 ± 1.8	19.5 ± 2.8	6.9 ± 4.2	7.3 ± 2.5	18.8 ± 2.6	44.8 ± 1.7	37.59*
Near sets	44.3 ± 2.5	31.4 ± 3.7	11.6 ± 2.8	11.4 ± 3.1	24.3 ± 5.9	55.2 ± 2.5	23.81*
$F_{1,46}$	0.19	6.58	0.87	1.05	0.74	11.51	*p<0.01
P value	0.6635	0.0149	0.3564	0.3129	0.3955	0.0018	

(Shaded cells correspond to significant values.)

As illustrated in Figure 3.4, the lift-off phase is longer for the near than far reaches. The relative duration of the lift-off phase (% of MT) increases with target eccentricity from the mid-sagittal plane.

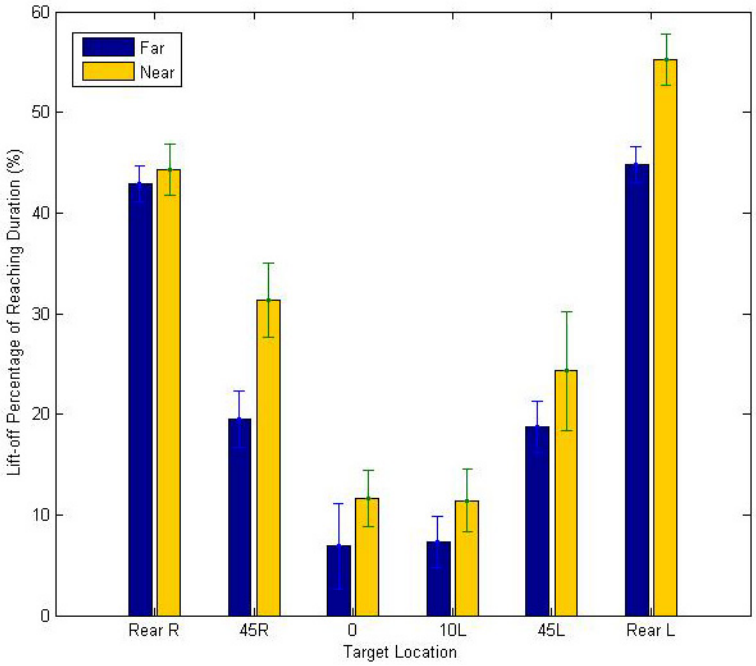

Figure 3.4. Relative duration of lift-off phase as a function of target azimuth and distance

Temporal modeling for the lift-off phase

Given the trend of the lift-off phase portion in the full reach relative to the target azimuth shown in Figure 3.4 and Figure 3.6, a parabolic curve may be used to estimate

the relationship between the lift-off phasic portion and target azimuth in terms of real time unit or hand traveling distance.

First, the lift-off phase portion with respect to the total reaching duration is taken into consideration. To describe variations in the lift-off phase temporal percentage as a function of reaching direction, a 2nd order regression was used to model the relationship as shown Figure 3.5.

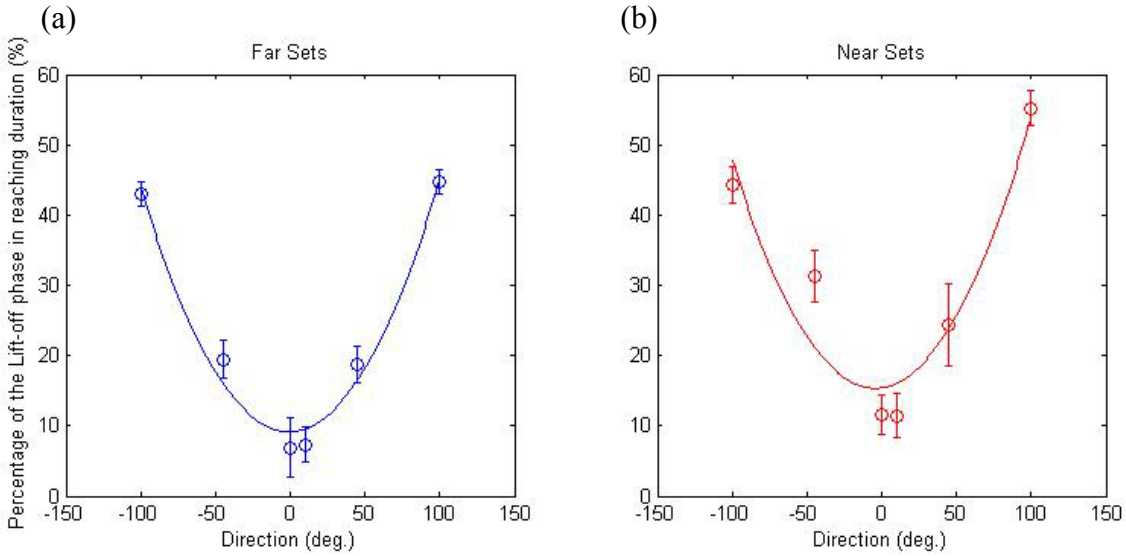

Figure 3.5. Curve fitting for the percentage of lift-off phase in reaching duration as a function of the target azimuth. a) Far sets; b) Near sets.

Derived from the 2nd order regression in a least square sense, the following equations represent these variations in the duration of the lift-off phase for far and near targets, respectively:

$$P_t^{Far} = 0.0035\theta^2 + 0.0055\theta + 9.16$$
$$P_t^{Near} = 0.0035\theta^2 + 0.0302\theta + 15.42 \qquad \text{(Eq. 3.2)}$$

where θ represents the target azimuth angle (in degree). The coefficients of determination (R^2) for the far and near group are 0.98 and 0.90 respectively. The vertexes of these two parabolic models are located at $\theta \approx 0.8^\circ$ and $\theta = 4.3^\circ$ for the far and near set, respectively. The magnitudes of the vertexes are 9.16% and 15.4%

3.4.3 Hand traveling distance of the lift-off phase

As shown in Figure 3.6, the hand traveling distance during the lift-off phase relative to the total reach distance also shows a parabolic relationship as a function of target azimuth (Figure 3.4).

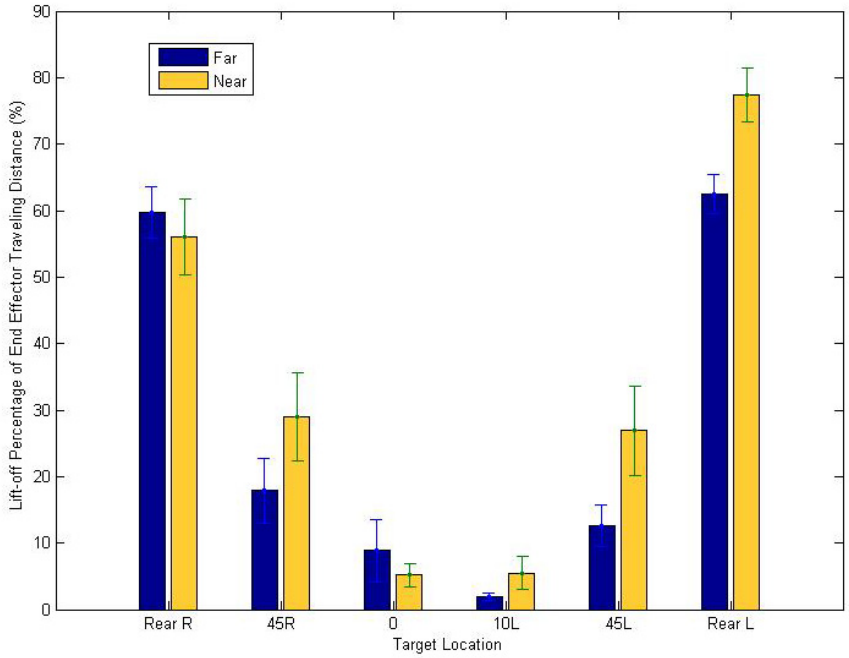

Figure 3.6. Fractional hand traveling distance of the lift-off phase as a function of target azimuth and distance.

The two-way ANOVA indicates a significant difference in fractional hand traveling distance for target azimuth and distance ($p < 0.05$) with F ratios of 80.48 and 1.68 respectively. There is no interaction between these two factors ($F=1.93$, $p = 0.09$). It also indicates that the traveling distance of the lift-off phase has a stronger dependence on the target azimuth than distance. Variation among subjects is relatively small in general. The proportion of hand traveling distance during the lift-off phase exhibits a significant difference between the far and near reach set.

Table 3.3. Percentage of lift-off phase in hand traveling distance with respect to target azimuth and distance

%	Rear Right	45º Right	0º Front	10º Left	45º Left	Rear Left	$F_{5,138}$
Far sets	59.8 ± 3.8	17.9 ± 4.9	8.9 ± 4.6	2.0 ± 0.5	12.6 ± 3.2	62.5 ± 2.9	53.9*
Near sets	56.1 ± 5.8	29.0 ± 6.7	5.2 ± 1.7	5.5 ± 2.5	26.9 ± 6.8	77.4 ± 4.0	32.91*
P value	0.5973	0.1876	0.4653	0.1862	0.0655	0.005	
$F_{1,46}$	0.28	1.81	0.55	1.82	3.62	9.03	*p<0.01

(Shaded cells correspond to significant values.)

Fractional hand traveling distance modeling for the lift-off phase

The lift-off phase portion of the total hand traveling distance is modeled by a 2nd order regression. Variations in hand travel during the lift-off phase expressed in percent of the total hand traveling distance was described as a function of target azimuth for each distance, as shown Figure 3.5 and Eq. 3.3.

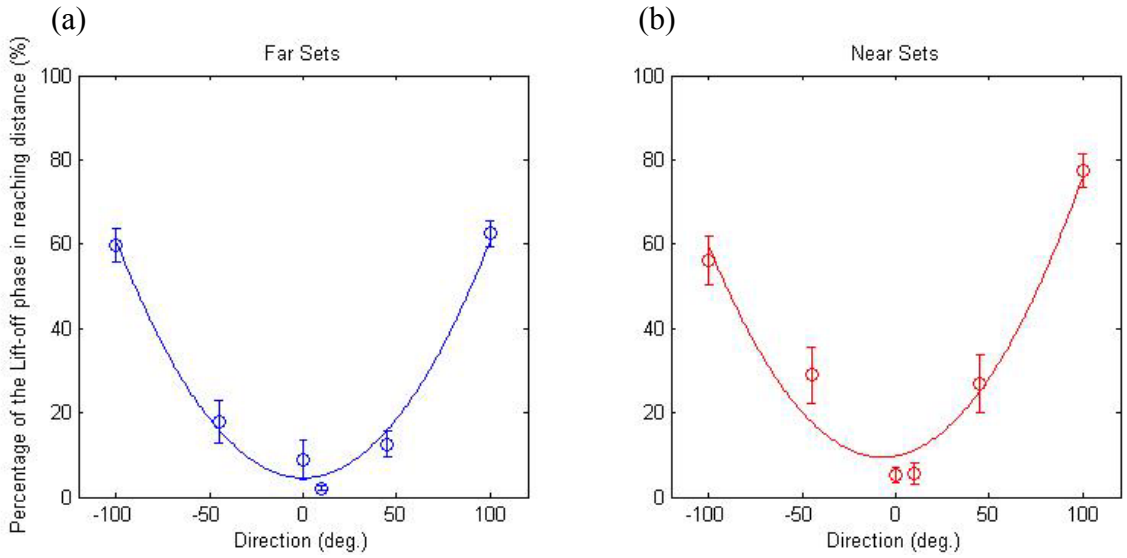

Figure 3.7. Curve fitting for the percentage of hand travel during the lift-off phase as a function of target azimuth. a) Far sets; b) Near sets.

$$P_d^{Far} = 0.0056\theta^2 + 0.0001\theta + 4.56$$
$$P_d^{Near} = 0.0058\theta^2 + 0.0823\theta + 9.76 \quad \text{(Eq. 3.3)}$$

where θ represents the target azimuth angle (in degree). The coefficients of determination (R^2) for the far and near group are 0.99 and 0.95 respectively. The vertexes of these two

parabolic models are located at $\theta \approx 0$ and $\theta = 7.1^{\circ}$ for the far and near set, respectively. The magnitudes of the vertexes are 4.6% and 9.7%

3.5 Discussion

3.5.1 Temporal scaling

From the temporal perspective, the present results suggest that kinematics of the end effector during an unconstrained reaching movement can be estimated from target distance and azimuth relative to trunk orientation. The TP/MT ratio is approximately 0.5 regardless of reaching distance (Figure 3.3). The comparison of the TP/MT ratio for near and far distance strongly indicates that reaching movement may be scaled for different hand traveling displacement, which is in agreement with previous results (Magescas et al., 2006; Wallace et al., 1990). Due to the temporal coupling effect between the MT and TP, the present results suggest that kinematics of the end effector during an unconstrained reaching movement can be estimated from target distance. Additionally, it has been reported that the velocity of wrist and finger aperture shows the same kinematic scaling factor in reach-to-grasp movements (Castiello, 1996; Jakobson & Goodale, 1992). This suggests that the kinematic scaling can be effectively apply to other body segments, such as torso or arm joint within a given temporal coordination scheme.

Furthermore, the peak velocity shows a dependency on target location. The peak velocity is slower for near than far targets and slower for medial targets close to the sagittal plane than more eccentric targets (Figure 3.1). For each target azimuth, the average peak velocity ratio between the far and near reaches is about 0.6 which corresponds to the target distance ratio (0.8/1.2 = 0.67 arm length). This suggests that the movement plan might be pre-planned and scaled to fit a specific need. In Eq. 3.2, the proportion of the lift-off phase is described as a function of target location. The average ratio of lift-off proportion between the near and far set is also about 0.6. The combination of results concerning the target dependency of the peak velocity and phase duration suggests that the relative contribution of feed-forward and feedback control modes may follow the same pattern. Based on the kinematic scaling and the composition of the control mode in reach movements, it may be assumed that transition to the slower

feedback control mode may be initiated sooner for close and central targets as the hand enters sooner the visual field of view for these targets.

Given the 2nd-order regression models for estimation of end effector horizontal peak velocity (Eq. 3.1) and the constant TP/MT ratio, the temporal aspect of reaching movements performed at self-imposed speed may be modeled dynamically for targets located within the reach envelope. These results also provide a foundation to model the time requirements (e.g. duration, acceleration time) using bell-shaped velocity profiles associated with feed-forward control (Flash et al., 1985).

The peak velocity models show a more pronounced effects of target azimuth for the near than far targets. In addition, the hand velocity is similar for eccentric near and far targets. Since the targets were centered about the shoulder vertical axis and not the head, the left target should appear closer than the right target. Similar peak velocity for both side imply that the egocentric coordinate system may be centered at the shoulder. Alternatively, the determination of movement kinematic may rely more on a low level control related to the musculoskeletal system than the CNS (Winter, 2005). Furthermore, the hand velocity is much greater for the most eccentric targets than the medial targets for the near set. Despite the absence of explicit constraint on movement speed, higher movement velocity for the more eccentric targets might be preprogrammed to maintain a similar total movement time for all targets. This result indicates that the open-loop control mode of the movements is largely preprogrammed as a function of target azimuth. Hence, it is hypothesized that the programming of movement velocity may be derived from both the visual information and the necessary time to acquire that visual information.

3.5.2 Lift-off phase

As illustrated by Figure 3.4 and Figure 3.6, the lift-off phase is longer for eccentric than the medial reaches. This might result from the expectation and pre-mapping for the reaching environment with a graphical instruction cue for each reaching trial. However, the precise spatial relationship between the subject and the target can only be dependent on visual information. Thus, the timing of the transition between the two initial movement phases (lift-off and transport phase) might depend on the timing of spatial mapping.

The empirical models expressed in Eq. 3.2 and Eq. 3.3 indicate that the lift-off phase proportions of the total movement time and hand traveling distance are both functions of target location. The coefficients of the 2nd order term (θ^2), which represents the curvature, are similar for the far and near targets. These coefficients are approximately 0.0035 and 0.0057 for the phase duration and fractional hand traveling distance, respectively. The vertex of the curve was slightly different for the far and near set with respect to target azimuth. Since the models look alike, it suggests common properties and that a generic movement pattern scaled for time, distance and orientation may be used for these reaches. This scaling property significantly simplifies the programming of movements and their simulation. The ratio of the vertex magnitude in the MT domain is about 0.6, which is close to ratio of target distance (0.67), which further supports the scaling effect. The results presented in this chapter provide information about the duration of the lift-off phase and hand traveling distance during that phase which will be used for defining the temporal aspect of the coordination model of reach movements presented in Chapter 6.

CHAPTER 4

Elbow Swivel Angle Modeling During Visually-Guided Reach Movements

4.1 Abstract

Reducing degree-of-freedom (DoF) redundancy is a major issue for human movement simulation. To address this issue in the case of reaching movements the use of the elbow swivel angle (ESA) was considered. Experiments collecting eye and body segment movements during reach movements were conducted to investigate the relationship between visual information, elbow swivel angle and movement control mode transition. ESA profile presents curvature changes, which may be associated with movement corrections, during reach movements. Combining the eye and body segment movement data, the field of view was reconstructed to determine when the hand spatial position was available to the central nervous system (CNS). The result shows that movement correction might not immediately occur when the visual information about the hand is available. For reaching movements to frontal targets in the ±45º range relative to the saggital plane, the results indicate that time variations of ESA in the feed-forward control mode may be described by a simple first-order lag response. The modeled elbow swivel angle function can be implemented to facilitate realistic human motion simulation.

4.2 Introduction

The multiple joints of the upper body and the arms confer to the mechanical linkage system large degrees of freedom (DoF). This redundancy of DoF is one of the major issues that need to be resolved to model, simulate and predict human movements Zhang et al., 1998; Kang et al., 2005). Previous studies suggest that human movements

contain invariant features to cope with this DoF redundancy (Bernstein, 1967, Flash et al., 1985). Hence, various approaches utilizing control theories and optimization methods and inverse kinematics have been proposed (Flash *et al*., 1985, Hogan 1985, Zhang and Chaffin, 1998, 1999 and 2000, Galloway *et al*., 2002). Furthermore, hand reaching movements are multi phasic (Meyer et al., 1988; Jeannerod et al. 1984, 1988; Prablanc et al., 1988, Kim, 2005), as they usually include a feed-forward (open-loop) control mode followed by a feedback (closed-loop) phase corresponding to a bell-shaped velocity profile followed by variations corresponding to multiple corrections. The aim of this work is to find a good indicator for control mode transition and further the understanding of human upper body coordination.

Models based on optimization criteria, such as minimum-work and minimum-torque-change, did not provide good predictions of empirical data (Klein Breteler et al. 2003; Admiraal et al. 2004). Previous studies indicate that reach movements models based on feed-forward and feedback modes of control, which have been identified in movements (Woodworth, 1899; Meyer et al., 1988, Jeannerod et al., 1984 1988, Prablanc et al., 1988) provide better simulations (Todorov & Jordan, 2002; Kim, 2005). Hence, this study investigates the relationship between these modes of control, their phase transitions and the utilization of visual and/or proprioceptive feedbacks.

In order to reduce the DoF of human upper body linkage system, the utilization of the elbow swivel angle (ESA) proposed by Korein (1985) and developed by Tolani and Badler (1996) was included in the present study. An experimental approach was used to find the relationship between ESA and the content of visual information. Synchronized body motion tracking and eye tracking systems were used to record the displacement of the shoulder, elbow, wrist, and eye ball, to determine the trajectory of upper body segment joints, gaze orientation and the associated field of view. By observing the prevailing behavior of ESA variations with hand displacement, it was found that changes in this ESA profile could be used as an indicator for the transition of movement phases as a function of the visual information about hand location. This information also allows to estimate the transition between feed-forward and feedback control modes.

4.3 Methods

4.3.1 Participants

Eight young adults (three females and five males) participated in the experiments. Participants had an average age of 27 years and an average stature of 1.78 m. Their average arm reaching length was 65.8 cm. All participants were right-handed and free from any neuromuscular disorders. All signed an informed consent for participation in an experiment approved by the internal review board of the University of Michigan.

4.3.2 Experimental design

Material

Twelve targets were distributed along horizontal concentric circles centered at the right shoulder (Figure 2.3a) with an elevation corresponding to elbow height. The targets were divided into two groups, near and far, as a function of their distance from the shoulder, which was defined by the radii of two circles. Radii (distances) for the near and far group corresponded to 80% and 120% of arm reaching length, which is defined as the distance between the acromion and the tip of the index finger when the elbow is fully extended.

Equipment

Eye movements were recorded by an Eye Tracking System (ASL Eye-Trac®) to determine the direction of gaze during each movement (see section 2.3.5). Whole-body movements were recorded and quantified by an infrared motion tracking system including eight cameras (Qualysis® ProReflex 240-MCU). Twenty-two retro-reflective markers were placed on selected body landmarks (Figure 2.3b). The two motion tracking systems were synchronized. After collecting anthropometric data including stature, reach length, seat height, elbow height and shoulder height in the seated posture, optical reflective markers and the eye tracking system were placed onto the participant and each system was carefully calibrated to obtain an accurate direction of gaze and the corresponding field of view.

Procedure

During the experiment, the participant was instructed to reach each target in a random order at a comfortable self-imposed pace. Each trial (movement to a target) started from an initial posture in which the elbow angle is 90° and the hand is placed on a given starting location in front of the shoulder while the eyes fixate a reference visual target placed at eye level in the mid sagittal plane. For each trial, the target to be reached was indicated on a panel placed in front of the subject beyond the reach destination. The subject was also instructed to return to the initial posture and gaze after each reaching movement.

The procedures were reviewed and approved by the University of Michigan Health Sciences Institutional Review Board for compliance with appropriate guidelines, state and federal regulations.

4.3.3 Field of view reconstruction

Centered around the gaze vector, the foveal and peripheral field of view were reconstructed with angles of view of 2.5º and 20 º, respectively (Atchison & Smith, 2000), as illustrated in Figure 4.1.

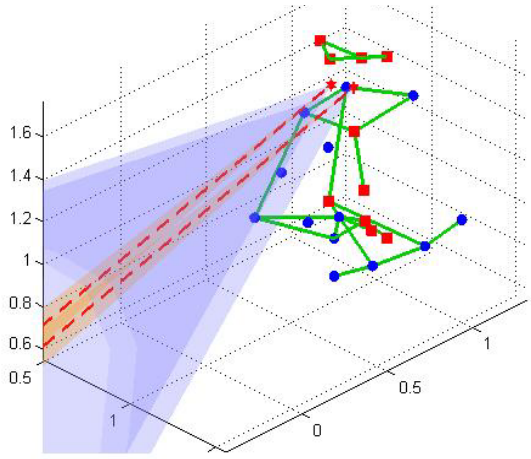

Figure 4.1. Reconstruction of Foveal Field of View (FFoV- light), Peripheral field of view (PFoV- dark) from gaze orientation (dash lines).

4.3.4 Data analysis

Body segment kinematics and eye movement data were sampled at 60 Hz and synchronized. Kinematic data of the hand and joint angles were used to quantify timing characteristics body segment movements. The beginning of each movement was determined using a 2% threshold of hand peak velocity. In order to compare data between subjects, the traveling distance (displacement projected on the horizontal plane) was normalized by subject's arm length. The direction of gaze and field of view (Figure 4.1) were reconstructed from the combination of motion and eye tracking data to find the instants at which the hand enters the foveal field of view.

Computation of the elbow swivel angle

Figure 4.2a illustrates the definition of the elbow swivel angle (Korein, 1985, Kang *et al.*, 2005). Centered on the vector from the shoulder to the wrist and in a plane perpendicular to that vector, the radius of a circle is defined by the position of the elbow. As shown in Figure 4.2b, the center of the circle is denoted as "**o**", $\vec{z}$ is a vertical vector and its projection on the circle is denoted as $\vec{v}$. Originating from "**o**", $\vec{e}$ is the vector pointing to the elbow on the circle circumference. Hence, the swivel angle denoted θ, is thereby defined by the angle between $\vec{v}$ and $\vec{e}$,. The swivel angle is positive for counterclockwise rotation along the shoulder-wrist vector.

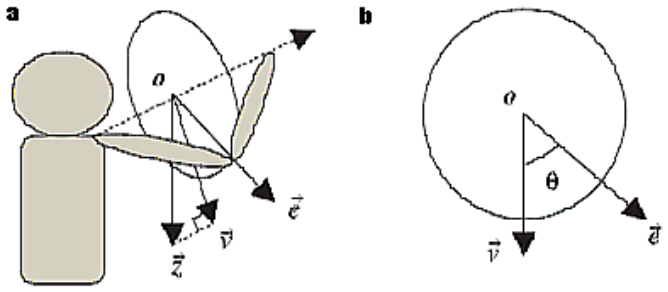

Figure 4.2. Definition of the swivel angle θ. (Kang *et al*., 2005)

Determination of the eye-on-hand during reach

In this study, the term 'eye-on-hand' (EOH) indicates the instant at which the hand enters the foveal field of view (FFoV). In order to determine this instant, two markers on the wrist and one on the knuckle on the back of the hand are used to represent

the hand, and a coordinate transformation was performed. As opposed to the transformation stated in section 2.3.4, expressing the position of hand markers in the local coordinate system of the FFoV was necessary to determine the intersection of the hand trajectory and the FFoV.

From Eq. 2.1, the rotational matrix from the local eye coordinate system to the global reference frame can be obtained by:

$$R(t) = R_{eye}^{global}(t) = R_{head}^{global}(t) \cdot R_{eye}^{head}(t) \qquad \text{(Eq. 4.1)}$$

In addition, the coordinate transformation needs not only rotating the reference axes but also translating the origin to the position of an eye (left or right eye). Given the instantaneous eye position ($p_{eye}^{\ global}$), the homogeneous transformation matrix for the hand markers from the global reference frame to the local coordinate system of an eye can be expressed as:

$$H_{global}^{FFoV}(t) = \begin{bmatrix} R^T & -R^T p_{eye}^{\ global} \\ 0 & 1 \end{bmatrix} \qquad \text{(Eq. 4.2)}$$

And the position of the hand makers expressed in the local FFoV coordinate system can be calculated by:

$$\begin{bmatrix} p_{hand}^{\ FFoV}(t) \\ 1 \end{bmatrix} = H_{global}^{FFoV}(t) \cdot \begin{bmatrix} p_{hand}^{\ global}(t) \\ 1 \end{bmatrix} \qquad \text{(Eq. 4.3)}$$

where $p_{hand}^{\ FFoV}(t)$ and $p_{hand}^{\ global}(t)$ denote the position of the hand marker expressed in the local FFoV coordinate system and the global reference frame, respectively. During a reach movement, the appearance of the hand in the FFoV can be identified by the intersection of the hand markers expressed in the local coordinate system and the conic volume of FFoV.

Elbow swivel angle profile with eye-on-hand

The elbow swivel angle during reach movements was computed from the recorded body segment movement data. To define the elbow swivel angle profile (ESA) as a function of hand traveling stance, time variation of the derived elbow swivel angle was analyzed in relation to the hand horizontal displacement during reaching.

In order to assess the change in the ESA relative to the visual feedback, the mean curvature and its standard deviation of the movement section preceding EOH was computed for each trial. When EOH occurs, the local curvature was computed to determine if the change of curvature at that point was larger than the standard deviation indicated above. If the EOH occurs prior to the first half of the total movement time, the mean curvature and standard deviation of the first half of the ESA was computed and used to determine significant curvature changes in the following portion of the ESA trajectory with the eye-on-hand.

Modeling parameter

Most human movement simulation softwares are quasi-static as movements are parameterized by linear/angular displacement of body segments but not by time. The model of elbow movements developed in this chapter includes a time parameterization by correlating the swivel angle with the hand displacement during reaching. This feature will facilitate the integration of the empirical model into most human movement simulation software driven by the movement of the hand.

4.4 Results

4.4.1 Elbow swivel angle vs. normalized hand traveling distance

Examples of elbow swivel angle profiles (ESA) with respect to the normalized hand displacement are shown in Figure 4.3 and Figure 4.4 for reaching to the rear far right target and profiles of four subjects reaching to the far 45º front right target, respectively. The elbow swivel angle is multi-phasic with a significant curvature change close to the end of the reach (Figure 4.3a and Figure 4.4a). Since the elbow was not fully extended in the final posture (section 2.4.3), these curvature changes in the ESA profile might not result from the computation error or other artifacts due to a fully stretched arm. The comparison of the ESA between rear and frontal reaches, suggest that this multi-phasic feature in the ESA profile corresponds to a movement adjustment/correction. Figure 4.4 shows that the swivel angle profiles are similar among subjects with a deviation close to the end of the movements. This result indicates that the swivel angle

profile in terms of the normalized hand traveling distance may capture an invariant feature of reach movements.

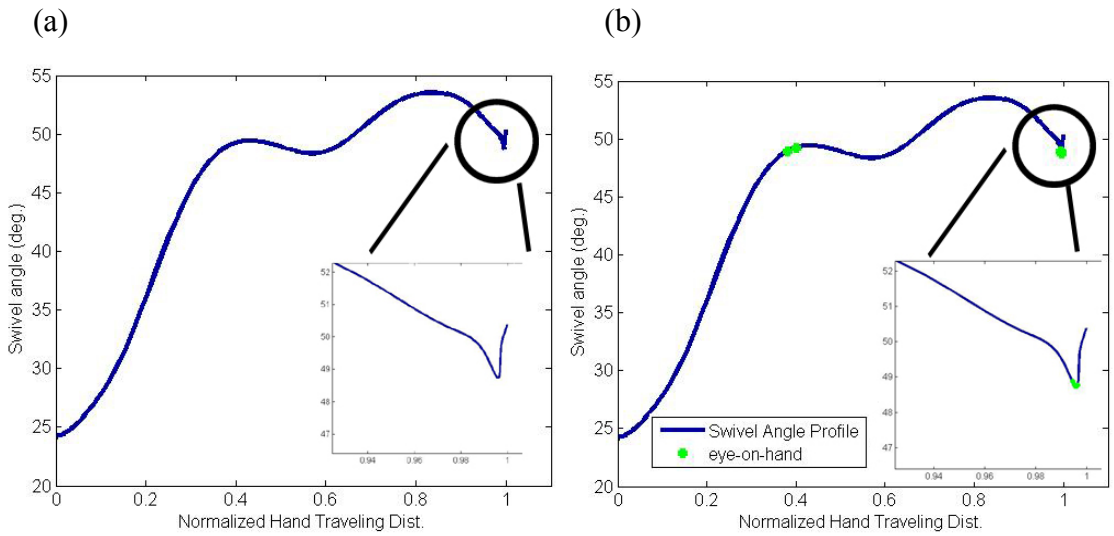

Figure 4.3. Example of elbow swivel angle profile of a rear reach. (a) reaching to rear far right target (F1); (b) ESA profile with indications of eye-on-hand

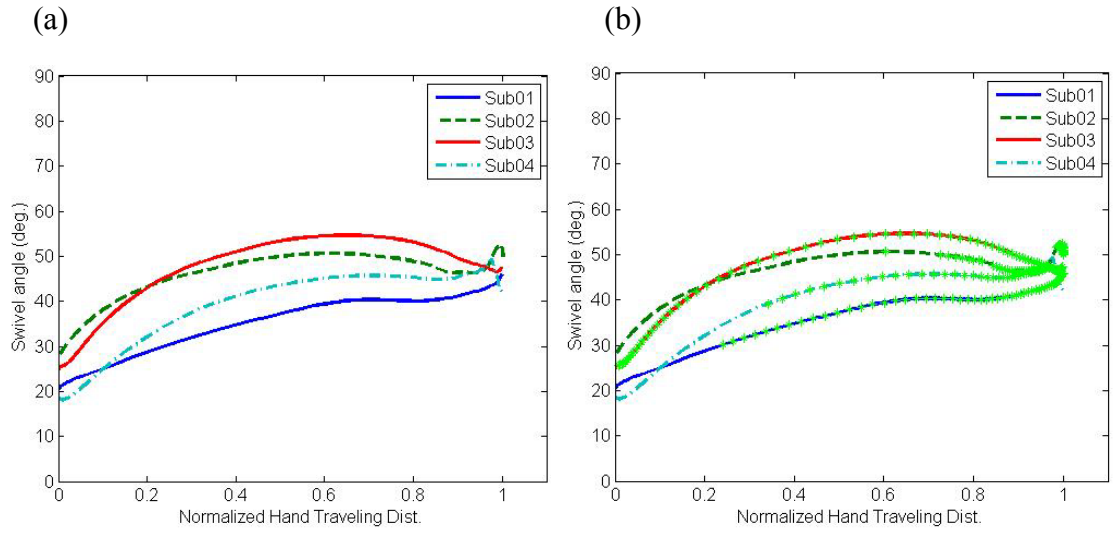

Figure 4.4. Example of elbow swivel angle profile of frontal reaches (a) reaching to 45° right far target (F2) from 4 subjects; (b) same ESA profile with indications of eye-on-hand.

For a rear reach, the combination of gaze with hand movements indicates that the hand enters the foveal field of view (eye-on-hand, EOH) during and at the end of the reach, as illustrated in Figure 4.3. For the rear targets, changes in the swivel angle profile

occur immediately after EOH and at the end of the movement (Figure 4.3b This result suggests that when the hand is in the visual field of view movement corrections based on visual feedback may take place. For the frontal targets (Figure 4.4), EOH occurs earlier due to the task spatial configuration and shorter search for the target. For these targets, the ESA profiles may not show a noticeable change in the early stage of the movement, even the EOH happens more or less in the mid of the reach. However, ESA always shows a remarkable curvature change at the end of the movement. This curvature change was related to movement correction and estimated by the ESA profile variation larger than the standard deviation of the portion of movement prior to EOH (Figure 4.4b). This suggests that movement adjustments are likely to be driven by the visual feedback. However, visual events cannot be used alone as indicator of movement phase transition. In other word visual feedback may be necessary but not sufficient to identify a transition. For the front reach, these results suggest that the control mode transition between the feed-forward and feedback mode may be indicated by the combination of the eye-on-hand moments and the curvature change of the elbow swivel angle profile.

4.4.2 Feed-forward control mode and transition

From the movement data of all subjects, the variance of ESA profile is much greater for rear than frontal reaches. Hence, the present study focuses on movements to frontal targets. According to this observation, the swivel angle profile for frontal reaches may be composed of two parts delimited by the initiation of the continuous eye-on-hand period and the curvature change in the elbow swivel angle profile. Before the eye-on-hand occurs and if there is only mild curvature change in the swivel angle profile, this first part may be regarded as the feed-forward (open-loop) control mode phase with respect to the utilization of visual information. Hence, the percentage of the hand traveling distance during that feed-forward phase may be determined as a function of the target azimuth and distance, as illustrated in Figure 4.5.

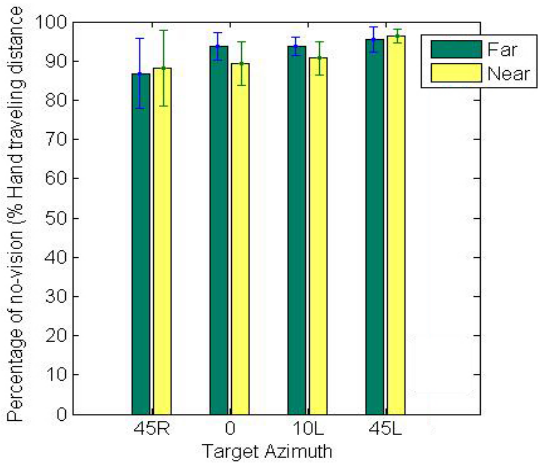

Figure 4.5. Percentage of feed-forward control mode in hand traveling distance with respect to target location (target azimuth and distance)

Table 2.2 presents the results of the statistical analysis (ANOVA) for the feed-forward control mode phase relative to the hand traveling distance. The result indicates that the proportion of the feed-forward control mode phase is not significantly influenced by the target location. For the frontal reaches, the average percentages of the feed-forward phase are 90.8% and 91.7 for the far and near set, respectively.

Table 4.1. ANOVA results for the feed-forward control mode proportion of hand traveling distance

(%)	45º Right	0º Front	10º Left	45º Left	p
Far set	86.8 ± 8.8	93.8 ± 3.6	93.7± 2.2	95.5± 3.1	0.78
Near set	88.2± 9.6	89.4±5.5	90.7± 4.2	96.4± 1.7	0.92
$F_{1,46}$	0.04	0.02	0.01	0.02	
p	0.85	0.88	0.92	0.90	

4.4.3 Elbow movement modeling

Given the determination of phase transition for the frontal reaches, the first part – the feed-forward phase of the elbow swivel profile may therefore be extracted. Examples of elbow swivel profiles from four subjects during the feed-forward phase are shown in Figure 4.6. During the feed-forward (open-loop) phase, all swivel angle profiles are

similar and change monotonously for frontal reaches, which suggests that a simple model may be used to reproduce this phase.

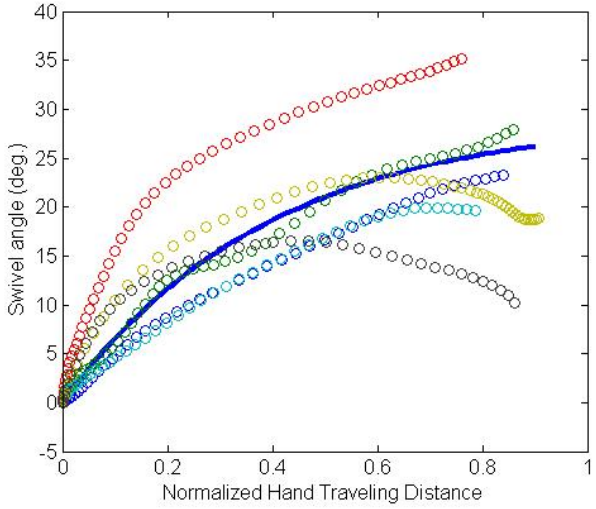

Figure 4.6. Swivel angle profiles for four subjects (Reach to 45° right far target). The solid line represents a fitted nonlinear least square model.

The elbow swivel angle profile exhibits the behavior of a first order lag response based on a feed-forward control mechanism. Hence, the elbow swivel angle displacement (S(x)) normalized to hand displacement was modeled by a general equation of a first-order lag response as follow:

$$S(x) = A(1 - e^{-kx}) \qquad \text{(Eq. 4.4)}$$

where A represents the steady state amplitude and k refers to the gain of the system. These parameters are estimated by a statistical nonlinear least square model for each target location. The corresponding pairs of parameters are listed in Table 4.2. As expected, coefficient A and k are target dependent for the frontal reaches. The associated models are illustrated in Figure 4.7.

Table 4.2. Model parameter estimates and R^2 coefficients

		A	k	R^2
45˚ right (F/N2)	Far	0.51	2.53	0.83
	Near	0.35	1.84	0.85
0˚ front (F/N3)	Far	0.47	3.47	0.90
	Near	0.39	1.49	0.91
10˚ left (F/N4)	Far	0.48	4.68	0.79
	Near	0.40	1.19	0.74
45˚ left (F/N5)	Far	0.50	2.83	0.87
	Near	0.53	2.04	0.88

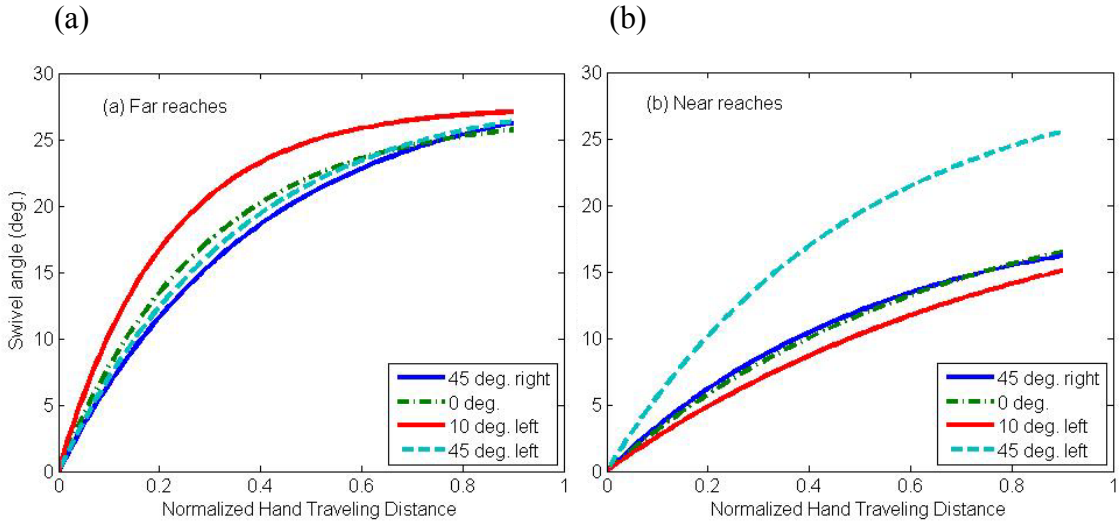

Figure 4.7. Predicted swivel angle vs. normalized hand displacement for far (a) and near (b) targets.

4.5 Discussion

Determining phase transition from feed-forward to feedback control is one of the crucial steps to understand and model the coordination of reach movements. Previous studies have reported that the final feedback phase contributes to movement accuracy (Crossman & Goodeve, 1983; Meyer et al., 1988) and foveal vision is used for the end-point control that takes places in the final phase of movements (Paillard, 1996). Thus, the availability of the spatial relationship between the current position of the hand and the target location is necessary for movement adjustment in the feedback control phase. The

characteristics of the elbow swivel profile reveal a multi-phasic behavior whose change are likely to correspond to the availability of visual information about the hand. The present results indicate that the presence of the eye-on-hand during the reach movement combined with a curvature change in the elbow swivel angle profile may be used to estimate the phase transition from a feed-forward (open-loop) to a feedback (closed-loop) control mode.

The elbow swivel profiles are multi-phasic. As the far reach indicates (Figure 4.3), reach movements requiring higher coordination of body segments show an early occurrence of the curve change, which corresponds to an early movement adjustment. Furthermore, the coincidence of the curvature change and instant of eye-on-hand (the hand-in-foveal field of view, Figure 4.3) suggests that visual feedback might be used to initiate a movement correction.

Nevertheless, the elbow swivel angle profile for the frontal reaches, which shows an early occurrence of eye-on-hand, do not present a change in curvature until the end of a reach. This indicates that movement corrections do not have to occur immediately after vision is available, since there might be no need at that moment. Nevertheless, a remarkable curvature change close to the end of ESA profile may serve as an indicator for control mode transition. On the other hand, merely using ESA profile to determine the phase transition might be misleading because movement correction might be made based on other sensory feedback such as proprioception. To determine the initiation of the feedback control mode transition, the combination of the ESA curvature change and eye-on-hand is suggested to be a better indicator than using one or the other along.

As the timing of a remarkable curvature change in ESA profile occurs late during the frontal reach movements, a substantial proportion of movement is controlled in the feed-forward control mode or is dependent on a feedback control based on proprioception or the efferent copy. However, since that movement phase corresponded to a monophasic ESA curve without obvious corrections on the hand trajectory, the phase was modeled by a first-order lag response.

The model of the ESA presented here corresponds to the feed-forward phase of reaching movement for the frontal targets (± 45° about the mid saggital plane). According to the coefficients of determination (R^2) of the ESA modeling functions presented in

Table 6.3, the prediction based on the feed-forward control mechanism is slightly better for the near (Figure 4.6a) than the far targets (Figure 4.6b) in general. This difference in prediction may be due to a hand traveling distance shorter for near than far reaches.

Overall, the prediction based on a lag function provides reasonable outcomes for the frontal reaches associated with high R^2 values in general. This implies that the ESA and its model based on the lag response might properly capture an invariant feature in reach movements. As previously suggested (Korein, 1985; Tolani and Badler, 1996), the elbow swivel angle has been used to reduce the DoF redundancy of the human upper body system. However, the analytical approach for computing the inverse kinematics utilizing ESA (Tolani and Badler, 1996) was rarely used to model movements. Hence, the use of the present model supplements the analytical approach and provides realistic postures in simulation of 3-D reach movements.

CHAPTER 5

Role of visual feedback in multi-joint coordination of reach movements

5.1 Abstract

Kinematic characteristics and coordination of reaching movements may differ with and without visual guidance. The contribution of visual feedback to the respective phases of reach movements was investigated in this study by quantifying the final position errors of the hand, variation of torso movements and changes in the elbow swivel angle. The results indicate that, as expected, the hand final position error increases without visual feedback. The hand final position error also increases with the size/weight of manipulated object and with reaching distance. The pattern of body segment coordination is less variable under the no-vision than the vision condition and no significant change in torso movements was observed when reaching without vision. However, the elbow swivel angle shows a significant difference in movement pattern and magnitude of change. This behavior is more pronounced for a target distance greater than arm length, but is not significantly affected by the movement azimuth. The offset of reach movement errors suggests that the egocentric coordinate system used for movement planning and control may be centered at the head.

5.2 Introduction

Vision is a major feedback mechanism for controlling the spatial accuracy of reaching movements (Prablanc et al., 1979). Hence, differences in reaching accuracy between reaches with and without visual feedback have been extensively investigated (Soechting et al., 1989; McIntyre et al., 1998; Van Beers et al., 2002; Admiraal et al.,

2003; Hondzinski & Kwon, 2009). According to Van Beers et al. (2002), the central nervous system (CNS) may use visual information for determining the direction of reaching/pointing while proprioceptive information is used for controlling the movement distance, when the end-effector is visible. Furthermore, the frame of reference the CNS might use was extensively investigated by experimental paradigms with different visual conditions such as end effector visible, target frame visible and no vision (Admiraal et al., 2004; McIntyre et al., 1998), or a moving base (Medendorp et al., 1999; Hondzinski & Kwon, 2009). In summary, previous studies suggest that the CNS might adapt the coordinate system between the head and the shoulder, and use control strategies relying on visual information for whole-body goal-directed movements.

However, the role of vision in movement planning and body segment coordination has received little attention. In recent studies, Medendorp et al. (2002) measured the quality of gaze control during heads translation in complete darkness. Another study examining the torso in addition to the hand under different visual conditions was also recently proposed (Hondzinski et al., 2009). With few exceptions (Kim, 2005; Sergio & Scott, 1998) most studies investigating reaching errors under vision and no-vision conditions have used a fixed reaching/pointing target setup for every participant without normalization for anthropometric differences.

An experiment was designed to further assess the contribution of visual feedback to movement control, and determine the contribution of visual information to movement coordination. In order to investigate upper body coordination of the torso and limb joints in reach movements this study included anthropometric considerations to normalize target locations. This normalization is necessary to identify coordination patterns independent of body segment length. In addition, reaching movements were performed with and without vision after visual calibration of the task space. The variance and characteristic changes in torso and elbow swivel angles were examined to estimate the effect of vision on movement organization and planning.

5.3 Methods

5.3.1 Experimental setup

The experimental setup was similar to those described in previous chapters. Briefly, eight frontal targets were distributed on two circles centered at participant's right acromion and corresponded to a far and a near set. Radii (distances) for the near and far groups corresponded to 80% and 120% of arm reaching length (Figure 5.1). The targets were distributed in the frontal area from 45º left, to medial 10º left and 0º front, and to 45° right on a flat-screen monitor placed horizontally in front of the subject (Figure 5.1).

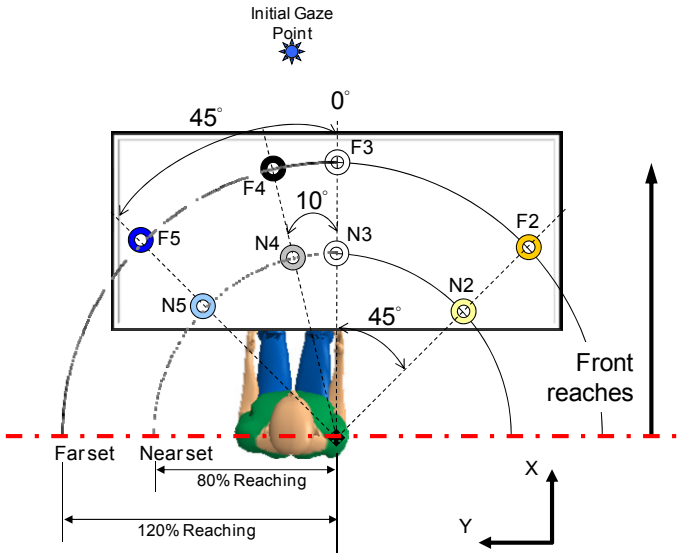

Figure 5.1. Experimental setup: The rectangle represents the video monitor on which the frontal targets are displayed.

The size of the manipulated objects was varied to investigate both the dimensional effect associated with visual perception and manipulation issues. In order to estimate the influence of the size and weight of the manipulated object, two cylinders with a diameter of 3.175 cm and 4.45 cm and respective weight of 18 g and 25 g were used.

Whole-body movements were recorded by an eight-camera motion tracking system (Qualysis® ProReflex 240-MCU).Twenty-two retro-reflective markers were placed on selected body landmarks on the upper body (Figure 2.3b). Eye movements were recorded simultaneously by an eye tracking system (ASL Eye-Trac®). Both systems were synchronized to record movements at a sampling rate of 60 Hz.

5.3.2 Experimental design

Twenty two right-handed individuals (11 males and 11 females) participated in this experiment as paid volunteers. The average age and stature of the participants were 24 ± 3.3 years and 1.70 ± 0.1 m, respectively. The average arm reaching length was 62.4 ± 4.1 cm. All Participants were free from any neuromuscular disorders. The experiment was divided into two sessions as follows:

A randomized sequence of front reaches was tested first. For this session, participants were asked to move a vertical cylinder from an initial location to a designated target (Figure 5.2) while holding it with a neutral hand posture. A reflective marker was placed on top of the cylinder. Four consecutive practice reaches to the same target were performed with full vision, and then replicated three times without vision (reaching in the dark with eyes open). Under the no-vision condition, the subject could not see the target nor the body segments. Reaches were performed with each object in two different trial series. Object size presentation was randomized between subjects only.

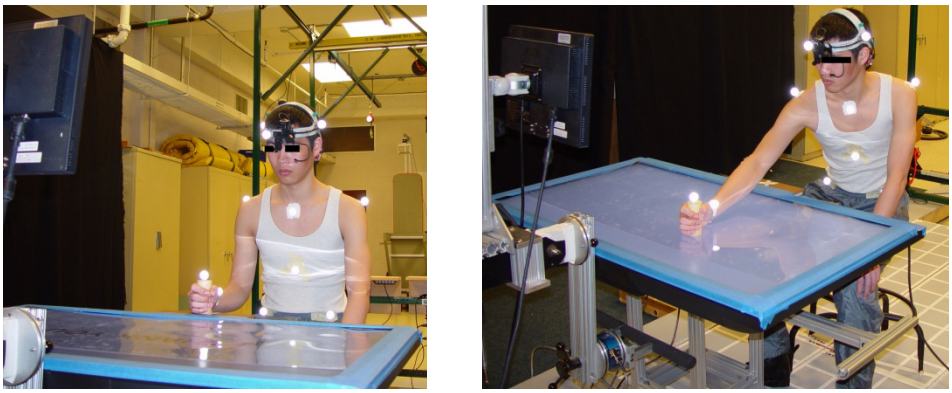

Figure 5.2. Example of the initial posture (left) and final posture at the target (right)

5.3.3 Data processing and analysis

In order to compare reaching performances between visual conditions, two types of reaching errors were distinguish: the *constant error (CE)*, which corresponds to the distance between the designed target location and the final position of the hand holding an object, and the *variable error (VE)*, which reflects the distribution of the reaching

positions toward a target location relative to the average pointing position to that target location. The distribution of the final reaching positions for a target location *i* (see Figure 5.1) is described by the 2-D covariance matrix S_i since the vertical component (z coordinate) was constrained by the height of the flat-screen monitor. The two orthogonal eigenvectors of the covariance matrix S_i depict the orientation of the variable errors. Their corresponding eigenvalues of the matrix give the range of the variable error along the eigenvectors. Furthermore, these eigenvalues can be scaled to compute the limits that contain 95% of the data (McIntyre et al., 1998; Morrison, 1976). Hence, the contours of the 95% confidence ellipse can be drawn with the two eigenvectors and their corresponding eigenvalues (λ_1 and λ_2) for the end position distribution. The eigenvector corresponding to the larger eigenvalue (λ_1) was referred to be the main axis of the distribution.

Since the target location were set up with respect to the arm length for each subject, reaching position data may be normalized by each subject reaching arm length (*l*) for a better comparison between individuals. Furthermore, centroids of final position distributions under the no-vision condition were obtained to represent the end position of the hand for each target location. Corresponding to the reaching distance (80% and 120% arm length), radial discrepancy (RD) is defined by:

$$RD = \overline{OP}_{centroid} - \overline{OP}_{target} \qquad \text{(Eq. 5.1)}$$

where $\overline{OP}_{centroid}$ and $\overline{OP}_{target}$ denote the distances from the right shoulder to the error centroid and to the associated target, respectively. Hence, a positive RD indicates an average overshooting tendency while a negative RD indicates undershooting.

Torso axial rotation, lateral bending and flexion angles as well as the elbow swivel angle were quantified to reveal movement strategies and corresponding coordination schemes. Since the reaching movements were unconstrained and performed at a self-imposed speed, torso and elbow swivel angles (ESA) were expressed with respect to the hand (wrist) traveling distance instead of the real time. In addition, the wrist traveling distance was also normalized by each subject's arm length to allow between-subjects comparisons.

Torso angles as a function of the wrist displacement are systematically monophasic. To be consistent within the present work, the single-valued curvature of the torso- wrist displacement curve (TWC) was used to represent the torso movement characteristics. For each trial, TWC was fitted to a 2^{nd} order function using the least mean square method. Hence, the curvature of the fitted function may represent the mean curvature of the TWC. The variance of TWC curvature between trials was computed for each target location in both visual conditions,. The curvature was computed for each torso angle. The curvature variance was used to compare the variability of torso movements under vision and no-vision condition.

The variance of the mean curvature for the ESA profiles was also quantified for each visual condition. However, ESA's may be implicitly associated with phase transition (Chapter 4). Therefore, the amplitude (overall variance) and the magnitude (difference between the initial and end value) of the ESA profile were computed to determine changes during a reach movement as a function of target azimuth, target distance and visual conditions.

For the data analysis, Student's t test and ANOVA were used for statistical analysis to identify the influence of target locations and manipulated objects on the reaching precision (CE and VE), and body segment movements (torso angles and the elbow swivel angle), as well as the effect of visual feedback on body segment movement characteristics.

5.4 Results

5.4.1 Reaching error without visual feedback

Figure 5.3 and Figure 5.4 shows the distribution of the normalized final hand position when reaching under vision and no-vision with the small (left panels) and large (right panels) object, respectively. Final positions of the 95% confidence region for reaching to each target location, across subjects, are expressed by ellipses for the no-vision condition. In all figures the origin coincides with the location of the right shoulder/acromion. As expected, the error distribution is significantly greater when reaching without than with vision ($t = 155.9$, $p<0.01$).

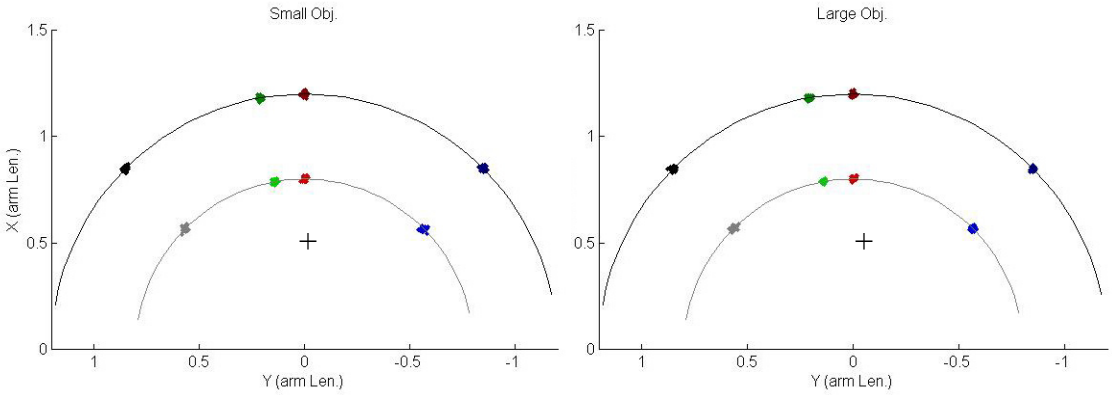

Figure 5.3. Final reaching position distribution with vision for small (left) and large (right) object. The origin of each plot corresponds to the vertical axis of the right shoulder; the average initial position of the hand over all subjects is indicated by '+'.

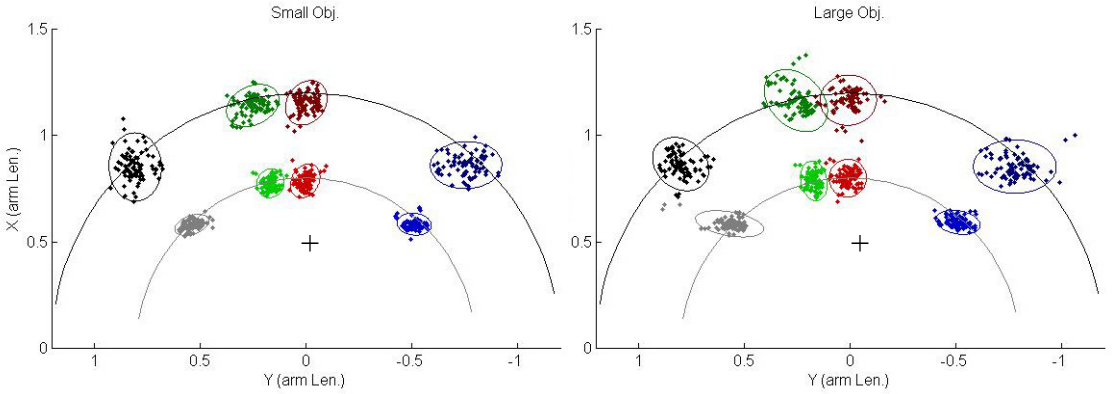

Figure 5.4. Final reaching position distribution without vision for small and large (left and right panels) manipulated object. Ellipses denote the 95% confidence region of the distribution. The origin of each plot corresponds to the vertical axis of the right shoulder; the average initial position of the hand over all subjects is indicated by '+'.

The ANOVA indicates no significant difference in the normalized CE between genders. A 3-way ANOVA including target azimuth, distance and object size as main factors (Table 5.1) was performed for the no-vision condition. The result shows that target location (azimuth and distance) only has a significant influence on the CE. No interaction exists between any two of the factors. In the no-vision condition, the CE is significantly larger ($t = 34.8$; $p < 0.05$) for the far (8.5% ± 5% arm length) than the near (5.14% ± 3%) set of targets.

Table 5.1. ANOVA table for CE

VE:	DoF	F	p
Obj size (S)	1	5.19	0.11
Distance (D)	1	228.2	< 0.01
Azimuth (A)	3	31.43	< 0.01
S × D	1	3.52	0.16
S × A	3	0.43	0.75
D × A	3	4.11	0.14

(Shaded cell corresponds to significant values)

CE variations a function of target azimuth are presented in Figure 5.5. Averaged over the two object sizes, the CE's are significantly larger (t_{near} = 11.7, t_{far} = 8.8, $p<0.01$) for reaches to 45 º right than 45º left by 1.8% and 3.1% for the near and far set, respectively. For reaches to the most eccentric targets (± 45º azimuth), the lateral error component (in global coordinate system) is significantly ($t = 2.62$; $p < 0.05$) larger (1.8%) than the longitudinal error. However, there is no significant difference between the x and y component for medial reaches (0º front and 10º left).

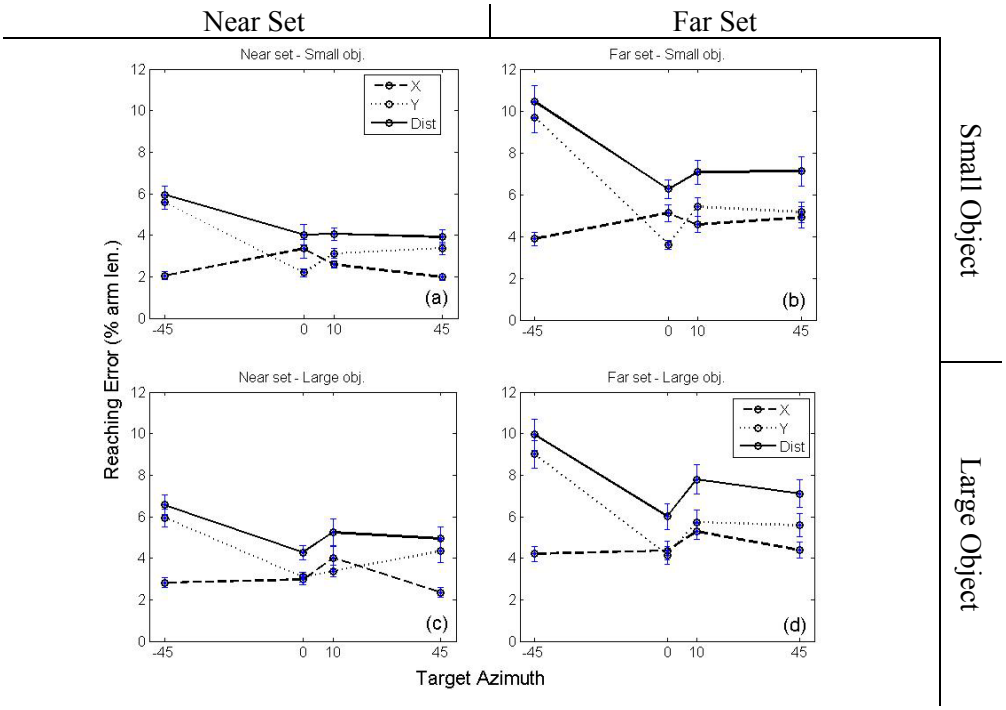

Figure 5.5. Constant errors of reach positions vs. target azimuth in the no-vision condition: small and large object (upper and lower panels); near and far set (left and right panels).

In addition, the variable error along the main axis (major VE, λ_1) reveals a reaching error tendency across subjects. The 3-way ANOVA including object size, target distance and target azimuth shows that VE in only significantly influenced by target distance and there is no interaction between any factors (Table 5.2). Table 5.3 presents the magnitudes of VE's along the major and minor axes (corresponding to eigenvalue λ_1 and λ_2). The major VE (λ_1) is significantly larger (1.4% on average) for the far than the near set($t = 467.5$, $p<0.01$).

Table 5.2. ANOVA table for VE

VE:	DoF	F	p
Obj size (S)	1	2.72	0.20
Distance (D)	1	12.57	0.04
Azimuth (A)	3	1.38	0.40
S × D	1	0.05	0.84
S × A	3	0.09	0.96
D × A	3	1.18	0.45

(Shaded cell corresponds to significant values.)

Table 5.3. Variable errors with respect to target location

		45º Right	0º Front	10º Left	45º Left
average eigenvalues		λ_1, λ_2	λ_1, λ_2	λ_1, λ_2	λ_1, λ_2
Small object	Near set	0.0067, 0.0026	0.0072, 0.0041	0.0047, 0.0041	0.0069, 0.0020
	Far set	0.0285, 0.0123	0.0125, 0.0081	0.0169, 0.0083	0.0258, 0.0153
Large object	Near set	0.0111, 0.0030	0.0079, 0.0078	0.0089, 0.0038	0.0265, 0.0031
	Far set	0.0383, 0.0159	0.0178, 0.0140	0.0291, 0.0146	0.0207, 0.0128

(All near and far pairs are significantly different; there is no significant difference between object sizes.)

The 3-way ANOVA performed on radial discrepancy (RD) indicates a significant influence of object size ($p = .028$), target distance ($p = .01$), and azimuth ($p = 0.029$), as indicated in Table 5.4. However, none of the interactions were significant ($p>0.05$). The

centroid of the error distribution was computed for each target over all subjects. Figure 5.6 illustrates the centroids of the final position distribution for no-vision reaches. The general tendency to undershoot the far targets seems to be larger for the right targets, as illustrated in figure 5.6.

Table 5.4. ANOVA table of radial discrepancy of centroids

VE:	DoF	F	p
Obj size (S)	1	15.99	0.028
Distance (D)	1	65.9	< 0.01
Azimuth (A)	3	13.79	0.029
S × D	1	0.02	0.89
S × A	1	0.36	0.79
D × A	3	0.83	0.56

(Shaded cells correspond to significant values)

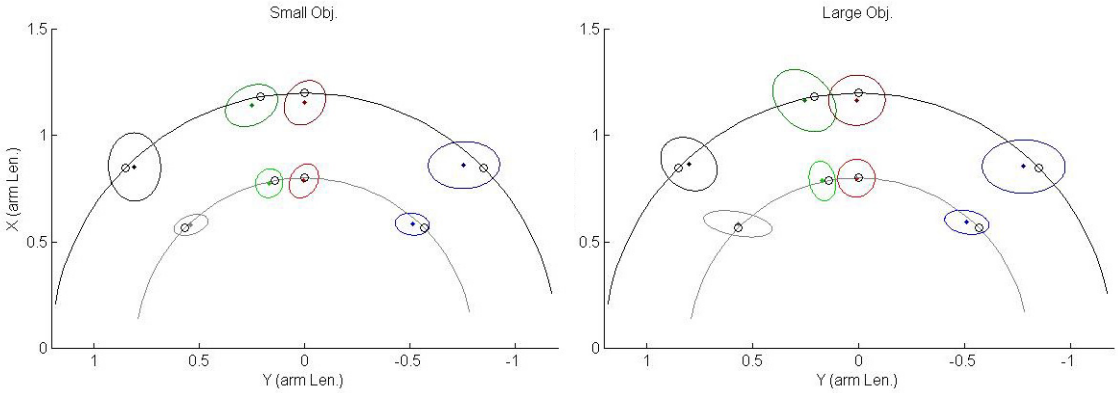

Figure 5.6. Centroids of final reach position distribution without vision for the small and large (left and right panel) object. Ellipses represent the 95% enclosure region of the distribution, circles represent the target locations, and dots represent the centroids of the final position distributions.

Table 5.5 shows that the magnitude of RD increases with target eccentricity and reaching distance in general. This means that the undershooting behavior might be greater for the more distant targets. In addition, undershooting is significantly larger (1.3% arm length) for the small than the large object ($t = 74.7$, $p<0.01$).

Table 5.5. Radial discrepancy of centroid from the designed reaching distance

(unit: % arm length)		45º Right	0º Front	10º Left	45º Left
Small object.	Near set	-2.49	-1.28	-0.62	-0.91
	Far set	-5.46	-4.57	-3.08	-2.70
Large object	Near set	-1.88	-0.01	+0.49	+1.55
	Far set	-4.48	-3.33	-0.76	-2.15

+: overshoot; -: undershoot

5.4.2 Visual feedback and movement coordination

Three torso joint angles and the elbow swivel angle were expressed as functions of the hand traveling distance. As indicated earlier, torso flexion is known to contribute to distance compensation (Chapter 2), while the elbow swivel angle may reflect the coordination between the shoulder and elbow joints (Chapter 4).

Torso angles

Typical examples of torso angle variations as a function of the horizontal wrist (hand) traveling distance are illustrated in Figure 5.7. The 2-way ANOVA shows that the curvature variability of all torso angles (torso axial rotation, lateral bending and flexion) is not significantly different between visual conditions (Table 5.6).

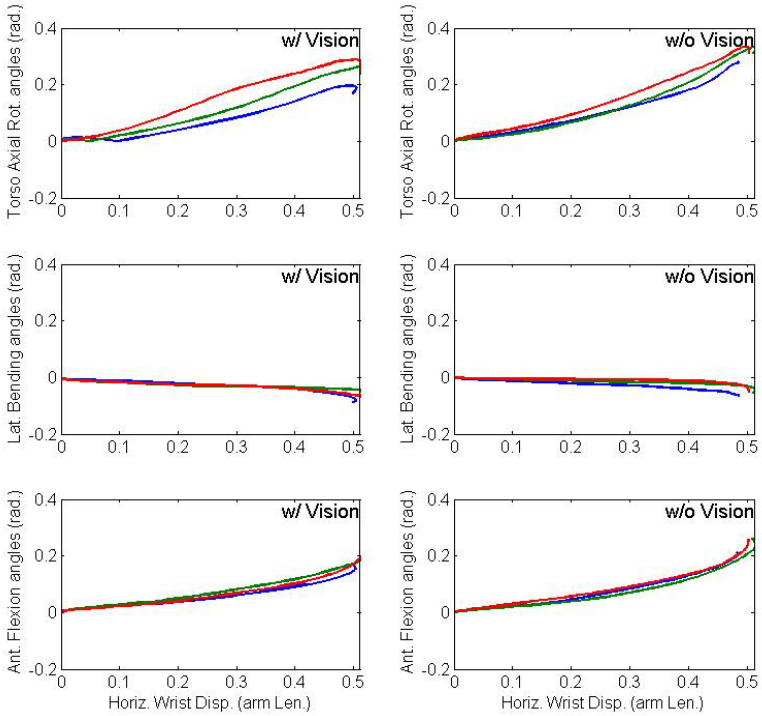

Figure 5.7. Typical example of torso angles of reaching to 45º left near target with (left) and without (right) visual feedback (trials from one subject data)

Table 5.6. 2-way ANOVA table for each torso angle and object size

	Axial rotation			Lateral bending			Anterior flexion		
Small Obj.	DoF	F	p	DoF	F	p	DoF	F	p
Vision (V)	1	0.62	0.43	1	0.18	0.67	1	0.72	0.40
Target location (T)	7	29.41	< 0.01	7	1.27	0.27	7	4.84	< 0.01
V× T	7	1.49	0.17	7	0.85	0.55	7	0.36	0.93
Large Obj.	DoF	F	p	DoF	F	P	DoF	F	P
Vision (V)	1	0.06	0.80	1	1.39	0.24	1	0.43	0.51
Target location (T)	7	24.89	< 0.01	7	1.49	0.17	7	3.06	< 0.01
V× T	7	0.63	0.73	7	1.84	0.08	7	0.92	0.49

(Shaded cells correspond to significant values.)

In addition, curvature variations of torso axial rotation and anterior flexion are significantly larger when reaching to the near than the far targets (Figure 5.8). Averaged over all target azimuths, the axial rotation variance difference between near and far set

are 1.67 and 1.89 for the small and large object group respectively; while those for anterior flexion are 0.22 and 0.32, respectively.

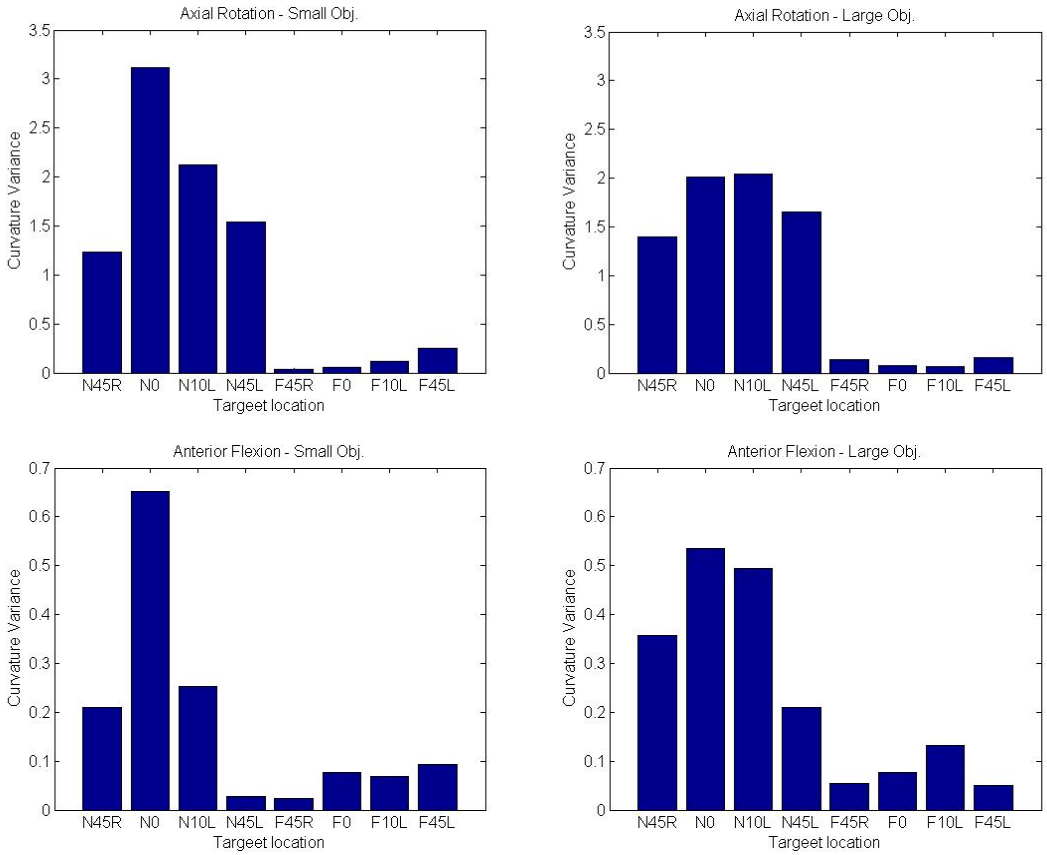

Figure 5.8. Curvature variation of torso axial rotation (upper panels) and anterior flexion (lower panels) when reaching with a small (left panels) and large (right panels) object.

Elbow swivel angle

The 4-way ANOVA performed on the curvature variance of elbow swivel angle (ESA) profiles (Table 5.7) shows no significant difference between the vision and no vision conditions. Object sizes and target azimuth have no significant effect on the variance. However, similar to the results for torso angles, the ESA variance is significantly larger for the near than the far reaches by 0.71 and 0.59 with a small and large object in hand, respectively (Figure 5.9).

Table 5.7. 4-way ANOVA table for the ESA curvature variance

	DoF	F	p
Vision (V)	1	0.44	0.52
Object size (S)	1	1.81	0.20
Azimuth (A)	3	2.84	0.08
Distance (D)	1	58.3	< 0.01
V×S	1	0.1	0.76
V×A	3	0.9	0.47
V×D	1	3.07	0.10
S×A	3	0.56	0.65
S×D	1	0	0.96
A×D	3	2.8	0.08

(Shaded cell corresponds to significant values.)

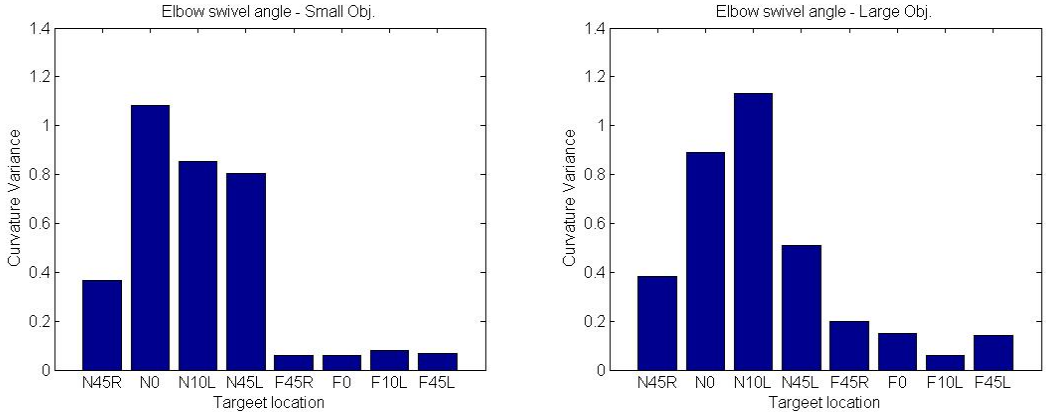

Figure 5.9. Curvature variation of ESA when reaching with a small (left panel) and large (right panel) object.

Typical examples of ESA time profiles when reaching to the far left and near right 45º azimuth targets are shown in Figure 5.10 a and b, respectively. Two characteristics emerged as a function of the visual condition. First, the number of ESA jerks and the amplitude of ESA variations are larger for reaches with vision than without vision (Figure 5.10a). Second, the ESA displacement magnitude is smaller in the no-vision than the vision condition (Figure 5.10b). These two characteristics can be reflected respectively by the *amplitude* (overall variance) and the *magnitude* (difference between the initial and end value) of the ESA profile.

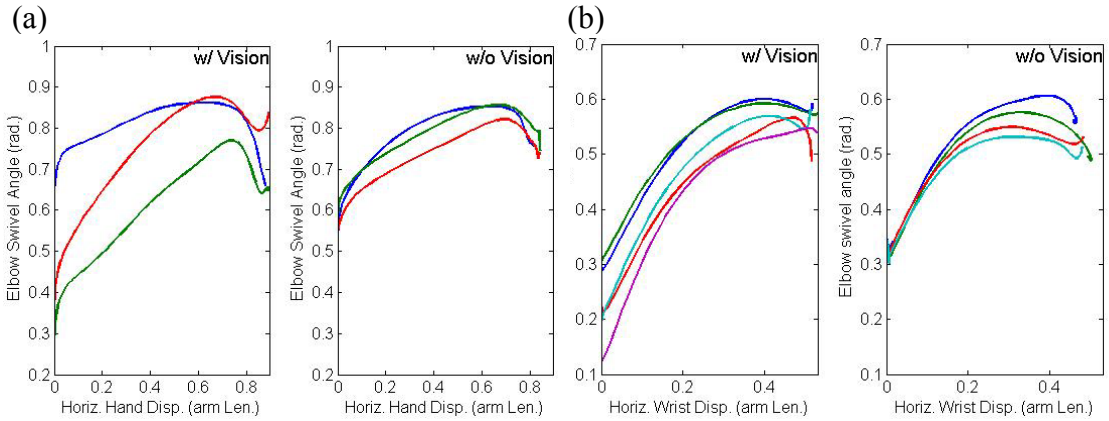

Figure 5.10. Typical examples of elbow swivel angle for reaches with and without visual feedback. Reaching to a) target location F5 (45º left), b) reaching to target location N2 (45º right) with the small object (trials from one subject data)

The 2-way ANOVA (Table 5.8) indicates that the magnitude and amplitude of ESA variations are both significantly influenced ($p < 0.01$) by the visual conditions. The magnitude of ESA change is larger with vision than without vision by 3.67° and 3.73° for reaches with the small and large object, respectively. The average amplitude of the ESA is 3.05° and 3.70° larger with than without vision for the small and larger object, respectively (Figure 5.11).

Table 5.8. 2-way ANOVA table of ESA's magnitude and amplitude

	Amplitude			Magnitude		
Small Obj.	DoF	F	p	DoF	F	P
Vision (V)	1	28.2	< 0.01	1	18.4	< 0.01
Target location (T)	7	34.9	< 0.01	7	1.8	0.08
V× T	7	0.24	0.97	7	0.47	0.85
Large Obj.	DoF	F	P	DoF	F	P
Vision (V)	1	17.9	< 0.01	1	11.2	< 0.01
Target location (T)	7	22.9	< 0.01	7	0.22	0.98
V× T	7	0.45	0.86	7	0.32	0.94

(Shaded cells correspond to significant values.)

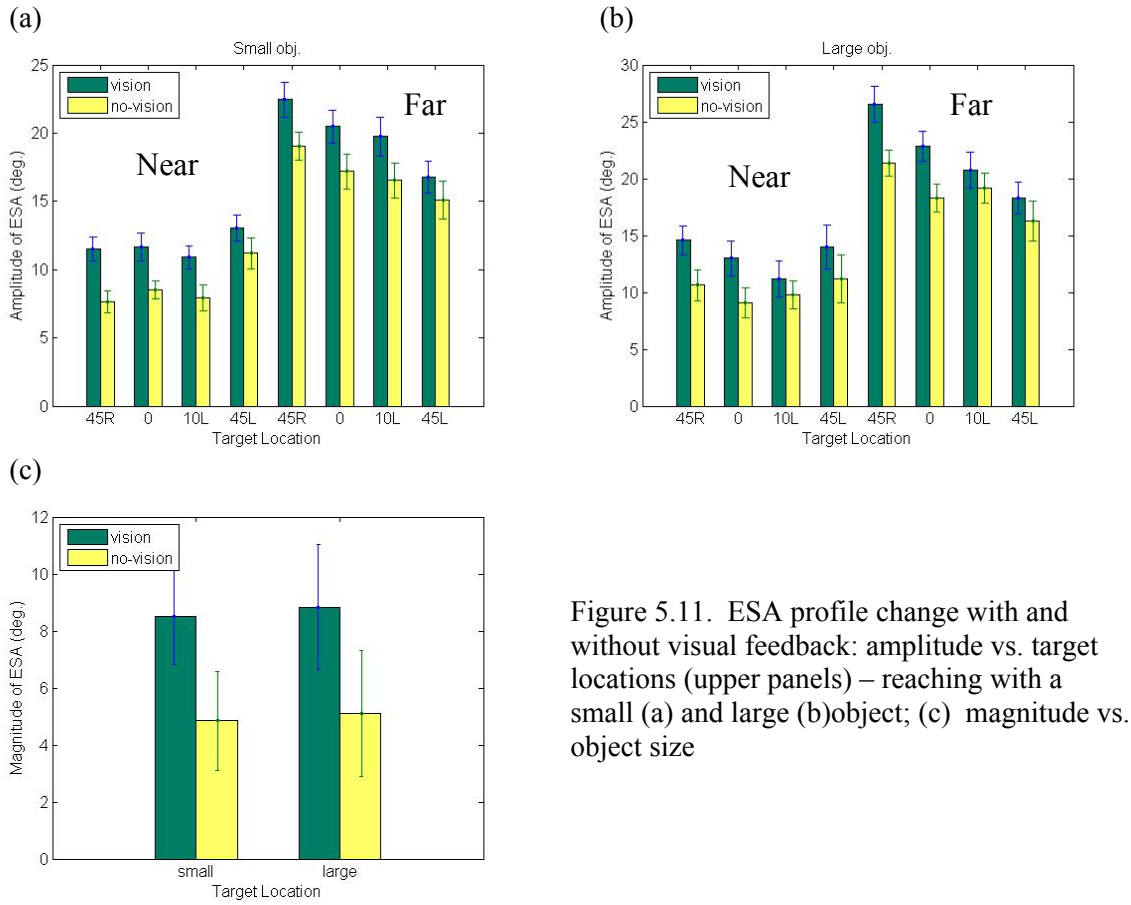

Figure 5.11. ESA profile change with and without visual feedback: amplitude vs. target locations (upper panels) – reaching with a small (a) and large (b)object; (c) magnitude vs. object size

5.5 Discussion

5.5.1 Reaching precision

The precision of the hand final position greatly depends on visual feedback. As may be expected, distal reaches (far set) also display higher constant errors in general and both constant and variable errors increase with the eccentricity of target azimuth. The ratio of constant errors for the near and far sets (5.14%/8.5% = 0.60) is similar to the ratio of corresponding reaching distances (0.8/1.2 arm length = 0.67). The discrepancy between right and left reaches also shows a ration of 0.58 between the far and near reaches. This may be associated with the scaling effect presented earlier.

The component analysis of the CE shows a larger contribution of the error to the lateral direction when reaching to the eccentric targets without vision. Furthermore, torso

axial rotations still present when reaching without vision. Hence it may be assumed that the egocentric coordinate system used for movement planning might be constrained to the original spatial mapping based on visual information and does not rotate to fit the specific goal when visual perception of space is unavailable. This interpretation is in accordance with Soechting and Flanders's proposition (1989), which suggests that reaching error occur because subjects implement a linear approximation to the transformation from extrinsic to intrinsic coordinates.

According to Van Beers et al. (2002), the central nervous system may use the visual information for determining the direction of reaching/pointing and proprioceptive information for controlling the movement distance, when the end effector is visible. However, the present work examining the dispersion of the final hand location shows an undershooting effect when reaching without visual feedback. It implies that the visual feedback also contributes to the control of movement distance.

Additionally, the movement undershoots were greater for far and eccentric targets than near and medial targets. Note that target locations corresponding to 0° and 10° left are in front of the shoulder and close to the front of the head. The undershooting behavior when visual information is not available suggest that the origin of the coordinate system in which the movement is planned is centered at the head while the origin of motor command designed when vision was available, remains centered at the shoulder when vision is no longer available.

5.5.2 Effect of visual feedback on body segment coordination

Torso angles (torso axial rotation, lateral bending and anterior flexion) show a significant consistency for both reaches with and without visual feedback. The variability of torso movement curves among repetitions shows no significant difference between two visual conditions. It implies that the CNS might try to reduce the level of body segment recruitment and maintain the system degree of freedom when visual feedback is not available. Movement correction may be limited in the absence of visual information in order to maintain reaching accuracy. Furthermore, only torso axial rotation and anterior flexion increase significantly with reaching distance, which reflects the contribution of the torso to reach movements. Hence, a similar motor command planned in the same

coordinate system might be used and maintained by the CNS when vision is unavailable for movement corrections.

The strategy adopted for movements without visual feedback may be designed to reduce the level of overall displacement of body segments. This limitation of joint movement amplitude may be used to reduce the level of coordination and control among body segments. Evidence can be found in the reduction of the elbow swivel angle magnitude, displacement and variability when reaching without vision. This strategy also reduces flexibility in arm movements, which may explain a compensatory increase in torso flexion in some reaches without visual guidance (see Figure 5.10).

In conclusion, coordination of body segments and control strategies might rely on the availability of feedback information. The precision of final reaching accuracy also greatly depends on visual feedback. Furthermore, the distribution of final position errors without visual feedback does not seem to be correlated with target azimuth relative to the shoulder. It is suggested that a frame of reference centered at the head might be used for reaching movements.

CHAPTER 6

Multi-phasic Coordination Model of Visually Guided Reach Movements to Frontal Targets

6.1 Abstract

Coordination of body segment in reach movements includes temporal and spatial aspects. Based on results related to the timing of body segment movement initiation and joint angular displacements, an upper body coordination model is proposed as an end effector driven, direction-based model for unconstrained reach movements to targets located in the frontal space. The temporal relationships are associated with visual feedback. For versatility and flexibility purposes, this model was developed in the normalized time domain defined by the total hand movement time. Based on empirical data, the proposed coordination model includes the visual feedback and generates temporally-coordinated body segments movements with respect to the visual acquisition of the target in the feed-forward control phase. Simulation of body segment movements is based on control theory. Simulation results are compared with empirical data to validate the model structure and outcomes associated with movement coordination features.

6.2 Introduction

Previous results suggested that the temporal and spatial behaviors of body segments in reaching tasks are generally context dependent (Chapter 2, 3, and 4). It has been also suggested that body segment movements might use pre-planned postures to achieve accurate gaze orientation, spatial representation of target location and movement sequencing in reach movements (Rossenbaum et al., 1995; Kim, 2005). Furthermore,

visual feedback may influence the organization body segment movements in reach activities (Chapter 5; Soechting et al., 1990; Admiraal et al., 2003).

In the present work, reach movements were divided into three phases relative to the visual information about the target to be reached. The first phase, or lift-off phase, is defined as the portion of movement before gaze reaches the target. Most joints movements are initiated during this phase in general (Chapter 2), but may not have a specific directional content (Kim, 2005). Then the transport phase is initiated when gaze is on target (GOT). Following the transport phase is the landing phase when the end-effector is within the foveal field of view and gaze remains on the target.

Reach movements have been characterized by a process including two successive control modes consisting of a feed-forward phase followed by a slow feedback phase (Jeannerod, 1984; Woodworth, 1899). The first two phases are generally assumed to use a feed-forward (open-loop) control mechanism since visual feedback of body segment is rarely available during these two phases and velocity profiles do not reveal corrections (Abend et al., 1982; Hoff & Arbib, 1993). During the landing phase, the hand is close to the target and within the foveal field of view. Hence, visual and/or proprioceptive feedback may then be used to adjust the movement trajectory. Previous studies indicated that foveal vision is used for the end-point control taking place in the final phase of movements (Paillard, 1996), and visual information of both the target and the hand can provide an exocentric (work space) frame of reference (Sober & Sabes, 2003). However, the landing phase represents only a small proportion (less than 10%) of a whole reach movement time (Chapter 3). The coordination model proposed in the present study focuses on the movement organization during the first two phases governed by feed-forward control only.

As stated in Chapter 2, a straightness error of less than 12% for targets in the ± 45° range about the sagittal plane lead to the assumption that reach movements along these directions could be considered fairly straight in the horizontal plane. In addition, the hand movement velocity presents consistent bell shapes and sinusoidal profiles in the horizontal and vertical directions, respectively. These results are in agreement with previous results (Morasso, 1981, Abend, 1982) suggesting that humans tend to choose unique trajectories with a fairly straight and smooth path. Furthermore, a movement

scaling effect (Plamondon et al., 1995; Grinyagin et al., 2005, Srinivasan, 2009) is observed in the horizontal plane. This scaling is indicated by a time-to-peak to total movement time (TP/MT) ratio of 0.5 for close and far similar targets, as presented in Chapter 3. The peak velocity in the horizontal plane occurs in the middle of the total movement time (MT) of the hand. These results provide the basis to model a generalized hand movement trajectory as a reference for the coordination model.

6.3 Methods

Based on the previous studies and observation from experimental data (Figure 6.1), a generalized hand trajectory can be determined with a bell-shaped and sinusoidal velocity profiles in the horizontal plane and vertical direction, respectively. The generalized hand trajectory is used as a reference for temporal modeling and for the correlation between hand traveling distance and time.

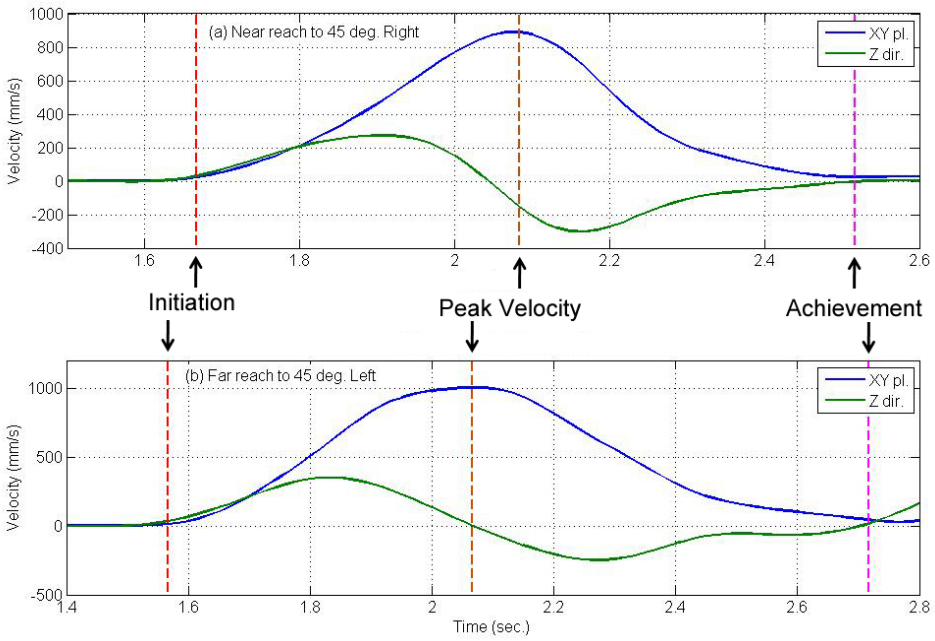

Figure 6.1. Typical example of the hand velocity profiles. Near (a) and far (b) reaches to ± 45º azimuth targets.

Given τ a time factor which normalizes MT to 2π, the proposed coordination model may be expressed in the normalized time domain (τ). The goal of the proposed coordination model is to describe and predict the temporal-coordinated upper body segment movements during the feed-forward control mode of reach movements. This model is based on results obtained in the previous studies and is driven by a generalized hand trajectory. The position of the elbow can therefore be derived from inverse kinematics and the swivel angle model (Chapter 4) while the position of the shoulder is derived from torso movements.

The timing sequence of initiation and termination of body segment movements are relative to the timing of gaze on target (GOT). Hence, this model can be expressed in the normalized time domain. For the spatial aspect, body segment movements are modeled based on the response of a feed-forward control mechanism. Currently, the proposed coordination model simulates the feed-forward phase of reaches beyond the anatomical frontal plane.

6.3.1 Model components

Figure 6.2 shows the structure of the proposed coordination model. The input of the model is target location (azimuth and distance). In the proposed coordination model, the hand trajectory, temporal and spatial modules are the three major components. First the hand trajectory module generates a generic hand movement model in the normalized time domain. This model provides a reference for the total movement (MT) time and the hand travel distance. Then the temporal module determines the GOT, the initiation and duration of each torso angle profile and the elbow swivel angle profile, as a function of the stated input. Furthermore, the spatial module determines the angular displacements of torso angles (axial rotation, lateral bending, and flexion) and the elbow swivel angle as a function of the movement duration and the specified target.

When combining the results of the temporal and spatial modules, the outputs of the coordination model are determined in the normalized time domain. These outputs are:

1) The timing of gaze-on-target (GOT).
2) The generalized hand trajectory represented by the horizontal and vertical components.

3) The initiation time, durations, and angular displacement of the torso axial rotation, lateral bending, and flexion angles.
4) The initiation and displacement of the elbow swivel angle.

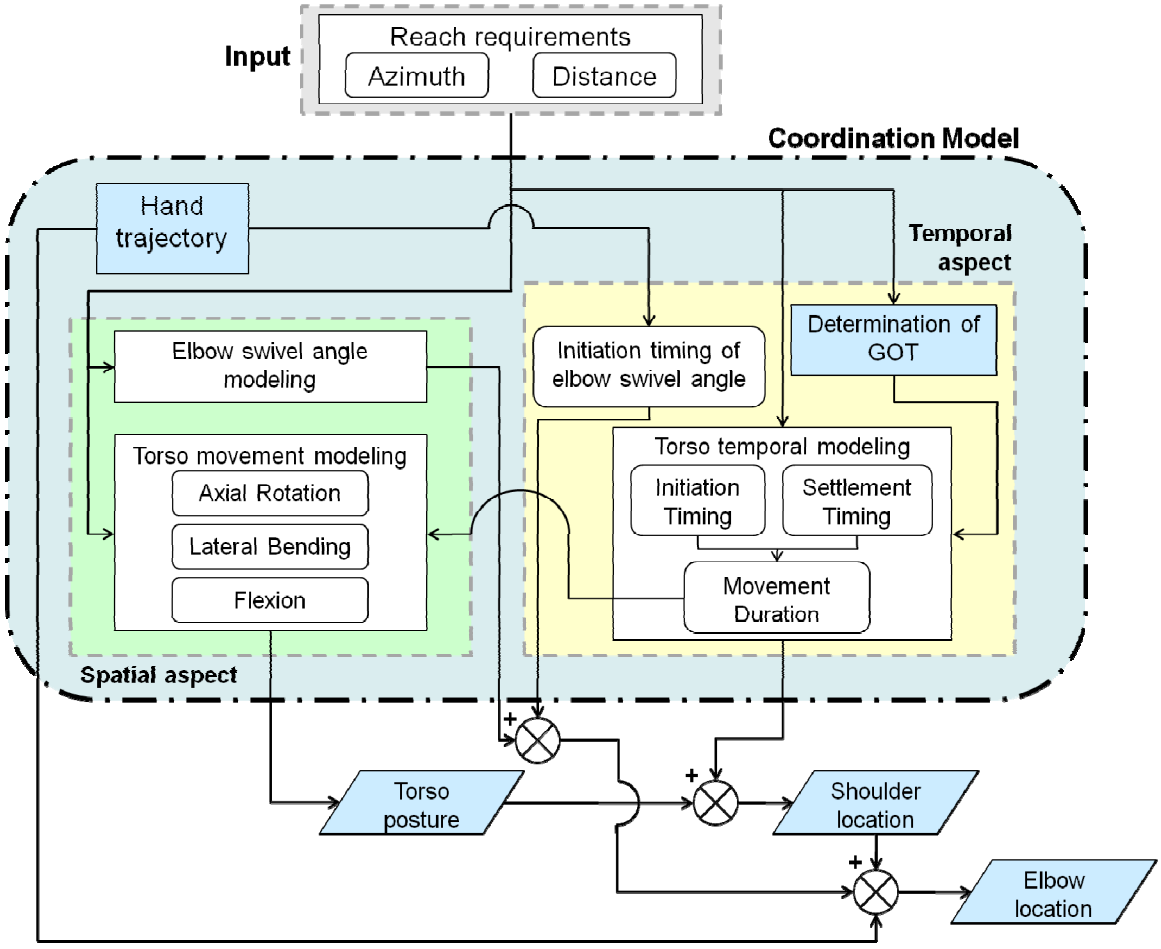

Figure 6.2. Diagram of the coordination model scheme

6.3.2 Correlation between the hand traveling distance and movement time

Since the temporal modeling is relative to the total movement time, the kinematics of the hand movement needs to be generalized to facilitate modeling. The hand movement trajectory is assumed to be planar and may be decomposed into a vertical component and the horizontal component associated to an azimuth. Given τ as a time factor which normalizes MT to 2π, the generalized hand trajectory model can therefore be expressed in the normalized time domain (τ). Since the TP/MT ratio is equal to 0.5, the

horizontal peak velocity of the modeled hand trajectory occurs at of the mid duration of MT. Therefore, the velocity in the horizontal (v_{xy}) and vertical direction (v_z) at the time t during a reach movement can therefore be expressed as a function of the normalized time factor as below:

$$v_{xy} = A_{xy} \sin(\frac{\tau}{2}) = A_{xy} \sin(\frac{\pi}{T}t) \qquad \text{(Eq. 6.1)}$$

$$v_z = A_z \sin(\tau) = A_z \sin(\frac{2\pi}{T}t) \qquad \text{(Eq. 6.2)}$$

where τ denotes the normalized time factor and $\tau = \frac{2\pi t}{T}$; T denotes MT, while A_{xy} and A_z are the amplitude (peak velocity) of the horizontal and vertical velocity respectively.

Velocity profiles corresponding to $A_{xy} = 1$ and $A_z = 0.2$ are illustrated in Figure 6.3.

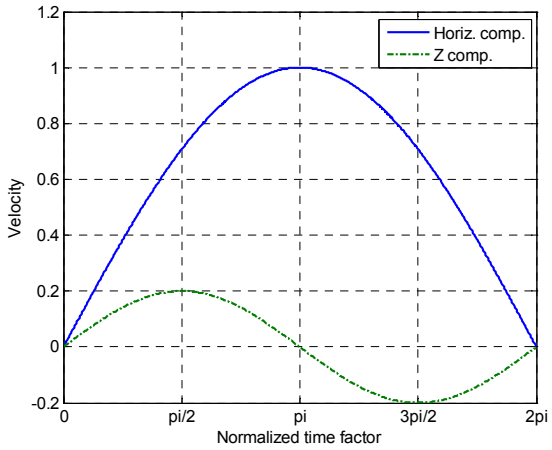

Figure 6.3. Generalized velocity profiles corresponding to the horizontal and vertical components of a hand movement in the normalized time domain.

Hand displacements in the horizontal and vertical directions can be determined by the time integration of Eq. 6.1 and Eq. 6.2:

$$d_{xy} = -A_{xy} \frac{T}{\pi} \cos(\frac{\pi}{T}t) + C_{xy} \qquad \text{(Eq. 6.3)}$$

$$d_z = -A_z \frac{T}{2\pi} \cos(\frac{2\pi}{T}t) + C_z \qquad \text{(Eq. 6.4)}$$

where C_{xy} and C_z are constants. Given the initial condition $d_{xy}\big|_{t=0} = d_z\big|_{t=0} = 0$, C_{xy} and C_z may be determined as follow:

$$C_{xy} = A_{xy}\frac{T}{\pi} \quad ; \quad C_z = A_{xy}\frac{T}{2\pi}$$

Hence, Eq. 6.3 and Eq. 6.4 can be expressed as

$$d_{xy}(t) = A_{xy}\frac{T}{\pi}\left(1-\cos(\frac{\pi}{T}t)\right) \qquad \text{(Eq. 6.5)}$$

$$d_z(t) = A_z\frac{T}{2\pi}\left(1-\cos(\frac{2\pi}{T}t)\right) \qquad \text{(Eq. 6.6)}$$

When a reach is achieved at time t = T, the horizontal displacement, $d_{xy}(t=T)$, equals the total hand traveling distance D_{xy}. Hence, the amplitude A_{xy} can be obtained by:

$$d_{xy}(t=T) = A_{xy}\frac{T}{\pi}\big(1-\cos(\pi)\big) = 2A_{xy}\frac{T}{\pi} = D_{xy}$$

$$\Rightarrow\ A_{xy} = \frac{\pi}{2}\frac{D_{xy}}{T}$$

In addition, the maximum vertical displacement (D_z) is reached when time t = T/2. The amplitude A_z can also be found by:

$$d_z(t=\frac{T}{2}) = A_z\frac{T}{2\pi}\big(1-\cos(\pi)\big) = A_z\frac{T}{\pi} = D_z$$

$$\Rightarrow\ A_z = \pi\frac{D_z}{T}$$

Substituting A_{xy} and A_z into the equations of hand displacements, Eq. 6.3 and Eq. 6.4 can be rewritten as:

$$d_{xy} = \frac{D_{xy}}{2}\left(1-\cos(\frac{\pi}{T}t)\right) = \frac{D_{xy}}{2}\left(1-\cos(\frac{\tau}{2})\right) \qquad \text{(Eq. 6.7)}$$

$$d_z = \frac{D_z}{2}\left(1-\cos(\frac{2\pi}{T}t)\right) = \frac{D_z}{2}\big(1-\cos(\tau)\big) \qquad \text{(Eq. 6.8)}$$

Eq. 6.7 and Eq. 6.8 are used to describe a generalized hand trajectory with a bell-shaped velocity profile in a 2-D plane. Furthermore, the relationship between the fractional hand traveling distance and the percentage of movement time (% MT) can be obtained from the equation of the hand horizontal displacement (Eq. 6.7) as follows:

$$\frac{d_{xy}}{D_{xy}} = \frac{1}{2}\left(1 - \cos(\pi \frac{t}{T})\right) \quad \text{(Eq. 6.9)}$$

$$\frac{t}{T} = \frac{1}{\pi}\cos^{-1}(1 - \frac{2d_{xy}}{D_{xy}}) \quad \text{(Eq. 6.10)}$$

These two equations are used to convert the movement from normalized time domain to kinematic (hand traveling distance) domain.

6.3.3 Lift-off phase

The instant at which the gaze is on-target (GOT) was assumed to correspond to the termination of the lift-off phase. It serves as an indicator to the transition from the lift-off to the transport phase. From Chapter 3, the lift-off phase percentage of MT is modeled as a function of target location. It can be expressed as:

$$P_t^{Far} = 0.0035\theta^2 + 0.0055\theta + 9.16$$
$$P_t^{Near} = 0.0035\theta^2 + 0.0302\theta + 15.42 \quad \text{(Eq. 3.2)}$$

where θ represents the target azimuth angle (in degree).

Therefore, the instant of GOT in the normalized time domain τ can also be determined as a function of the target location by:

$$\tau_{GOT} = 2\pi \frac{t_{GOT}}{T} = 2\pi P_t^{Far/Near}(\theta) \quad \text{(Eq. 6.11)}$$

Torso angle initiation timing

In Chapter 2, the initiation timings of joint angles were determined relatively to the GOT. Thus, the initiation of torso movements, represented by three angles can be determined for a given GOT instant.

As shown by the results in section 2.4.4, the initiation timings of torso angles are significantly influenced by target distance and azimuth. The results are summarized in Table 2.10. The negative sign indicates an initiation prior to GOT.

Table 6.1. Torso initiation timing

	Rear left			Frontal (45º left – 45º right)			Rear right		
% MT	AR	LB	AF	AR	LB	AF	AR	LB	AF
Far	-51.9%	-19.8%	-42.7%	-23%	-19.8%	-5.6%	-35.4%	-19.8%	-42.7%
Near			-60.5%			-18.2%			-60.5%

AR: Axial Rotation; LB: Lateral Bending; AF: Anterior Flexion

Combining the GOT (Eq. 6.11) and torso initiation timing (Table 2.10), the initiation timing for each torso angle for frontal reaches in the normalized time domain can be determined by:

$$\tau_{AR}^{Init.} = \tau_{GOT} - 2\pi \frac{t_{AR}^{Init.}}{T} = 2\pi(P_t^{Far/Near}(\theta) - 0.23) \qquad \text{(Eq. 6.12)}$$

$$\tau_{LB}^{Init.} = \tau_{GOT} - 2\pi \frac{t_{LB}^{Init.}}{T} = 2\pi(P_t^{Far/Near}(\theta) - 0.198) \qquad \text{(Eq. 6.13)}$$

$$\tau_{AF}^{Init.Far} = \tau_{GOT} - 2\pi \frac{t_{AF}^{Init.Far}}{T} = 2\pi(P_t^{Far}(\theta) - 0.056)$$
$$\tau_{AF}^{Init.Near} = \tau_{GOT} - 2\pi \frac{t_{AF}^{Init.Near}}{T} = 2\pi(P_t^{Near}(\theta) - 0.182) \qquad \text{(Eq. 6.14)}$$

If a body segment was initiated before the hand movement initiation, the timing as negative value in the normalized time domain. If necessary, the origin of the normalized time axis may be shifted to the earliest initiating time among all torso angles. As long as the initiation timing for the hand and GOT are shifted accordingly, the performance of the coordination model would not be affected.

6.3.4 Torso movement and temporal modeling

The duration of the respective movements also needs to be determined. The termination time, or stop time (ST), is used to denote the time at which each torso angle reaches a final value. From the experimental data collected earlier (Chapter 2), the torso STs were determined for each angle by using a 98% threshold of the total angular changes during the reach movement, and were represented by the percentage of MT

relative to the GOT. The results of the two-way ANOVA determining the influences of target azimuth and distance on STs are shown in Table 6.2. Figure 6.4 shows the duration of the torso angle movements, which were determined by the respective initiation and termination times with respect to the GOT instant.

Table 6.2. ANOVA table corresponding to torso angles termination time

Torso joints	Axial Rotation			Lateral Bending			Anterior Flexion		
	DoF	F	p	DoF	F	p	DoF	F	p
Azimuth	5	39.99	< 0.01	5	10.88	< 0.01	5	15.6	< 0.01
Distance	1	10.46	< 0.01	1	11.26	< 0.01	1	16.6	< 0.01
Azim. × Dist.	5	0.79	0.56	5	3.96	< 0.01	5	1.04	0.40

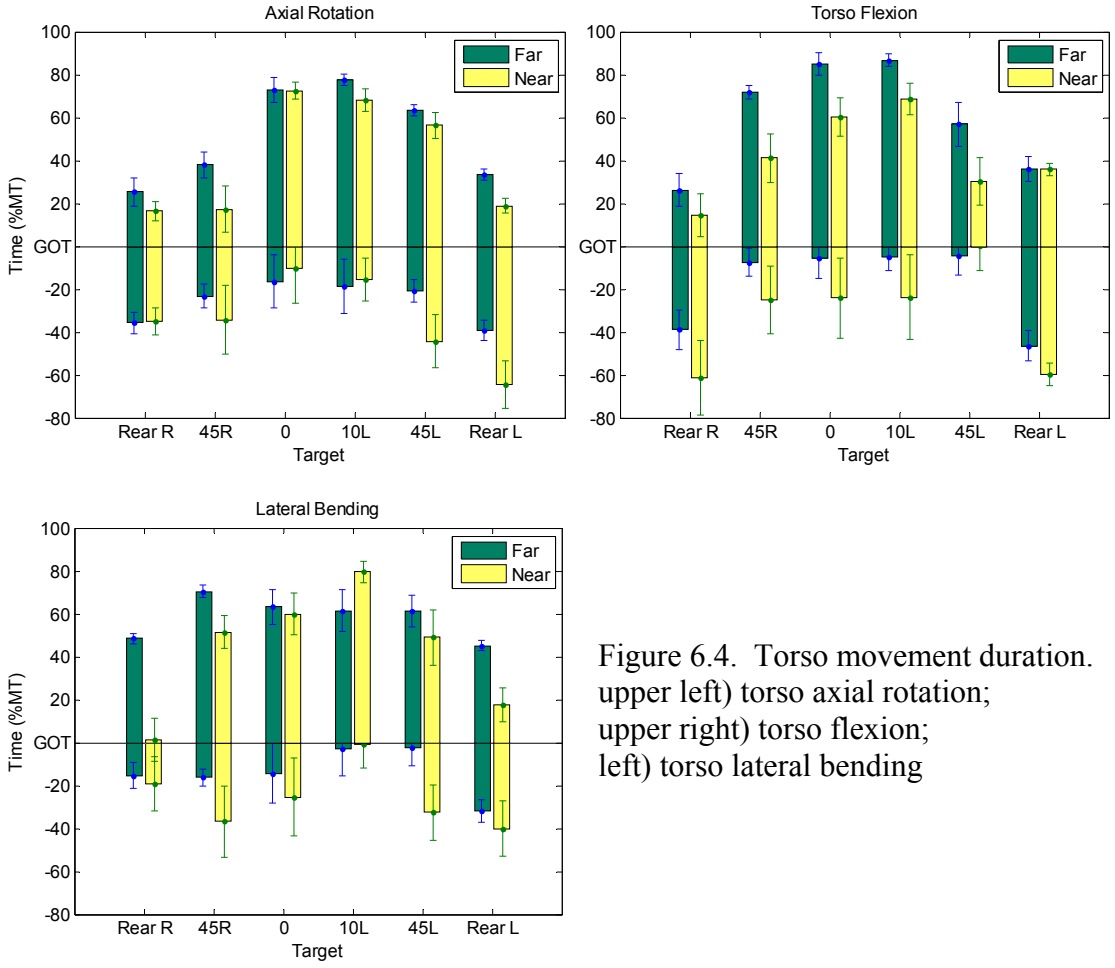

Figure 6.4. Torso movement duration.
upper left) torso axial rotation;
upper right) torso flexion;
left) torso lateral bending

Tukey's honestly significant difference criterion was used to do the compare the effects of target azimuths with the same distance on the termination time for each torso angle. The result shows that torso lateral bending only shows differences between rear and frontal reaches. For the frontal reaches, there is no significant influence of distance ($p < 0.05$). For the frontal reaches, the average termination timing of lateral bending is 62% MT after GOT.

For the torso axial rotation and flexion angles, parabolic distribution trends are observed for the average termination time as a function of target azimuth (Figure 6.4). Hence, the termination time of these two torso angles were modeled by 2nd-order functions. In addition, there is no significant difference ($p > 0.05$, HSD test) between the termination time for the 0º and 10º degree left reaches. Since the frame of reference for movement planning was suggested to be centered at the head (Chapter 5), data corresponding to the 10º left target were used to represent medial reaches for modeling the termination time of torso axial rotations and anterior flexions. The least square regression models of the termination time are represented by Eq. 6.15, Eq. 6.16 and Figure 6.5.

$$ST_{AR}^{Far} = -0.0037\theta^2 + 0.0870\theta + 65.59$$
$$ST_{AR}^{Near} = -0.0037\theta^2 + 0.0902\theta + 53.40 \quad \text{(Eq. 6.15)}$$

$$ST_{AF}^{Far} = -0.0048\theta^2 + 0.0121\theta + 78.22$$
$$ST_{AF}^{Near} = -0.0024\theta^2 + 0.0683\theta + 48.19 \quad \text{(Eq. 6.16)}$$

where θ represents the target azimuth angle (in degree), subscript AR and AF stand for torso axial rotation and anterior flexion respectively. The dimension of the models is the percentage of MT (% MT).

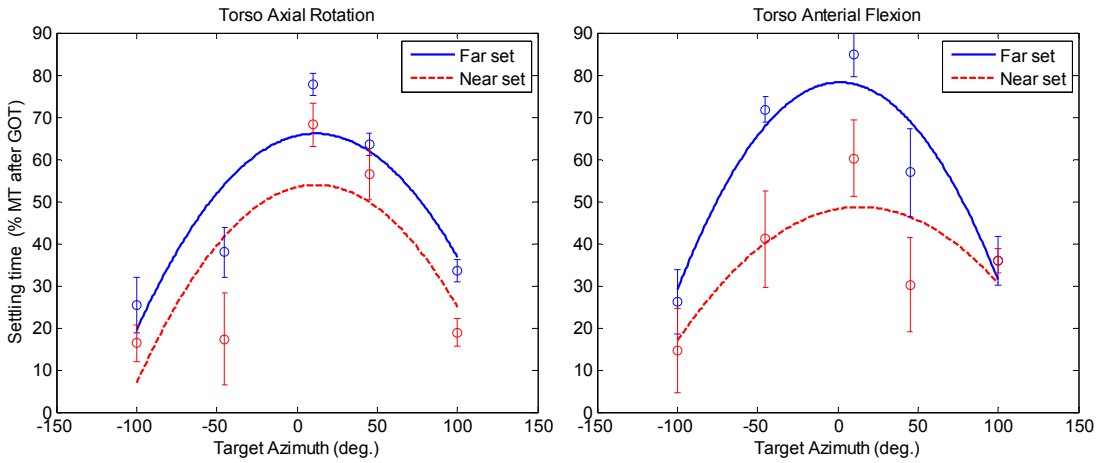

Figure 6.5. Regression models for torso termination times of torso axial rotation (left) and torso flexion (right).

Given the modeled torso termination time (an average for lateral bending, and Eq. 6.15 and Eq. 6.16 was determined relative to the GOT, the instant at which each component of the torso movement ends for frontal reaches in the normalized time domain can be determined by:

$$\tau_{AR}^{Term.} = \tau_{GOT} + 2\pi ST_{AR}^{\ Far} = 2\pi(P_t^{Far/Near}(\theta) + ST_{AR}^{Far/Near}(\theta)) \qquad \text{(Eq. 6.17)}$$

$$\tau_{LB}^{Term.} = \tau_{GOT} + 2\pi \frac{t_{LB}^{Term.}}{T} = 2\pi(P_t^{Far/Near}(\theta) + 0.62) \qquad \text{(Eq. 6.18)}$$

$$\tau_{AF}^{Term.} = \tau_{GOT} + 2\pi ST_{AF}^{\ Far} = 2\pi(P_t^{Far/Near}(\theta) + ST_{AF}^{Far/Near}(\theta)) \qquad \text{(Eq. 6.19)}$$

By combining these results with the initiation time expressed in Eq. 6.12 to Eq. 6.14, the duration of these torso angular movements (T_φ) can be expressed as:

$$\begin{aligned} T_{AR} &= \tau_{AR}^{Term.} - \tau_{AR}^{Init.} \\ &= 2\pi\left(P_t^{Far/Near}(\theta) + ST_{AR}^{Far/Near}(\theta) - (P_t^{Far/Near}(\theta) - 0.23)\right) \\ &= 2\pi\left(ST_{AR}^{Far/Near}(\theta) + 0.23)\right) \end{aligned} \qquad \text{(Eq. 6.20)}$$

$$\begin{aligned} T_{LB} &= \tau_{LB}^{Term.} - \tau_{LB}^{Init.} \\ &= 2\pi\left(P_t^{Far/Near}(\theta) + 0.62 - (P_t^{Far/Near}(\theta) - 0.198)\right) \\ &= 2\pi\left(0.818\right) \end{aligned} \qquad \text{(Eq. 6.21)}$$

$$T_{AF} = \tau_{AF}^{Term.} - \tau_{AF}^{Init.}$$
$$= \begin{cases} 2\pi\left(ST_{AF}^{Far}(\theta) + 0.056\right) & \text{for the far reaches} \\ 2\pi\left(ST_{AF}^{Near}(\theta) + 0.182\right) & \text{for the near reaches} \end{cases} \quad \text{(Eq. 6.22)}$$

6.3.5 Body segment movements in the feed-forward control phase

The joint angle variations of the body segment movements, such as the torso and arm, need to be determined for the computed movement times. The elbow swivel angle movement is determined by the first-order lag response proposed in Chapter 4, and the angular displacement of the torso axial rotation, lateral bending and flexion angles are used in combination with the response of a feed-forward control to determine the movement and position of body segments during reach movements.

Elbow swivel angle

Given the initial posture, the elbow angle is 90° and the hand is in a starting location in front of the shoulder, the initial value of the elbow swivel angle is zero. Hence, the initial condition for the modeled ESA is set to zero to be consistent with the experimental condition. The ESA (Chapter 4) is modeled as a function of the fractional hand traveling distance (x) as follows:

$$S(x) = A(1 - e^{-kx})$$
$$x = \frac{d_{xy}}{D_{xy}} : \text{fractional hand traveling distance} \quad \text{(Eq. 4.1)}$$

where A denotes the amplitude of the elbow swivel angle and k denotes the gain of the arm system. As shown in Table 6.3, these two coefficients are functions of the target location.

Table 6.3. Estimated parameters for ESA modeling

		45º right	0º front	10º left	45º left
A	Far	0.51	0.47	0.48	0.50
	Near	0.35	0.39	0.40	0.53
k	Far	2.53	3.47	4.68	2.83
	Near	1.84	1.49	1.19	2.04

For frontal reaches, the coefficient A does not vary significantly with target azimuth for far targets. Hence, the average value 0.49 is used for far reaches. However, for near reaches, A is different for left and right reaches. Hence, A is set to be 0.38 and 0.53 for medial- right and left reaching, respectively. The gain of the model (coefficient k) varies as a function of target location. A 2nd-order parabolic curve was used to fit k as a function of target azimuth (θ) for the far and near set, respectively, as follows (see Figure 6.6):

$$k^{Far} = -0.0007\theta^2 + 0.0049\theta + 4.0689 \qquad \text{(Eq. 6.23)}$$

$$k^{Near} = 0.0003\theta^2 + 0.0018\theta + 1.3203 \qquad \text{(Eq. 6.24)}$$

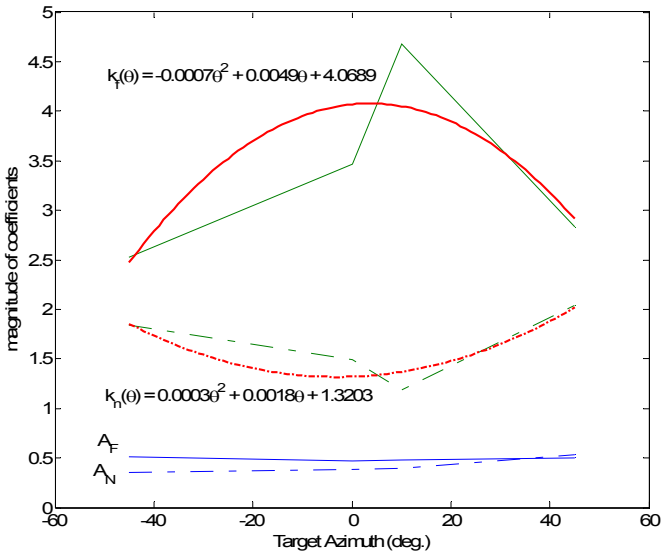

Figure 6.6. Coefficients for ESA modeling. Solid and dash lines correspond to the far and near target sets, respectively.

Since the proposed coordination is modeled in the normalized time domain, the ESA model needs to be converted using Eq. 6.9 to be expressed in the normalized time domain as well:

$$S(\tau) = A(1 - e^{-k\frac{d_{xy}}{D_{xy}}}) = A(1 - e^{-\frac{k}{2}\left(1-\cos(\pi\frac{t}{T})\right)}) = A(1 - e^{-\frac{k}{2}\left(1-\cos(\frac{\tau}{2})\right)}) \qquad \text{(Eq. 6.25)}$$

where A is 0.49, 0.38 and 0.53 for all reaching in the far set, the medial-right and left reaching in the near set, respectively.

Given a generalized hand trajectory and corresponding shoulder location, the movement and position of the elbow may be derived from inverse kinematics and the elbow swivel angle profile model.

Kinematic modeling of Torso movements

From the experimental results presented in section 2.4.3, the torso axial rotation may be represented by a quasi-linear function of target azimuth for both target distances; while the lateral bending and flexion are quasi-linear as a function of the target azimuth for the far frontal reaches. Since torso lateral bending and flexion were negligible for near reaches, these two torso angles are set to 0 for these reaches. In any case, the angular displacements of the axial rotation (φ_{AR}), lateral bending (φ_{LB}) and flexion (φ_{AF}) for the far and near set may be expressed as a function of target azimuth, θ (in degree) as follows:

$$\begin{aligned} \phi_{AR}^{Far} &= 0.45\theta + 23.8 \\ \phi_{AR}^{Near} &= 0.32\theta + 10.1 \quad \text{(unit: deg.)} \end{aligned} \qquad \text{(Eq. 6.26)}$$

$$\begin{aligned} \phi_{LB}^{Far} &= -0.27\theta + 1.7 \\ \phi_{LB}^{Near} &= 0 \quad \text{(unit: deg.)} \end{aligned} \qquad \text{(Eq. 6.27)}$$

$$\begin{aligned} \phi_{AF}^{Far} &= -0.11\theta + 10.9 \\ \phi_{AF}^{Near} &= 0 \quad \text{(unit: deg.)} \end{aligned} \qquad \text{(Eq. 6.28)}$$

The trajectories present the characteristic response of a symmetric bang-bang control (Carlton, 1981) in general (Figure 6.7). For the torso joint angular movements, it is assumed that the magnitudes of acceleration for the first and second half of the movement are the same constant, but with opposite signs. Acceleration occurs in the first half while the second half corresponds to a deceleration.

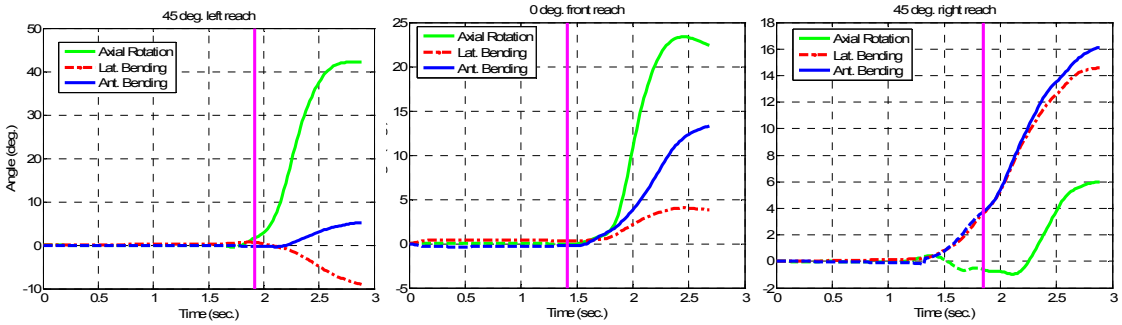

Figure 6.7. Examples of torso angular movement during reaches. The vertical bar represents the GOT time.

Let constant K represents the magnitude of acceleration (or deceleration), T_φ the duration of torso movement in the normalized time domain, and the movement initiation time is zero. For a symmetric bang-bang control, acceleration can be expressed by:

$$\ddot{\phi}_1\Big|_{\tau=T_\phi/2}^{\tau=0} = K \quad and \quad \ddot{\phi}_2\Big|_{\tau=T_\phi}^{\tau=T_\phi/2} = -K$$

Integration of both sides of these equations with respect to the normalized time (τ) gives the velocity function for each period:

$$\dot{\phi}_1\Big|_{\tau=T_\phi/2}^{\tau=0} = K\tau + C_1 \quad and \quad \dot{\phi}_2\Big|_{\tau=T_\phi}^{\tau=T_\phi/2} = -K\tau + C_2 \qquad \text{(Eq. 6.29a)}$$

From the initial and final condition $\tau = 0$, $\dot{\phi}_1 = 0$ and $\tau = T_\varphi$, $\dot{\phi}_2 = 0$, then $C_1 = 0$ *and* $C_2 = KT_\phi$. Hence, Eq. 6.29a can be rewritten to be:

$$\dot{\phi}_1\Big|_{\tau=T_\phi/2}^{\tau=0} = K\tau \quad and \quad \dot{\phi}_2\Big|_{\tau=T_\phi}^{\tau=T_\phi/2} = -K(\tau - T_\phi) \qquad \text{(Eq. 6.29b)}$$

Integrating these equations with respect to τ gives the angular displacement function for each period:

$$\phi_1\Big|_{\tau=T_\phi/2}^{\tau=0} = \frac{1}{2}K\tau^2 + C_{11} \quad and \quad \phi_2\Big|_{\tau=T_\phi}^{\tau=T_\phi/2} = -\frac{1}{2}K\tau^2 + KT_\phi\tau + C_{21} \qquad \text{(Eq. 6.30a)}$$

From the initial condition $\tau = 0$, $\phi_1 = 0$, and the continuity of movement $\tau = T_\varphi/2$, $\phi_1 = \phi_2$, then C_{11} and C_{21} are obtained:

$$C_{11} = 0 \quad and \quad C_{21} = -\frac{KT_\phi^2}{4}$$

And the angular displacement (Eq. 6.30a) can be rewritten to be:

$$\phi_1\Big|_{\substack{\tau=0\\ \tau=T_\phi/2}} = \frac{1}{2}K\tau^2 \quad and \quad \phi_2\Big|_{\substack{\tau=T_\phi/2\\ \tau=T_\phi}} = -\frac{1}{2}K\tau\left(\tau - 2T_\phi\right) - \frac{KT_\phi^{\,2}}{4} \qquad \text{(Eq. 6.30b)}$$

The final (total) angular displacement is therefore achieved when substituting $\tau = T_\varphi$:

$$\phi_2(T_\phi) = \frac{KT_\phi^{\,2}}{4}$$
$$K = \frac{4\phi_2(T_\phi)}{T_\phi^{\,2}} \qquad \text{(Eq. 6.31)}$$

Based on a given total angular displacement for each torso angle described by Eq. 6.26 to Eq. 6.28, the magnitude of acceleration K (in Eq. 6.31) for each torso angle can be determined as a function of the target location. Given the initiation and termination time of the torso movement, the angular displacement of each torso angle can be respectively derived by Eq. 6.30b during reach movements.

6.4 Model implementation and simulation results

The proposed model was implemented in Matlab™ and simulated the temporal organization and movements of body segments and gaze as a function of the target to be reached. The computation time for the simulation of reach trial is, on average, less than 1 second when using a 3.6GHz clock speed Pentium® 4 class computer.

As illustrated by examples of the simulation results in Figure 6.8, the model predicts the torso axial rotation, lateral bending, flexion, and the elbow swivel angle along with the description of the generalized hand movement in the normalized time domain. The examples show that the model produces an early initiation of the torso angles for a far reach but not for the near reach as expected.

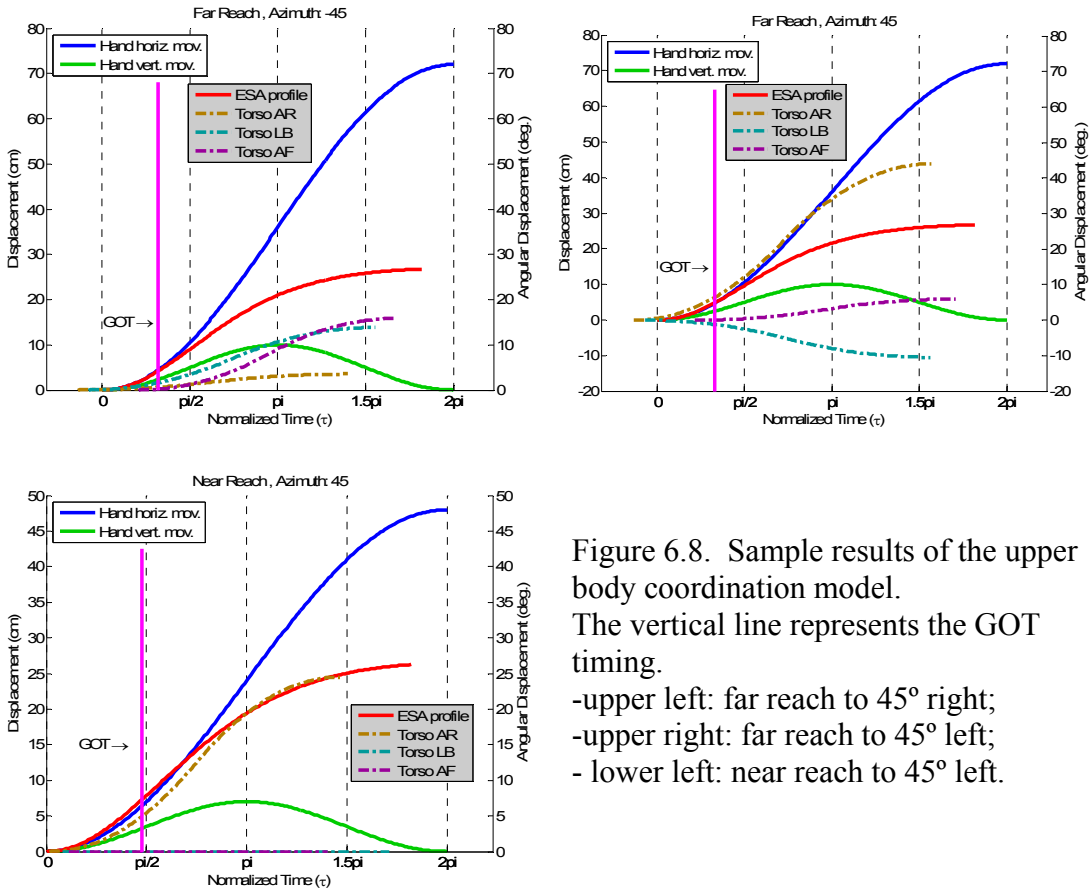

Figure 6.8. Sample results of the upper body coordination model.
The vertical line represents the GOT timing.
-upper left: far reach to 45º right;
-upper right: far reach to 45º left;
- lower left: near reach to 45º left.

The model predictions were compared to the empirical data obtained from a 26 year-old male participant (171 cm height with an arm length of 63 cm). The results corresponding to the 45º left far reach are presented in Figure 6.9. For this particular trial, the predicted time of GOT occurs slightly earlier than expected at 0.15 normalized time (1% MT, or 0.01 sec for this particular case).

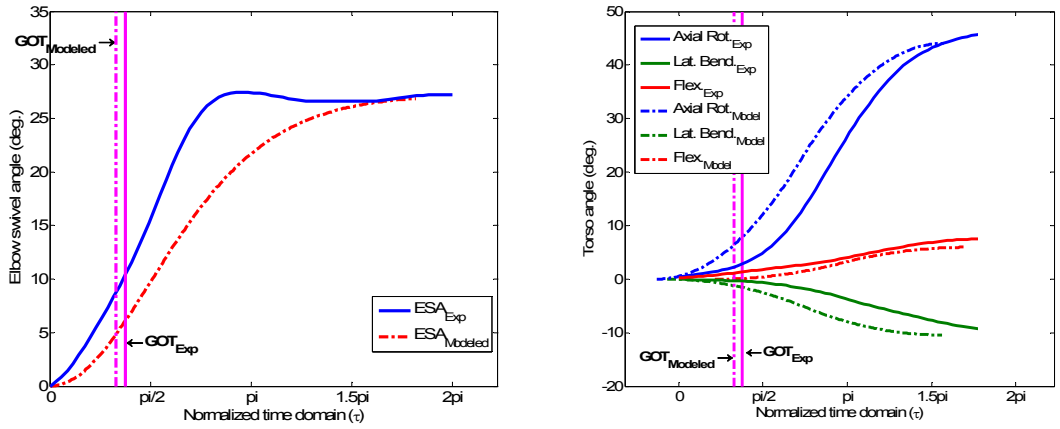

Figure 6.9. Comparison of model predictions and real data.
The vertical line represents the GOT time. left) elbow swivel angle; right) torso angles

The elbow swivel angle profile is barely underestimated (0.4°) by the model. For torso angular movements, the predicting curves are in agreement with empirical data. However, while the errors between the predicted and the empirical results are small for lateral bending (0.7º) and flexion1.7º, the error is 2.5º for axial rotation.

6.5 Discussion

Most movement models focus on the movement of the end-effector. Furthermore, these models have relied on optimization methods (Flash & Hogan, 1985; Kawato, 1992; Zhang et al., 1999; Torress & Zipser, 2002; Park et al., 2003). However, the overall organization of three-dimensional visually-guided reach movements does not necessarily rely on optimization within the context of unconstrained conditions (Feldman, 1986; Bizzi et al., 1992; Kim, 2005). The present coordination model uses a generalized hand movement to address the temporal modeling, and generates the movements of each upper body segment for the feed-forward phase along with the GOT instant as a function of target location. The preliminary comparison suggests that the prediction from the coordination model is reasonably good for the body segment kinematics and for the timing of visual acquisition of the target. However, the movement initiation for each joint angle is slightly anticipated when compared to experimental data. This early initiation may be due to the absence of a processing time delay after the GOT instant. A better

estimation of visual processing delay may be beneficial to improve the accuracy of the model.

Randomness in movement organization can be observed in both the coordination and the activities of the individual movement components. This might result either/or from the large variability of the human movement in temporal organization and noise of the sensorimotor system. Hence, the coordination of multiple movement phases and upper body subsystems may therefore vary slightly between individuals, depending not only on task requirements but also on individual characteristics. Since the proposed model is developed according to averaged empirical data, noise and individual differences are not reflected. The temporal organization of movement components may be further manipulated to exhibit a random behavior. A module may be developed to reflect the randomness and alternatives of reach movements. More specifically, different coordination patterns may be generated for each joint movement simulation by implementing a probability function in the initiation timings and total movement duration for each joint.

In the landing phase, which is governed by the feedback control, visual information about the position of the hand and spatial relationship between the target and the hand is available to guide the hand movements. Further movement refinement to achieve a certain level of precision is ensured by visual feedback. The current coordination model only covers the feed-forward phase with respect to the definition of movement control mode and the content of visual feedback. The coordination patterns in the landing phase need further investigation.

Nevertheless, the present coordination model can still provide the initial condition of each joint and body segment for the feedback control mode after the end of the transport phase. From the quantification of the feed-forward phase proportion (Chapter 4), the occurrence of the feedback phase is close to the end of reach movements and takes about 10% of the total movement time. Torso movements are usually over before the landing phase. Therefore, the initial condition for the torso is already determined for the feedback phase modeling. Only the shoulder and elbow movements require further modeling. It is also suggested that movement trajectories of each body segment in the

landing phase can be derived from existing inverse-kinematic control models (Dysart & Woldstad, 1996; Zhang, Kuo, and Chaffin, 1998; Wang, 1999; Kim, 2005).

CHAPTER 7

Summary and Conclusion

7.1 Principal Contributions

7.1.1 Movement control mode transition

Unconstrained three-dimensional (3D) reach movements can be divided into a series of movement phases. It has been reported that the final feedback phase contributes to movement accuracy (Crossman & Goodeve, 1983; Meyer et al., 1988) in which foveal vision is used for end-point control (Paillard, 1996). Therefore, gaze orientation was used to indicate phase transition in the present work. Hence, the characteristics and correlation between the visual information and the body segment movements were investigated.

In the present work, reach movements are hypothesized to consist of three movement phases which include the lift-off, transport and landing phases (Kim, 2005). The period of body segment movement preceding the instant at which gaze aims at a target is defined as the lift-off phase. From the experimental approach, the timing of gaze on target was quantified and modeled as a function of the target location (distance and azimuth). This result provides a basis to model the timing of body segment movements.

The transport phase, starting at the time of gaze on target, was ended when the hand approached the target. Since the major change from the transport phase to the landing phase is the transition of control mode, from feed-forward to feedback, it was found that the elbow swivel angle trajectory (ESA profile) presented a movement correction feature (curvature change) that could be used as an indicator of phase transition. The present work also shows that the determination of this phase transition

may not be only determined by the ESA profile kinematically but also by the availability of the visual information about the hand.

7.1.2 Temporal aspects of movement coordination with respect to visual feedback

It has been reported that torso angular movements are initiated almost simultaneously, but usually not end at the same time during a reach (Paillard & Amblard, 1985; Jeannerod, 1988). However, with the high-precision motion tracking techniques, the result from the present work reveals that the initiation time of each torso angle might not be the same. The sequence of initiation of torso movements defined by three angles is dependent on reaching goals. On the contrary, the sequence of initiation of the movement of the arm joints shows a consistent proximo-distal distribution in which the shoulder moves first, followed by the elbow.

A significant correlation between the initiation of torso angle movements and the time of gaze-on-target was observed. For torso angles (axial rotation, lateral bending and flexion), the initiation times always precede the time of gaze-on-target. This indicates that torso movements are consistently initiated during the lift-off phase. Since the visual information about the target location does not account for the initiation times of the torso angles for the frontal reaches, this result supports the preplanning of an initial open-loop control of the movement. The initiation strategy may be a general characteristic of human movement behavior since in the present context movement time was not constrained.

Furthermore, the duration of the lift-off phase is longer for eccentric than medial targets and may be described by a 2^{nd}-order least square regression function of the target azimuth. A longer lift-off phase may be associated with the a requirement of eye and head to bring the gaze on target, as suggested by Kim (2005) who showed that head movements are rarely present for medial target with azimuth less than 10°, while head movements are systematically present for target of eccentricity greater than 10°.

The temporal scaling effect of the end effector (hand) is in agreement with previous studies (Plamondon et al., 1995; Grinyagin et al., 2005). The present work shows that the ratio of time to peak velocity and total movement time is approximately 0.5. The magnitude of the peak velocity was found to be a function of target azimuth and distance in the context of unconstrained movements. These results also provide a basis to

model the time requirements (e.g. duration, acceleration time) associated with the bell-shaped velocity profile (Flash et al., 1985). The peak velocity model shows a more pronounced target azimuth effects for the near than far targets. The hand peak velocity is higher for reaches to near eccentric targets than medial targets. Under the context of unconstrained reach movement, the variation of velocity as a function of target azimuth may reflect a general characteristic of human movement. It may be possible that eccentric targets are perceived being further than the medial ones. The visual perception bias may result from the longer visual search time – as supported by the longer lift-off phase duration, and, as proposed in Chapter 5 as the egocentric reference of frame for movement coordination might be located at the head to be in concordance with the visual feedback. Hence, the distance bias resulting from the visual perception might induce a higher peak velocity in order to compensate a "perceived" longer reaching distance and maintain the total movement time almost constant.

Additionally, the sum of the durations of the lift-off and transport phases is not significantly influenced by target azimuth for frontal reaches. The results also indicate that about 90% of the total movement time corresponds to the feed-forward control mode for frontal reaches. Given that the duration of the lift-off phase increases with target eccentricity, this also suggests that the higher velocity for the more eccentric target might be preprogrammed in order to compensate for the longer lift-off phase. This result indicates that the feed-forward (open-loop) control mode of the movements is largely preprogrammed as a function of target azimuth. Hence, it is hypothesized that the programming of movement velocity may be derived from both the visual information and the necessary time to acquire that visual information

7.1.3 Role of visual feedback in movement coordination and control

Coordination of body segments and control strategies may depend on the availability of feedback information. The precision of the final reaching accuracy also greatly depends on visual feedback (McIntyre et al., 1998; Admiraal et al., 2004). Furthermore, the distribution of final position errors without visual feedback was observed to be correlated with target azimuth and distance relative to the shoulder. The manipulated object size is not significantly affecting the reaching precision.

According to Van Beers et al. (2002), the central nervous system may use the visual information for determining the direction of reaching/pointing and proprioceptive information for controlling the movement distance, when the end-effector is visible. However, the present work examining the dispersion of the final end effector location shows an undershooting tendency when reaching without visual feedback. As opposed to the proposition of Van Beers et al. this result implies that the visual feedback also contributes to the control of movement distance. In addition, the component analysis shows a larger contribution of the constant error (CE) to the lateral direction when reaching to the eccentric targets without vision. An interpretation of this behavior may be that the egocentric coordinate system for movement planning is constrained to the original spatial mapping and does not shift to fit a specific goal when the visual perception of the space is unavailable (Soechting and Flanders, 1989).

Previous studies suggest that the origin of the reference frame of human movement planning may be situated in between the shoulder and the head (McIntyre et al., 1997; Admiraal et al., 2003). However, it has also been proposed that movement direction is specified relative to an origin at the current location of the hand, while movement extent may be affected by the workspace learned during baseline movement experience (Sainburg et al., 2003). The error bias observed in the present study shows that the undershooting is smaller for reaches to the target in front of the head than the target in front of the shoulder when reaching without vision. This result leads to the hypothesis that the egocentric coordinate system may be centered at the head for reach movement planning and control. However, the origin of the egocentric coordinate system is not in contradiction with the movement direction based on the current hand location.

Movement planning seems to differ between visual conditions. The variability of torso movement between repetitions shows no significant difference between the two visual conditions. However, variations in the elbow swivel angle are significantly smaller without than with vision. This result may reflect an attempt to reduce the degrees of freedom (less flexibility/ higher constraint) in order to limit error variations and/or a drift in the error in the absence of vision. This hypothesis is in agreement with the demonstration that vision and the motor command are used to calibrate proprioception (Feldman and Latash, 1982), whose primary function is to correct movement errors while

vision is used to estimate movement distance (Bagesteiro et al., 2006). In addition, without vision the end–effector position errors drift with repetition (Brown et al., 2003), which also suggest the loss of an absolute reference (Gauthier et al. 1981). Hence, immediately after vision suppression movements may be replicated more systematically to avoid error dispersion.

7.1.4 Model of upper body coordination for reach movements

Kim (2005) reported that the global task goal (visually-guided reach movement) satisfies the fulfillment of each segment-specific goal (visual guidance and hand displacement). Hence, it would be of interest to understand how the CNS organizes the scheduling of activities to pursue these segment-specific movements in order to reach the desired target. The results of Chapter 2 show that the temporal initiation sequencing of joints and their relationship with gaze orientation are target goal dependent. Accordingly, it is suggested that the CNS would prioritize the activities of each subsystem and regulate their coordination so that the outcome of one subsystem (space representation) can effectively be used for the subsequent action (hand reach movement). Hence, coordinated movements among body segments and joints in a three-dimensional space should exhibit a correlation with the visual condition to generate a sequence of multiple phases corresponding to the activity of each individual subsystem and control mode.

The above hypotheses were used as the basis for a coordination model. The principle of the proposed coordination model for unconstrained three-dimensional movements was that the sequenced activities of each subsystem and movement phase are evaluated for a specific goal (target) in order to plan for the sequencing of gaze and joint movements. It was assumed that movement coordination during the initial and intermediate phases (the lift-off and transport phases) is direction-based and end-effector driven, and both phases are encoded in an egocentric reference frame.

Focusing on the first two movement phases (the lift-off and transport phases), which are governed by a feed-forward control mode, the proposed coordination model includes a temporal and spatial module to determine the sequencing and kinematic behaviors, respectively. With an input of the reaching target azimuth and distance, the proposed coordination model could provide the information about the sequencing of body

segment movements and the timing of gaze-on-target along with the angular displacement trajectories for the torso axial rotation, lateral bending, flexion and the elbow swivel angle. It currently works for the frontal reaches in the ±45º range relative to the saggital plane only.

7.1.5 Summary of contributions

In summary, the present work furthers the understanding of upper body coordination and movement control as follows:

1) For unconstrained reaching movements, the kinematic characteristics of the hand movements are a function of target azimuth and distance.
2) A new indicator of movement control mode transition was proposed and quantified as functions of target azimuth and distance.
3) Sequencing of arm joint initiation and the temporal characteristics of torso movements were modeled for unconstrained reach movements to frontal targets.
4) The role of visual feedback in multi-joint coordination of reach movements was preliminarily investigated and the movement planning strategies under no-vision condition attempt to reduce the system degree of freedom and to maintain/repeat more systematically the motor command learned with vision. In addition, the reference frame used to program movements seems to be centered at the head in the absence of vision.
5) A vision related movement coordination model of unconstrained three-dimensional reach movements was developed to predict the temporal coordination and kinematics of multiple subsystems.

7.2 Limitations of the present work

The proposed coordination model is developed based on empirical data collected from young healthy adults. Further study to different population, such as older

individuals, and neurologically or visually-impaired patients, is suggested to investigate different coordination patterns and compensation mechanisms.

The present study adopted a seated posture to eliminate postural instability and considered only movement planning of the upper extremities. However, reach movements in the standing or other postures might require the recruitment of more body segments and result in different coordination patterns. The end postures of the hand in the present study correspond only to supinated and neutral postures and did not require complex wrist movements. Different hand postures are likely to affect the elbow swivel angle, which needs to be investigated to complement the current coordination model.

The proposed coordination model for visually-guided reach movements is currently applicable to frontal reaches in the ± 45º range relative to the saggital plane and for the feed-forward control mode only. Validation of the model should be achieved by quantifying the predictions errors and the sensitivity to target azimuth, distance and elevation. In addition, it is suggested that the robustness of the model should be examined with a wide range of input conditions.

7.3 Future research directions

7.3.1 Validation and expansion of multi-phasic movement coordination

Based on the literature and findings of the present study, it may be proper to divide reach movements into three movement phases and two movement control modes. Nevertheless, the intrinsic attributes of each phase are remaining open debates. The purpose of the lift-off phase has not yet been clearly understood. In the present work, it was suggested that the lift-off phase may contribute to the preparation of movement. From this perspective, it is suggested that the lift-off phase prepare the hand to move in the direction of the target based on a cognitive mapping of the task space. This phase may also be used to calibrate proprioception to the initial condition of joint variables. Another aspect is that the lift-off phase may be used to "loosen" the inertia of body segments during the early phase of movements and elevate muscle tone for movement preparation. In any case, experimental evidence would be necessary to further support these hypotheses. From the same perspective, the selection of the control modes for each phase of reach movement is largely based on the gaze-body segment kinematic interaction. One way to further validate this hypothesis relative

to the transition of movement phases would be to conduct experiments in which visual feedback may be manipulated to interfere with its expected utilization. Hence, if visual information disappears when necessary, will that suppression trigger the re-initiation of a movement sequence?

The proposed coordination model is currently limited to the prediction of frontal reaches in the ± 45º range relative to the saggital plane. Although the proposed model requires only the definition of azimuth and distance and uses pre-defined hand kinematic information in the normalized time domain, a broader range of values for these two types of factors (target location and movement kinematics) would enable the expansion of the coordination model. For instance, a study covering a wider range of target azimuth to the side and rear locations is desirable to identify more specifically differences between front and rear movement directions and between left and right hemisphere in the frontal space.

7.3.2 Probabilistic model for movement variability

Randomness in movement organization can be observed in both the coordination and the activities of the individual movement components. This might result either/or from the large variability of the human movement in temporal organization and noise of the sensorimotor system. More specifically, different coordination patterns can be generated for each joint movement simulation by implementing a probability function affecting the scheduling of segment movements. Furthermore, the sensitivity to movement perturbations needs to be assessed. The interaction between body segments might result in a reorganization of coordination rather than individual segmental corrections. Hence such investigation would contribute to further understand the attribute of the coordination controller and movement control properties.

7.3.3 Movement coordination with external requirements

Simulation of feedback control (as observed in the landing phase) requires further development. Movement patterns may be influenced by external constraints. For example, reorganization of body segment coordination should be necessary when obstacles must be

avoided. In addition, some body segment movement might be limited and constrained in some situations, such as reaching with a safety belt, or reaching in a narrow space.

From the energy and momentum perspective, several different human movements were studied and simulated with a combination of simple muscle model and activation timings (Alexander, 1990, 1991). Optimization schemes have been used to model human movements. However, optimization may be the privilege of well-learned movements that may be based on the reduction of a cost function. It may be of interest to determine whether coordination of body segment movements could be also based on the optimization of a cost function, such as energy consumption or end effector trajectory smoothness.

Bibliography

Abend W., Bizzi E., Morasso P. (1982) Human arm trajectory formation. Brain 105:331-348.

Abrams R.A., Meyer D.E., Kornblum S. (1990) Eye-hand coordination: oculomotor control in rapid aimed limb movements. J Exp Psychol Hum Percept Perform 16(2):248–267.

Adamo, D., & Martin, B. (2009). Position sense asymmetry. Experimental Brain Research, 192(1), 87-95.

Admiraal, M. A. Keijsers, N. L. W., & Gielen, C. C. A. M. (2003). Interaction between gaze and pointing toward remembered visual targets. *Journal of Neurophysiology, 90*(4), 2136.

Admiraal, M. A., Kusters, M. J. M. A. M., & Gielen, S. C. A. M. (2004). Modeling kinematics and dynamics of human arm movements. *Motor Control, 8*(3), 312.

Alberts JL, Saling M, Adler CH, Stelmach GE (2000) Disruptions in the reach-to-grasp actions of Parkinson's patients. Exp Brain Res 134:353–362

America Heart Association Statistics Committee and Stroke Statistics Subcommittee (2006) Heart Disease and Stroke Statistics – 2006 update. Circulation 113:e85-151.

America Heart Association Statistics Committee and Stroke Statistics Subcommittee (2007) Heart Disease and Stroke Statistics – 2007 update. Circulation 115:e69-171.

Andersen, R. A. (1987). Inferior parietal lobe function in spatial perception and visuomotor integration. In: *Handbook of Physiology. The Nervous System. Higher Functions of the Brain.* Bethesda, MD: Am. Physiol. Sot., sect. 1, vol. V, pt 2, chapt. 12, p. 483-5 18.

Andrews, J.G., (1995). Euler's and lagrange's equations for linked rigid body models of three-dimensional human motion. In Allard, P., Stokes, I.A.F., Blanchi, J. (Eds.), Three-Dimensional Analysis of Human Movement Human Kinetics, Champaign, IL, pp. 145-175.

Ayoub, M.A., Ayoub, M.M., Walvekar, A.G., (1974). A biomechanical model for the upper extremity using optimization techniques. Human Factors 16, 585-594.

Bagesteiro LB, Sarlegna FR, Sainburg RL (2006) Differential influence of vision and proprioception on control of movement distance. *Exp Brain Res* 171: 358-370

Bastian A.J., Martin T.A., Keating J.G., Thach W.T. (1996) Cerebellar ataxia: abnormal control of interaction torques across multiple joints. J Neurophysiol 76:492–509

Bastian A.J., Zackowski K.M., Thach W.T. (2000) Cerebellar ataxia: torque deficiency or torque mismatch between joints? J Neurophysiol 83:3019–3030

Beer R.F., Dewald J.P.A., Rymer W.Z. (2000) Deficits in the coordination of multijoint arm movements in patients with hemiparesis: evidence for disturbed control of limb dynamics. Exp Brain Res 131:305–319

Bernstein N (1967). The coordination and regulation of movements. Pergamon, London

Bernstein N.A. (1996) Essay 6: on exercises and motor skill. In: Latash ML, Turvey MT (eds) Dexterity and its development. Lawrence Erlbaum, New Jersey, pp 171–205

Bizzi, E., Hogan, N., Mussa-Ivaldi, F. A. and Giszter, S. (1992). Does the nervous system use equilibrium-point control to guide single and multiple joint movements? Behavioral and Brain Sciences, 15, 603-613.

Brown LE, Rosenbaum DA, Sainburg RL (2003) Limb position drift: implications for control of posture and movement. *J Neurophysiol* 90: 3105-3118

Brown, S. H., & Cooke, J. D. (1981). Responses to force perturbations preceding voluntary human arm movements. *Brain Research*, *220*, 350–355.

Buneo CA, Boline J, Soechting JF, Poppele RE (1995) On the form of the internal model for reaching. Exp Brain Res 104:467–479

Burgess, P. R., Wei, J. Y., Clark, F. J., and Simon, J. (1982) Signaling of kinesthetic information by peripheral sensory receptors. Annu. Rev. Neurosci. 5: 171-187.

Calton, L. G. (1981). Movement control characteristics of aiming reponses, *Ergonomics*, 23, 1091-1032.

Carlton, L. G. (1981). Visual information: The control of aiming movements. Quarterly *Journal of Experimental Psychology*, 33A, 87-93.

Carnahan, H., & Marteniuk, R. G. (1991). The temporal organization of hand, eye, and head movements during reaching and pointing. *Journal of Motor Behavior*, *23*(2), 109-119

Castiello U (1997) Arm and mouth coordination during the eating action in humans: a kinematic analysis. Exp Brain Res 115:552–556

Castiello U, Bennett K.M.B. (1997) The bilateral reach-to-grasp movement of Parkinson's disease subjects. Brain 120:593–604

Castiello U, Bennett K.M.B., & Stelmach G.E. (1993b) Reach to grasp the natural response to perturbation of object size. Exp Brain Res 94:163–178

Castiello U, Bennett K.M.B., & Stelmach GE (1993a) The bilateral reach to grasp movement. Behav Brain Res 56:43–57

Castiello, U. (1996). Grasping a fruit: selection for action. *J. Exp. Psychol. Hum. Percept. Perf.* **22**, 582–603

Chaffin, D.B., Faraway, J., Zhang, X. and Woolley, C. (2000). Stature, Age, and Gender Effects on Reach Motion Postures. Human Factors 42(3):408-420.

Chieffi S, Gentilucci M (1993) Coordination between the transport and the grasp components during prehension movements. Exp Brain Res 94:471–477

Churchill A, Vogt S, Hopkins B (1999) The coordination of two-effector actions: spoon feeding and intermanual prehension. Br J Psychol 90:271–290

Clifton RK, Muir DW, Ashmead DH, Clarkson MG (1993) Is visually guided reaching in early infancy a myth? Child Dev 64:1099–1110

Cohn, J. V., DiZio, P., & Lackner, J. R. (2000). Reaching during virtual rotation: context specific compensations for expected coriolis forces. Journal of Neurophysiology, 83(6), 3230–3240.

Cooke JD, Virji-Babul N (1995) Reprogramming of muscle activation patterns at the wrist in compensation for elbow reaction torques during planar two-joint movements. Exp Brain Res 106:169–176

Cordo, P., Bevan, L., Gurfinkel, V., Carlton, L., Carlton, M., Kerr, G. (1995) Proprioceptive coordination of discrete movement sequences : mechanism and generality. Canadian J. of physio. & pharmaco. 73(2):218-330

Cordo, P., Carlton, L., Bevan, L., Carlton, M., and Kerr, G. K. (1994) Proprioceptive coordination of movement sequences: Role of Velocity and Position Information. Journal of Neurophysio. 71:1848-1861.

Delleman, N. J., & Hin, A. J. S. (2000). Postural Behaviour in Static Gazing Upwards and Downwards, *SAE Technical Papers Series 2000-01-2173*, Warrendale, PA: Society of Automotive Engineers.

Delleman, N. J., Huysmans, M. A., & Kujit-Evers, L. F. M. (2001). *Postural behaviour in static gazing sidewards* (SAE Technical Papers Series, 2001-01-2093). Warrendale, PA: Society of Automotive Engineers.

Desmurget, M., & Prablanc, C. (1997). Postural Control of Three-Dimensional Prehension Movements. *Journal of Neurophysiology*. *77*, 452-464.

Desmurget, M., Prablanc, C., Rossetti, Y., Azi, M., Paulignan, Y., Urquizar, C., & Mignot, J. (1995). Postural and synergic control for three-dimensional movements of reaching and grasping. *Journal of Neurophysiology*, *74*(2), 905–910.

Devanne H., and Maton, B., (1998) Role of proprioceptive information in the temporal coordination between joints. - Exp Brain Res. 119:58-64

Dornay M., Uno Y., Kawato M., Suzuki R. (1992) Simulation of optimal movements using the minimum-muscle-tension-change model. In: Moody J.E., Hanson S.J.

Lippmann R.P. (eds) Advances in neural information processing systems, vol 4. Morgan Kauffmann, San Mateo, pp 627-634

Dysart, M. J., & Woldstad, J. C. (1996). Posture Prediction for Static Sagittal-Plane Lifting. *Journal of Biomechanics*, *29*(10), 1393-1397.

Feldman AG, Latash ML (1982) Interaction of afferent and efferent signals underlying joint position sense: empirical and theoretical approaches. *J Mot Behav* 14: 174-193

Feldman, A. G. (1966). Functional turning of nervous system with control of movement or maintenance of a steady posture. Controllable parameters of the muscle. *Biophysics*, *11*, 565–578.

Feldman, A. G. (1986). Once more on the equilibrium point hypothesis (lambda model) for motor control. *Journal of Motor Behavior*, *18*, 17-54.

Fetters L, Todd J (1987) Quantitative assessment of infant reaching movements. J Mot Behav 19:147–166

Fitts, P.M. (1954). The Information Capacity of the Human Motor System in Controlling the Amplitude of Movement. Journal of Experimental Psychology 47:381-391.

Flanagan J.R., Johansson R.S. (2003) Action plans used in action observation. Nature 424(6950):769–771

Flash T., Hogan N. and Richardson M.J.E. (2003) Optimization principles in motor control. In: Arbib M (ed) Handbook of brain theory and neural networks, 2nd edn. MIT Press, Cambridge, MA, pp.827-831

Flash, T. and Hogan N. (1985). The Coordination of Arm Movements: an Experimentally Confirmed Mathematical Model. Journal of Neuroscience 5:1688–1703.

Forssberg H, Eliasson AC, Kinoshita H, Johansson RS, Westling G (1991) Development of human precision grip. I. Basic coordination of force. Exp Brain Res 85:451–457

Forssberg H, Kinoshita H, Eliasson AC, Johansson RS, Westling G, Gordon AM (1992) Development of human precision grip. II. Anticipatory control of isometric forces targeted for object's weight. Exp Brain Res 90(2):393–398

Fuller, J. H. (1992). Head movement propensity. *Experimental Brain Research*, *92*(1), 152–164.

Galloway J.C. and Koshland G.F. (2002). General coordination of shoulder, elbow and wrist dynamics during multijoint arm movements. Experimental Brain Research 142:125-136

Gandevia, S. C. and Burke, D. (1992) Does the nervous system depend on kinesthetic input to control natural limb movements? Behav. Brain Sci. 15: 615-633.

Gauthier GM, Roll JP, Martin B, Harlay F (1981) Effects of whole-body vibrations on sensory motor system performance in man. *Aviat Space Environ Med* 52: 473-479

Gauthier, G. M., Martin, B. J., & Stark, L. (1986). Adapted head and eye movement responses to added-head inertia. *Aviation, Space, and Environmental Medicine*, *57*, 336–342.

Gauthier, G. M., Vercher, J. L., & Blouin, J. (1995). Egocentric visual target position and velocity coding: role of ocular muscle proprioception. *Annals of Biomedical Engineering*, *23*, 423–435.

Gentilucci M, Castiello U, Corradini ML, Scarpa M, Umilta C, Rizzolati G (1991) Influence of different types of grasping on the transport component of prehension movements. Neuropsychology 29:361–378

Georgopoulos, A.P., Kalaska, J.F., & Massey, J.T. (1981). Spatial trajectories and reaction times of aimed movements: Effects of practice, uncertainty and change in target location. *Journal of Neuroscience*, 46: 725-743

Ghez C, Sainburg R (1995) Proprioceptive control of interjoint coordination. Can J Physiol Pharmacol 75:273–284

Ghez, C., Gordon, J., Ghilardi, M. F., Christakos, C. N., and Cooper, S. E. (1990) Roles of proprioceptive input in the programming of arm trajectories. Cold Spring Harbor Symp. Quant. Biol. 55: 837-847,

Gibson AR, Horn KM, Van Kan PL (1998) Construction of reach to grasp. Novartis Found Symp 218:245–251

Gielen, C.C.A.M., Vrijenhoek, E. J., Flash, T., & Neggers, S.F.W. (1997). Arm position constraints during pointing and reaching in 3-D space. *Journal of Neurophysiology, 78*(2), 660.

Gottlieb GL, Song Q, Almeida GL, Hong D, Corcos D (1997) Directional control of planar human arm movement. J Neurophysiol 78:2985–2998

Graaf J.B. de, Denier van der Gon J.J., Sittig A.C. (1991a) Directional information during slow goal-directed arm movements. Soc Neurosci Abstr 17(2): 1110

Graaf J.B. de, Denier van der Gon J.J., Sittig A.C. (1994) Misdirections in slow, goal-directed arm movements are not primarily visually based. Exp Brain Res 99: 464-472

Graaf J.B. de, Sittig A.C., Denier van der Gon J.J. (1991b) Misdirections in slow goal-directed arm movements and pointer-setting tasks. Exp Brain Res 84:434-438

Gribble PL, Ostry DJ (1999) Compensation for interaction torques during single- and multijoint limb movement. J Neurophysiol 82:2310–2326

Guitton, D., & Volle, M. (1987) Gaze control in humans: eye-head coordination during orienting movements to targets within and beyond the oculomotor range. Journal of Neurophysiology, 58, 427.

Hasan, Z. (1992) Role of proprioceptors in neural control. Curr. Opin. Neurobiol. 2: 824-829.

Helsen, W. F., Elliott, D., Starkes, J. L., & Ricker, K. L. (2000). Coupling of eye, finger, elbow, and shoulder movements during manual aiming. *Journal of Motor Behavior*, *32*(3), 241–248.

Hoff B, Arbib MA (1993) Models of trajectory formation and temporal interaction of reach and grasp. J Mot Behav 25:175–192

Hofsten C von (1979) Development of visually directed reaching: the approach phase. J Hum Mov Stud 5:160–178

Hofsten C von (1991) Structuring of reaching movements: a longitudinal study. J Mot Behav 23:280–292

Hofsten C von, Roennqvist L (1988) Preparation for grasping an object: a developmental study. J Exp Psychol Hum Percept Perform 14:610–621

Hogan, N. (1985). The Mechanics of Multi-Joint Posture and Movement Control. Biological Cybernetics 52:315-331.

Hollerbach JM, Flash T (1982) Dynamic interactions between limb segments during planar arm movement. Biol Cybern 44:67–77

Holst, E. von (1973). Relative coordination as a phenomenon and as a method of analysis of central nervous function. In R. Martin (Ed. and Trans.), The collected papers of Erich von Holst: Vol. 1. The behavior physiology of anumals and man, pp. 35-135. Coral Gables, FL: University of Miami Press. (Original work published 1939)

Holst, E. von, and Saint Paul, U. von (1973). On the functional organization of drives. In R. Martin (Ed. and Trans.), The collected papers of Erich von Holst: Vol. 1. The behavior physiology of anumals and man, pp. 220-258. Coral Gables, FL: University of Miami Press.

Hondzinski, J. M., & Kwon, T. (2009). Pointing control using a moving base of support. *Experimental Brain Research, 197*(1), 81.

Hore, J., Watts, S., & Tweed, D. (1994) Arm position constraints when throwing in three dimensions. *J. Neurophysiol.* 72: 1171–1180.

Hore, J., Watts, S., & Vilis, T. (1992) Constraints on arm position when pointing in three dimensions: Donders' law and the Fick gimbal strategy. *J. Neurophysiol.* 68: 374–383.
Jackobson LS, Goodale MA (1991) Factors affecting higher order movement planning: a kinematic analysis of human prehension. Exp Brain Res 86:199–208

Jagacinski, R. J. & Flach, J. M. (2003). *Control theory for humans: quantitative approaches to modeling performance*. New Jersey: Lawrence Erlbaum Associates

Jakobson, L. S. & Goodale, M. A. (1992). Factors affecting higher-order movement planning: a kinematic analysis of human prehension. *Exp. Brain Res.* **86**, 199–208.

Jeannerod (1981) Intersegmental coordination during reaching at natural visual objects. In: Long L, Baddeley A (eds) Attention and performance IX. Erlbaum, Hillsdale, pp 153–168

Jeannerod M (1984) The timing of natural prehension movements. J Mot Behav 16:235–254

Jeannerod M (1986) The formation of finger grip during prehension: a cortically mediated visuomotor pattern. Behav Brain Res 19:99–116

Jeannerod M, Arbib MA, Rizzolatti G, Sakata H (1995) Grasping objects: the cortical mechanisms of visuomotor transformation. Trends Neurosci 18:314–320

Jeannerod M, Marteniuk RG (1992) Functional characteristics of prehension: from data to artificial neural networks. In: Proteau L, Elliott D (eds) Vision and motor control. Elsevier, North-Holland, pp 197–232

Jeannerod M, Paulignan Y, Weiss P (1998) Grasping an object: one movement, several components. Novartis Found Symp 218:5–20

Jeannerod, M. (1981). Intersegmental coordination during reaching at natural visual objects. In *Attention and performance IX* (ed. J. Long & A. Baddeley), pp. 153–168. Hillsdale, NJ: Lawrence Erlbaum Associates.

Jeannerod, M. (1984). The timing of natural prehension movements. *J. Mot. Behav.* **16**, 235–254.

Jeannerod, M. (1988). *The neural and behavioural organization of goal directed movements*. Oxford: Clarendon Press.

Johansson R.S., Westling G., Backstrom A., Flanagan J.R. (2001) Eye-hand coordination in object manipulation. J Neurosci 21(17):6917–6932

Jordan M.I., Flash T, Arnon Y. (1994) A model of the learning of arm trajectories from spatial deviations. J Cogn Neurosci 6:359-376

Kang T., He, J., and Tillery S. (2005). Determining natural arm configuration along a reaching trajectory. Exp Brain Res. 167:352-361

Katawa M. (1996) Trajectory formation in arm movements: Minimization principles and procedures. In:Zelaznik H (ed) Advances in motor learning and control. Human Kinetics, Champaign, IL, pp.225-259

Katawa M. (1999) Internal models for motor control and trajectory planning. Curr opin Neurobiol 9:718-727

Kawato M., and Wolpert D. (1998) Internal models for motor control. Novartis Found Symp. 218:291-304

Kim, K. H. (2005). Modeling of Head and Hand Coordination in Unconstrained Three Dimensional Movements. Doctoral Dissertation, The University of Michigan, Ann Arbor, MI.

Kim, K. H., Gillespie, R. B., & Martin, B. J. (2007). Head movement control in visually guided tasks: Postural goal and optimality. *Computers in Biology and Medicine, 37*(7), 1009.

Klein Breteler, M. D., Hondzinski, J. M., & Flanders, M. (2003). Drawing sequences of segments in 3D: Kinetic influences on arm configuration. *Journal of Neurophysiology, 89*(6), 3253.

Konczak J, Borutta M, Dichgans J (1997) The development of goad-directed reaching in infants. II. Learning to produce task-adequate patterns of joint torque. Exp Brain Res 113:465–474

Konczak J, Borutta M, Topka H, Dichgans J (1995) The development of goal-directed reaching in infants: hand trajectory formation and joint torque control. Exp Brain Res 106:156–168

Konczak J, Dichgans J (1997) The development toward stereotypic arm kinematics during reaching in the first 3 years of life. Exp Brain Res 117:346–354

Kuhtz-Buschbeck JP, Boczed-Funcke A, Illert M, Jöhnk K, Stolze H (1999) Prehension movements and motor development in children. Exp Brain Res 128:65–68

Kuhtz-Buschbeck JP, Stolze H, Boczed-Funcke A, Johnk K, Heinrichs H, Illert M (1998a) Kinematic analysis of prehension movements in children. Behav Brain Res 93:131–141

Kuhtz-Buschbeck JP, Stolze H, Jöhnk K, Boczed-Funcke A, Illert M (1998b) Development of prehension movements in children: a kinematic study. Exp Brain Res 122:424–432

Lackner JR (1973) Visual rearrangement affects auditory localization. Neuropsychologia 11:29-32

Lashley K.S. (1951). The problem of serial order in behavior. Cerebral Mechanisms in Behavior. pp.112-146

Magescas F, Prablanc C (2006) A joint-centred model accounts for movement curvature and spatial variability. Neuroscience Letters 403:114-118.

Magescas F, Urquizar C, and Prablanc C (2009) Two modes of error processing in reaching. Experimental Brain Research 193:337-350.

Mason CR, Gomez JE, Ebner TJ (2001) Hand synergies during reach-to-grasp. J Neurophysiol 86:2896–2901

Mason CR, Miller LE, Baker JF, Houk JC (1998) Organization of reaching and grasping movements in the primate cerebellar nuclei as revealed by focal muscimol inactivation. J Neurophysiology 79:537–554

McCloskey, D. I. (1973) Differences between the senses of movement and position shown by the effects of loading and vibration of muscles in man. Brain Res. 61:119-131

McCloskey, D. I. (1978) Kinesthetic sensibility. Physiol. Rev. 58: 763-820

McIntyre J, Stratta F, Lacquaniti F (1997) A viewer-centered reference frame for pointing to memorized targets in three-dimensional space. *J Neurophysiol* 78:1601–1618.

McIntyre,J., Stratta, F., & Lacquaniti, F. (1998). Short-term memory for reaching to visual targets: Psychophysical evidence for body-centered reference frames. *The Journal of Neuroscience, 18*(20), 8423.

McMahon T.A. (1984) Muscle, Reflexes, and Locomotion, Princeton University Press, NJ

Medendorp W.P. & Crawford J.D. (2002a). Visuospatial updating of reaching targets in near and far space. *Neuroreport* 13: 633–636,

Medendorp W.P., Van Asselt S., and Gielen C.C.A.M. (1999). Pointing to remembered visual targets after active one-step self-displacements within reaching space. *Exp Brain Res* 125: 50–60.

Medendorp W.P., Van Gisbergen J.A.M., and Gielen C.C.A.M. (2002b). Human gaze stabilization during active head translations. *J Neurophysiol* 87: 295–304.

Miller, L. E., Theeuwen, M., & Gielen, C.C.A.M (1992). The control of arm pointing movements in three dimensions. *Exp. Brain Res.* 90: 415–426.

Morasso P (1981) Spatial control of arm movements. Experimental Brain Research 42:223.

Morrison, D. F. (1976). *Multivariate Statistical Methods*. Tokyo: McCraw-Hill Kogakusha. 1976, p. 128-136

Neggers S.F., Bekkering H. (2000) Ocular gaze is anchored to the target of an ongoing pointing movement. J Neurophysiol 83(2):639–651

Okadome, T., & Honda, M. (1999). Kinematic construction of the trajectory of sequential arm movements. *Biological Cybernetics*, 80: 157-169.

Olivier I, Bard C (2000) The effects of spatial movement components precues on the execution of rapid aiming in children aged 7, 9, and 11. J Exp Child Psychol 77:155–168

Olivier, I., Hay, L., Bard, C., and Fleury, M. (2007) Age-related diVerences in the reaching and grasping coordination in children: unimanual and bimanual tasks, Experimental Brain Research 179:17-27

Orban de Xivry JJ, Bennett SJ, Lefevre P, Barnes GR. (2006) Evidence for synergy between saccades and smooth pursuit during transient target disappearance. J Neurophysiol 95(1):418–27.

Paillard, J., & Amblard, B. (1985). Static versus kinetic visual cues for the processing of spatial relationships. In D. J. Ingle, M. Jeannerod & D. N. Lee (Eds.), *Brain mechanism in spatial vision* (pp. 367–385). Amsterdam: Martinus Nijhoff.

Park, W., Chaffin, D., & Martin, D. (2004). Toward Memory Based Human Motion Simulation: Development and Validation of a Motion Modification Algorithm. *IEEE Transactions on Systems, Man and Cybernetics*, *34*(3), 376–386.

Peterka, R. J., & Benolken, M. S. (1995). Role of somatosensory and vestibular cues in attenuating visually induced human postural sway. Experimental Brain Research, 105(1), 101–110.

Prablanc C, Echallier JF, Komilis E, Jeannerod M (1979) Optimal response of eye and hand motor systems in pointing at a visual target. I. Spatio-temporal characteristics of eye and hand movements and their relationship when varying the amount of visual information. *Biol Cybern* 35:113–124.

Prablanc, C., Pélisson, D., & Goodale, M.A. (1986). Visual control of reaching movements without vision of the limb—I: Role of retinal feedback of target position in guiding the hand. *Experimental Brain Research*, *62*, 293–302.

Reed, M.P., Manary, M.A., and Schneider, L.W. (1999). Methods for measuring and representing automobile occupant posture. Technical paper 990959. SAE Transactions: Journal of Passenger Cars, Vol. 108.

Reed, M.P., Parkinson, M.B., and Chaffin, D.B. (2003). A new approach to modeling driver reach. Technical Paper 2003-01-0587. SAE International, Warrendale,PA.

Reed, M.P., Parkinson, M.B., and Wagner, D.W. (2004). Torso Kinematics in Seated Reaches. Technical paper 2004-01-2176. SAE International, Rochester, MI.

Ren L., Blohm G. and Crawford J.D. (2007) Comparing Limb Proprioception and Oculomotor Signals during Hand-guided Saccades. Experimental Brain Research 182:189-198

Roby-Brami, A., Jacobs, S., Bennis, N. & Levin, M.F. (2003). Hand orientation for grasping and arm joint rotation patterns in healthy subjects and hemiparetic stroke patients. *Brain Research, 969*(1-2), 217.

Roll, J. P., Bergenheim, M., and Ribot-Ciscar, E. (2000) Proprioceptive population coding of two-dimensional limb movements in humans: II. Muscle-spindle feedback during "drawing-like" movements. Exp Brain Res 134:311–321

Roll, J. P., Vedel, J. P., and Roll, R. (1989) Eye, head and skeletal muscle spindle feedback in the elaboration of body references. Prog. Brain Res. 80: 113-123, 1989.

Roll, R., Gilhodes, J. C., Roll, J. P., Popov, K., Charade, O., and Gurfinkel V. (2000) Proprioceptive information processing in weightlessness. Exp Brain Res 122:393–402

Rosenbaum D.A., Loukopoulos, L.D., Meulenbroek, R.G.J., Vaugan, J., & Engelbrecht, S.E. (1995). Planning reaches by evaluating stored postures. *Psychological Review,* 102:28-67

Rosenbaum, D. A., Meulenbroek, R. G. J., & Vaughan, J. (2001). Planning reaching and grasping movements: Theoretical premises and practical implications. *Motor Control*, *2*, 99–115.

Rothwell, J. C., Traub, M. M., Day, B. L., Obeso, J. A., Thomas, P. K., and Marsden, C. D. Manual (1982) Motor performance in a deafferented man. Brain 105 15-542.

Sabes, P. N. (2000). The Planning and Control of Reaching Movements, *Current Opinions in Neurobiology* 10, 740-746.

Sailer, U., Eggert, T., Ditterich, J., & Straube, A. (2005). Spatial and temporal aspects of eye-hand coordination across different tasks. *Experimental Brain Research, 134*, 163–173.

Sainburg RL, Ghez D, Kalakanis D (1999) Intersegmental dynamics are controlled by sequential anticipatory, error correction, and postural mechanisms. J Neurophysiol 81:1045–1056

Sainburg RL, Ghilardi M, Poizner H, Ghez C (1995) Control of limb dynamics in normal subjects and patients without proprioception.J Neurophysiol 73:820–835

Sainburg RL, Kalakanis D (2000) Differences in control of limb dynamics during dominant and nondominant arm reaching. J Neurophysiol 83:2661–2675

Sainburg RL, Lateiner JE, Latash ML, Bagesteiro LB (2003) Effects of altering initial position on movement direction and extent. *J Neurophysiol* 89: 401-415

Saling, M., Sitarova, T., Vejsada, R., and Hnik, P. (1992) Reaching behavior in the rat: absence of forelimb peripheral input. Physiol. Behav. 5 1: 185-191.

Sanes, J. N., Mauritz, K. -H., Dalakas, M. C., and Evarts, E. V. (1985) Motor control in humans with large-fiber sensory neuropathy. Hum. Neurobiol. 4:101-114.

Sauter, D., Martin, B., Di Renzo, N., & Vomscheid, C. (1991). Analysis of eye tracking movements using innovations generated by a kalman filter. Medical and Biological Engineering and Computing, 29(1), 63-69.

Schneiberg S, Sveistrup H, McFadyen B, McKinley P, Levin M (2002) The development of coordination for reach-to-grasp movements in children. Exp Brain Res 146:142–156

Sherrington, C. S. (1906) On the proprio-ceptive system, especially in its reflex aspects. Brain 29: 467-482.

Siebert T., Sust M., Thaller S., Tilp M. and Wagner H. (2007) An Improved Method to Determine Neuromuscular Properties Using Force Laws – from Single Muscle to Applications in Human Movements. Human Movement Science 26:320-341

Simoneau M, Paillard J, Bard C, Teasdale N, Martin O, Fleury M, Lamarre Y (1999) Role of the feedforward command and reafferent information in the coordination of a passive prehension task. Exp Brain Res 128:236–242

Sittig A.C., Graaf .J.B. de (1994) Orientation dependent misalignments in a visual alignments task. Vision Res. 34(17):2195-203.

Soechting, J. F. (1986). Coordination of arm movements in 3-dimensional space – sensorimotor mapping during drawing movement. *Neuroscience, 17*(2), 295.

Soechting, J. F., & Flanders, M. (1989a). Sensorimotor representations for pointing to targets in three-dimensional space. *Journal of Neurophysiology, 62*(2), 582.

Soechting, J. F., & Flanders, M. (1989b). Errors in pointing are due to approximations in sensorimotor transformations. *Journal of Neurophysiology, 62*(2), 595-608.

Soechting, J. F., & Ross, B. (1984). Osychophysical determination of coordinate representation of human arm orientation. *Neuroscience, 13*(2), 595.

Soechting, J.F., & Lacquaniti, F. (1981). Invariant characteristics of a pointing movement in man. *Journal of Neuroscience*, 1: 710-720

Soechting, J.F., Buneo, C.A., Herrmann, U., & Flanders, M. (1995). Moving effortlessly in three dimensions: Does Donders' law apply to arm movement? *Journal of Neuroscience*, 15: 6271-6280

Stahl, J. S. (1999). Amplitude of human head movements associated with horizontal saccades. Experimental Brain Research, 126(1), 41–54.

Stelmach GE, Castiello U, Jeannerod M (1994) Orienting the finger opposition space during prehension movements. J Mot Behav 26:178–186

Tipper, S. P., Howard, L. A., & Paul, M. A. (2001). Reaching affects saccade trajectories. *Experimental Brain Research*, *136*(2), 241–249.

Todorov, E., & Jordan, M. I. (2002). Optimal feedback control as a theory of motor coordination - nature neuroscience. *Nature Neuroscience, 5*(8/18/2008): 1226-1235.

Tolani D., Badler N. (1996). Real-time inverse kinematics of the human arm. Presence 5.4:393-401

Torres E, B & Zipser D. (2002). Reaching to grasp with a multi-jointed arm. I. A computational model. *Journal of Neurophysiol*ogy 88: 1-13.

Tresilian JR, Stelmach GE (1997) Common organisation for unimanual and bimanual reach-to-grasp tasks. Exp Brain Res 115:283–299

Tweed, D. & Vilis, T. (1987) Implications of rotational kinematics for the oculomotor system in three dimensions. *J. Neurophysiol.* 58: 832–849.

Tweed, D., Glenn, B., & Vilis, T. (1995). Eye-head coordination during large gaze shifts. *J. Neurophysiol.* 73: 766–779.

Uno Y, Kawato M, Suzuki R (1989) Formation and control of optimal trajectory in human multijoint arm movement. Biol Cybern 61:89-101.

van Beers, R. J., Wolpert, D. M., & Haggard, P. (2002). When feeling is more important than seeing in sensorimotor adaptation. *Current Biology, 12*(10), 834.

van den Bosch W.A., Leenders I., and Mulder P. (1999), Topographic anatomy of the eyelids, and the effects of sex and age, British Journal of Ophthalmology, 83:347-352.

Van der Kooij, H., Jacobs, R., Koopman, B., & van der Helm, F. (2001). An adaptive model of sensory integration in a dynamic environment applied to human stance control. Biological Cybernetics, 84(2), 103–115.

Vercher, J.L., Magenes. G., Prablanc, C., & Gauthier, G. M. (1994). Eye-head-hand coordination in pointing at visual targets: spatial and temporal analysis, *Experimental Brain Research*, *99*, 507-523.

Wang, X. (1999). Behavior-based inverse kinematics algorithm to predict arm prehension postures for computer-aided ergonomic evaluation. *Journal of Biomechanics*, *32*(5), 453–460.

Welch RB (1978) Perceptual modification: adaptation to altered sensory environments. Academic, New York

Winter, D. A. (2005). *Biomechanics and motor control of human movement*, New Jercy: John Wiley & Sons.

Wolpert D.M., Ghahramani Z., Jordan M.I. (1995) Are arm trajectories planned in kinematic or dynamic coordinates? An adaptation study. Exp Brain Res 103:460-470

Wolpert, D. M., Ghahramani, Z., & Jordan, M. I. (1994). Perceptual distortion contributes to the curvature of human reaching movements. *Exp. Brain Res.* 98: 153–156.

Won J. and Hogan N. (1995). Stability Properties of Human Reaching Movements. Experimental Brain Research 107:125-136

Woodworth, R. S. (1899). The accuracy of voluntary movements. Psychological Review (Monograph Supplement), 3, 1-114.

Woolley, C., Natalini, T., and Cascos, R. (2000). HUMOSIM 1999 Summer Data Collection: Anthropometric Measurements. Center for Ergonomics, University of Michigan, Ann Arbor, MI.

Yu, S.Y. and Martin, B.J. (2008). Upper Body Coordination in Reach Movements. SAE Technical Paper 2008-01-1917.

Zaal FT, Daigle K, Gottlieb GL, Thelen E (1999) An unlearned principle for controlling natural movements. J Neurophysiol 82:255–259

Zackowski KM, Thach WT, Bastian AJ (2002) Cerebellar subjects show impaired coupling of reach and grasp movements. Exp Brain Res 146:511–522

Zhang, X. and Chaffin, D. (1999) The Effects of Speed Variation on Joint Kinematics during Multisegment Reaching Movements, Human Movement Science, 18:741-757.

Zhang, X. and Chaffin, D. (2000) A Three-dimensional Dynamic Posture Prediction Model for Simulating In-vehicle Seated Reaching Movements: Development and Validation. Ergonomics, 43(9):1314-1330.

Zhang, X., Kuo, A.D., and Chaffin, D. (1998) Optimization-based differential kinematic modeling exhibits a velocity-control strategy for dynamic posture determination in seated reaching movements, Journal of Biomechanics 31:1035-1042